CENTER FOR X-RAY OPTICS

X-RAY DATA BOOKLET

LBL-PUB--490-Rev.

DE86 012650

Contributions by Janos Kirz, David T. Attwood, Burton L. Henke, Malcolm R. Howells, Kurt D. Kennedy, Kwang-Je Kim, Jeffrey B. Kortright, Rupert C. Perera, Piero Pianetta, John C. Riordan, James H. Scofield, Gary L. Stradling, Albert C. Thompson, James H. Underwood, Gwyn P. Williams, and Herman Winick.

Edited by Douglas Vaughan

Lawrence Berkeley Laboratory
University of California
Berkeley, California 94720

Second printing, with corrections, April 1986

This work was supported in part by the U.S. Department of Energy under Contract No. DE-AC03-76SF00098

AFFILIATIONS

David T. A[illegible], *Center for X-Ray Optics, LBL*
Burton [illegible], *Center for X-Ray Optics, LBL*
Malcolm R. [illegible], *Center for X-Ray Optics, LBL*
Kurt D. Kennedy, [illegible] *Laboratory*
Kwang-Je Kim, *Center for X-Ray Optics, LBL*
Janos Kirz, *State University of New York at Stony Brook*
Jeffrey B. Kortright, *Center for X-Ray Optics, LBL*
Rupert C. Perera, *Center for X-Ray Optics, LBL*
Piero Pianetta, *Stanford Synchrotron Radiation Laboratory*
John C. Riordan, *Maxwell Laboratories, Inc.*
James H. Scofield, *Lawrence Livermore National Laboratory*
Gary L. Stradling, *Los Alamos National Laboratory*
Albert C. Thompson, *Center for X-Ray Optics, LBL*
James H. Underwood, *Center for X-Ray Optics, LBL*
Douglas Vaughan, *Lawrence Berkeley Laboratory*
Gwyn P. Williams, *National Synchrotron Light Source*
Herman Winick, *Stanford Synchrotron Radiation Laboratory*

CONTENTS

PREFACE

Aside from a perceived need for such a compilation, the principal inspiration for this data booklet was the *Particle Properties Data Booklet*, which is compiled and published periodically by the Particle Data Group at the Lawrence Berkeley Laboratory. Indeed, Sections 1, 8.1, 8.2, and 8.3 of the present booklet have been borrowed, with permission and with only slight modification, from the 1984 edition of the particle data booklet.

Many other sections also draw heavily on work published elsewhere, as indicated in the text and figure captions. Furthermore, we are indebted to many colleagues whose names do not appear among the authors of the articles. Several willingly made illustrations and other material available to us, and we have tried to credit such contributions explicitly. Others served as reviewers and offered invaluable advice on several articles; their names appear among the contributors.

Despite these contributions and the efforts of the many authors, final decisions rested with only a few of us, as did responsibility for compiling the sections lacking by-lines. Blame for error is thus easy to assign.

David T. Attwood
Janos Kirz
Douglas Vaughan
16 August 1985

A NOTE ON THE CORRECTED EDITION

With this reprinting of the *X-Ray Data Booklet*, we have made only a few corrections, affecting pages 1-2, 2-6, 2-13, 2-27, 4-7, 4-9, 7-2, 7-3, and 7-4. We still plan a second, more extensively revised edition in the future. Consequently, if you find further errors or omissions, or can think of ways the booklet can be made more useful, please send your comments to Douglas Vaughan, Building 50, Room 149, Lawrence Berkeley Laboratory, 1 Cyclotron Road, Berkeley, California 94720.

SECTION 1

PHYSICAL CONSTANTS

Table 1-1 was adapted, with permission, from one that appeared in the April 1984 edition of the *Particle Properties Data Booklet*. A periodic table follows on page 1-4.

Table 1-1. Physical constants.[a]

Quantity	Symbol, equation	Value	Uncert. (ppm)
permeability of vacuum	μ_0	$4\pi\times10^{-7}$ H m^{-1}	—
		$= 12.566\ 370\ 614\ 4\times10^{-7}$ H m^{-1}	
speed of light	c (see note [m])	$2.997\ 924\ 58(1.2)\times10^{10}$ cm s^{-1} (10^8 m s^{-1})	0.004
permittivity of vacuum	$\epsilon_0 = 1/(\mu_0 c^2)$	$8.854\ 187\ 82(7)\times10^{-12}$ F m^{-1}	0.008
Planck constant	h	$6.626\ 176(36)\times10^{-27}$ erg s (10^{-34} J s)	5.4
Planck constant, reduced	$\hbar = h/2\pi$	$1.054\ 588\ 7(57)\times10^{-27}$ erg s (10^{-34} J s)	5.4
		$= 6.582\ 173(17)\times10^{-22}$ MeV s (10^{-16} eV s)	2.6
electron charge magnitude	e	$4.803\ 242(14)\times10^{-10}$ esu	2.9
		$= 1.602\ 189\ 2(46)\times10^{-19}$ coulomb	2.9
conversion constant	$\hbar c$	197.328 58(51) MeV fm (= eV nm)	2.6
electron mass	m_e	$0.511\ 003\ 4(14)$ MeV/c^2 = $9.109\ 534(47)\times10^{-28}$ g	2.8, 5.1
proton mass	m_p	$938.279\ 6(27)$ MeV/c^2 = $1.672\ 648\ 5(86)\times10^{-24}$ g	2.8, 5.1
		$= 1.007\ 276\ 470(11)$ amu $= 1836.151\ 52(70)\ m_e$	0.011, 0.38
deuteron mass	m_d	1875.628 0(53) MeV/c^2	2.8
atomic mass unit (amu)	(mass ^{12}C atom)/12 = (1 g)/N_A	$931.501\ 6(26)$ MeV/c^2 = $1.660\ 565\ 5(86)\times10^{-24}$ g	2.8, 5.1
fine structure constant	$\alpha = e^2/\hbar c$	1/137.036 04(11)	0.82
classical electron radius	$r_e = e^2/m_e c^2$	2.817 938 0(70) fm (10^{-15} m)	2.5
electron Compton wavelength	$\lambda\!\!\!^{-}_e = \hbar/m_e c = r_e\alpha^{-1}$	3.861 590 5(64)$\times10^{-11}$ cm (10^{-13} m)	1.6
Bohr radius ($m_{nucleus} = \infty$)	$a_\infty = \hbar^2/m_e e^2 = r_e\alpha^{-2}$	0.529 177 06(44)$\times10^{-8}$ cm (10^{-10} m)	0.82
Rydberg energy	$hcR_\infty = m_e e^4/2\hbar^2 = m_e c^2\alpha^2/2$	13.605 804(36) eV	2.6
Thomson cross section	$\sigma_T = 8\pi r_e^2/3$	0.665 244 8(33) barn (10^{-28} m^2)	4.9
Bohr magneton	$\mu_B = e\hbar/2m_e c$	$5\ 788\ 378\ 5(95)\times10^{-15}$ MeV gauss^{-1} (10^{-5} eV T^{-1})	1.6
nuclear magneton	$\mu_N = e\hbar/2m_p c$	$3\ 152\ 451\ 5(53)\times10^{-18}$ MeV gauss^{-1} (10^{-8} eV T^{-1})	1.7
electron cyclotron freq./field	$\omega_{ce}/B = e/m_e c$	$1\ 758\ 804\ 7(49)\times10^{7}$ rad s^{-1} gauss^{-1} (10^{11} rad s^{-1} T^{-1})	2.8
proton cyclotron freq./field	$\omega_{cp}/B = e/m_p c$	$9\ 578\ 756(28)\times10^{3}$ rad s^{-1} gauss^{-1} (10^{7} rad s^{-1} T^{-1})	2.8

gravitational constant	G_N	$6.672\,0(41)\times10^{-8}$ cm^3 g^{-1} s^{-2} (10^{-11} m^3 kg^{-1} s^{-2})	615
grav. accel., sea level, 45° lat.	g	980.62 cm s^{-2} (10^{-2} m s^{-2})	—
Avogadro number	N_A	$6.022\,045(31)\times10^{23}$ mol^{-1}	5.1
Boltzmann constant	k	$1.380\,662(44)\times10^{-16}$ erg K^{-1} (10^{-23} J K^{-1})	32
		$= 8.617\,35(28)\times10^{-5}$ eV K^{-1}	32
molar volume, ideal gas at STP	$N_A k(273.15\ \mathrm{K})/(1\ \mathrm{atmosphere})$	22 413.83(70) cm^3 mol^{-1} (10^{-6} m^3 mol^{-1})	31
Stefan-Boltzmann constant	$\sigma = \pi^2 k^4/60\hbar^3 c^2$	$5.670\,32(71)\times10^{-5}$ erg s^{-1} cm^{-2} K^{-4} (10^{-8} J s^{-1} m^{-2} K^{-4})	125

π = 3.141 592 653 589 793 238 $\quad$ e = 2.718 281 828 459 045 235 $\quad$ γ = 0.577 215 664 901 532 861

1 in. = 2.54 cm	1 newton = 10^5 dyne	1 eV/c^2 = $1.782\,676\times10^{-33}$ g	1 coulomb = $2.997\,924\,58\times10^9$ esu
1 Å = 10^{-8} cm	1 joule = 10^7 erg	$\hbar c$/(1 eV) = 1.239 854 μm	1 tesla = 10^4 gauss
1 fm = 10^{-13} cm	1 cal = 4.184 joule	1 eV/$\hbar$ = $2.417\,965\times10^{14}$ Hz	1 atm = $1.013\,25\times10^6$ dyne/cm^2
1 barn = 10^{-24} cm^2	1 eV = $1.602\,189\,2\times10^{-12}$ erg	1 eV/k = 11 604.8 K	0°C = 273.15 K

* Revised 1984 by Barry N. Taylor, based mainly on the "1973 Least-Squares Adjustment of the Fundamental Constants," by E. R. Cohen and B. N. Taylor, *J. Phys. Chem. Ref. Data* 2, 663 (1973). The figures in parentheses give the 1-standard-deviation uncertainties in the last digits of the main numbers; the uncertainties in parts per million (ppm) are given in the last column. The uncertainties of the output values of a least-squares adjustment are in general correlated, and the laws of error propagation must be used in calculating additional quantities.

The set of constants resulting from the 1973 adjustment of Cohen and Taylor has been recommended for international use by CODATA (Committee on Data for Science and Technology), and is the most up-to-date, generally accepted set currently available. Since the publication of the 1973 adjustment, new experiments have yielded better values for some of the constants: $N_A = 6.022\,097\,8(63)\times10^{23}$ mol^{-1} (1.04 ppm); $\alpha^{-1} = 137.035\,963(15)$ (0.11 ppm); and $m_p/m_e = 1836.152\,470(79)$ (0.043 ppm). However, since a change in the measured value of one constant usually leads to changes in the adjusted values of others, one must be cautious in using together the values from the 1973 adjustment and the results of more recent experiments.

** In October 1983, the Conférence Générale des Poids et Mesures adopted a new definition of the *meter*. The meter is the length of the path traveled by light in vacuum during a time interval of 1/299 792 458 s. Thus the speed of light is *defined* to be 299 792 458 m s^{-1}. For a discussion of this change, see B. W. Petley, *Nature* 303, 373 (1983).

PERIODIC TABLE

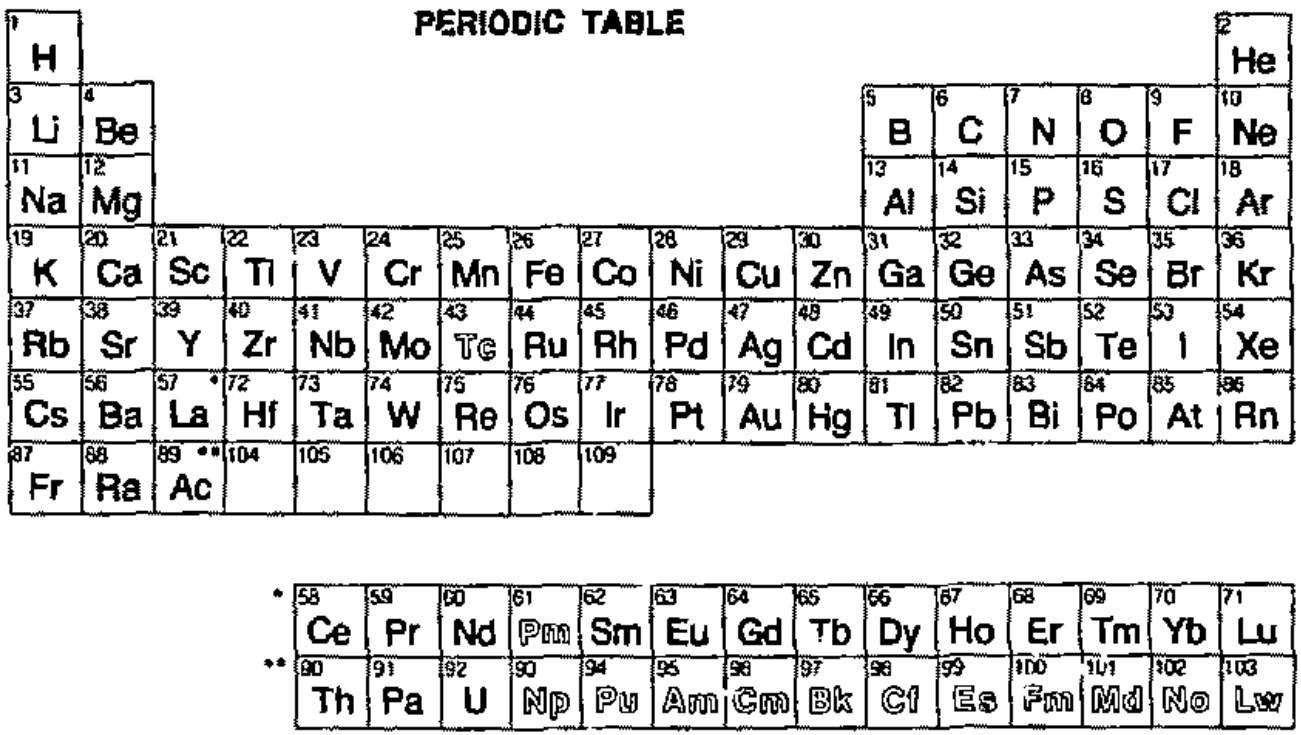

SECTION 2

THE ELEMENTS

2.1 PROPERTIES OF THE ELEMENTS

Table 2-1 lists the atomic weights, densities, melting and boiling points, first ionization potentials, and specific heats of the elements. Data were taken mostly from R. C. Weast, Ed. *CRC Handbook of Chemistry and Physics*, 65th ed. (CRC Press, Boca Raton, Florida, 1984). Atomic weights apply to elements as they exist naturally on earth or, in the cases of radium, actinium, thorium, protactinium, and neptunium, to the isotopes with the longest half-lives. Values in parentheses are the mass numbers for the longest-lived isotopes. Specific heats are given for the elements at 25°C. Densities for solids and liquids are given at 20°C unless otherwise indicated by a superscript temperature (in °C); densities for the gaseous elements are for the liquids at their boiling points.

Table 2-1. Properties of the elements.

Z	Element	Atomic weight	Density (g/cm³)	Melting point (°C)	Boiling point (°C)	Ionization potential (eV)	Specific heat (cal/g·K)
1	Hydrogen	1.00794	0.0708	−259.14	−252.87	13.598	3.41
2	Helium	4.00260	0.122	−272.2	−268.934	24.587	1.24
3	Lithium	6.941	0.533	180.54	1342	5.392	0.834
4	Beryllium	9.01218	1.845	1278	2970	9.322	0.436
5	Boron	10.81	2.34	2079	3550[c]	8.298	0.245
6	Carbon	12.011	2.26	3550	3367[s]	11.260	0.170
7	Nitrogen	14.0067	0.81	−209.86	−195.8	14.534	0.249
8	Oxygen	15.9994	1.14	−218.4	−182.962	13.618	0.219
9	Fluorine	18.9984003	1.108	−219.62	−188.14	17.422	0.197
10	Neon	20.179	1.207	−248.67	−246.048	21.564	0.246
11	Sodium	22.98977	0.969	97.81	882.9	5.139	0.292
12	Magnesium	24.305	1.735	648.8	1090	7.646	0.245
13	Aluminum	26.98154	2.6941	660.37	2467	5.986	0.215
14	Silicon	28.0855	2.32^{25}	1410	2355	8.151	0.168
15	Phosphorus	30.97376	1.82	44.1	280	10.486	0.181
16	Sulfur	32.06	2.07	112.8	444.674	10.360	0.175
17	Chlorine	35.453	1.56	−100.98	−34.6	12.967	0.114
18	Argon	39.948	1.40	−189.2	−185.7	15.759	0.124
19	Potassium	39.0963	0.856	63.25	760	4.341	0.180
20	Calcium	40.08	1.55	839	1484	6.113	0.153
21	Scandium	44.9559	2.989^{25}	1541	2831	6.54	0.1173
22	Titanium	47.88	4.53	1660	3287	6.82	0.1248
23	Vanadium	50.9415	$0.10^{18.7}$	1890	3380	6.74	0.116
24	Chromium	51.996	7.18	1857	2672	6.766	0.107
25	Manganese	54.9380	7.43	1244	1962	7.435	0.114
26	Iron	55.847	7.860	1535	2750	7.870	0.1035
27	Cobalt	58.9332	8.9	1493	2870	7.86	0.107
28	Nickel	58.69	8.876^{25}	1453	2732	7.633	0.1061
29	Copper	63.546	8.94	1083.4	2567	7.726	0.0924
30	Zinc	65.38	7.11^{25}	419.58	907	9.394	0.0922
31	Gallium	69.72	$5.877^{29.6}$	29.78	2403	5.999	0.088
32	Germanium	72.59	5.307^{25}	937.4	2830	7.899	0.077
33	Arsenic	74.9216	5.72	$817^{28 \text{ atm}}$	615[s]	9.81	0.0785
34	Selenium	78.96	4.78	217	684.9	9.752	0.0767
35	Bromine	79.904	3.11	−7.2	58.78	11.814	0.0537
36	Krypton	83.80	2.6	−156.6	−152.30	13.999	0.059
37	Rubidium	85.4678	1.529	38.89	686	4.177	0.0860

Table 2-1. Properties of the elements (continued).

Z	Element	Atomic weight	Density (g/cm³)	Melting point (°C)	Boiling point (°C)	Ionization potential (eV)	Specific heat (cal/g·K)
38	Strontium	87.62	2.54	769	1384	5.695	0.0719
39	Yttrium	88.9059	4.456[25]	1522	3338	6.38	0.0713
40	Zirconium	91.22	6.494	1852	4377	6.84	0.0660
41	Niobium	92.9064	8.55	2468	4742	6.88	0.0663
42	Molybdenum	95.94	10.20	2617	4612	7.099	0.0597
43	Technetium	(98)	11.48[a]	2172	4877	7.28	0.058
44	Ruthenium	101.07	12.39	2310	3900	7.37	0.0569
45	Rhodium	102.9055	12.39	1966	3727	7.46	0.0580
46	Palladium	106.42	12.00	1554	3970	8.34	0.0583
47	Silver	107.8682	10.48	961.93	2212	7.576	0.0562
48	Cadmium	112.41	8.63	320.9	765	8.993	0.0552
49	Indium	114.82	7.30	156.61	2080	5.786	0.0536
50	Tin	118.69	7.30	231.9681	2270	7.344	0.0519
51	Antimony	121.75	6.679	630.74	1950	8.641	0.0495
52	Tellurium	127.60	6.23	449.5	989.8	9.009	0.0481
53	Iodine	126.9045	4.92	113.5	184.35	10.451	0.102
54	Xenon	131.29	3.52	−111.9	−107.1	12.130	0.0378
55	Cesium	132.9054	1.870	28.40	669.3	3.894	0.0575
56	Barium	137.33	3.5	725	1640	5.212	0.0362
57	Lanthanum	138.9055	6.127[25]	921	3457	5.577	0.0479
58	Cerium	140.12	6.637[25]	799	3426	5.47	0.0459
59	Praseodymium	140.9077	6.761	931	3512	5.42	0.0467
60	Neodymium	144.24	6.994	1021	3068	5.49	0.0453
61	Promethium	(145)	7.20[25]	1168	2460	5.55	0.0442
62	Samarium	150.36	7.51	1077	1791	5.63	0.0469
63	Europium	151.96	5.228[25]	822	1597	5.67	0.0326
64	Gadolinium	157.25	7.8772[25]	1313	3266	6.14	0.056
65	Terbium	158.9254	8.234	1356	3123	5.85	0.0435
66	Dysprosium	162.50	8.525[25]	1412	2562	5.93	0.0414
67	Holmium	164.9304	8.769[25]	1474	2695	6.02	0.0394
68	Erbium	167.26	9.039[25]	1529	2863	6.10	0.0401
69	Thulium	168.9342	9.294[25]	1545	1947	6.18	0.0382
70	Ytterbium	173.04	6.953	819	1194	6.254	0.0287
71	Lutetium	174.967	9.841[25]	1663	3395	5.426	0.0285
72	Hafnium	178.49	13.29	2227	4602	7.0	0.028
73	Tantalum	180.9479	16.624	2996	5425	7.89	0.0334
74	Tungsten	183.85	19.3	3410	5660	7.98	0.0322

Table 2-1. Properties of the elements (continued).

Z	Element	Atomic weight	Density (g/cm^3)	Melting point (°C)	Boiling point (°C)	Ionization potential (eV)	Specific heat (cal/g-K)
75	Rhenium	186.207	20.98	3180	5627[b]	7.88	0.0350
76	Osmium	190.2	22.53	3045	5027	8.7	0.0310
77	Iridium	192.22	22.39[17]	2410	4130	9.1	0.0312
78	Platinum	195.08	21.41	1772	3827	9.0	0.0317
79	Gold	196.9665	18.85	1064.43	3080	9.225	0.0308
80	Mercury	200.59	13.522	−38.842	356.58	10.437	0.0333
81	Thallium	204.383	11.83	303.5	1457	6.108	0.0307
82	Lead	207.2	11.33	327.502	1740	7.416	0.0305
83	Bismuth	208.9804	9.730	271.3	1560	7.289	0.0238
84	Polonium	(209)	9.30	254	962	8.42	0.030
85	Astatine	(210)	—	302	337[b]	—	—
86	Radon	(222)	4.4	−71	−61.8	10.748	0.0224
87	Francium	(223)	—	27	677	—	—
88	Radium	226.0254	5	700	1140	5.279	0.0288
89	Actinium	227.0278	10.07[a]	1050	3200[b]	6.9	—
90	Thorium	232.0381	11.70	1750	4790	—	0.0281
91	Protactinium	231.0359	15.34[a]	<1600	—	—	0.029
92	Uranium	238.0289	18.92	1132.3	3818	—	0.0278
93	Neptunium	237.0482	20.21	640	3902[b]	—	—
94	Plutonium	(244)	19.80	641	3232	5.8	—
95	Americium	(243)	13.64	994	2607	6.0	
96	Curium	(247)	13.49[a]	1340	—	—	—
97	Berkelium	(247)	14[b]	—	—	—	—
98	Californium	(251)	—	—	—	—	—
99	Einsteinium	(252)	—	—	—	—	—
100	Fermium	(257)	—	—	—		—
101	Mendelevium	(258)	—	—	—		—
102	Nobelium	(259)	—	—	—		—
103	Lawrencium	(260)	—	—	—	—	—

[a]Calculated
[b]Estimated
[c]Sublimes

2.2 ELECTRON BINDING ENERGIES

Gwyn P. Williams

Table 2-2 gives the electron binding energies for the elements in their natural forms. The energies are given in electron volts relative to the vacuum level for the rare gases and for H_2, N_2, O_2, F_2, and Cl_2; relative to the Fermi level for the metals; and relative to the top of the valence bands for semiconductors. Values have been taken from Ref. 1 except as noted:

[a] Values taken from Ref. 2.
[f] Values taken from Ref. 3.
[g] One-particle approximation not valid owing to the extremely short lifetime of the core hole.
[b] Values derived from Ref. 1.

REFERENCES

1. J. A. Bearden and A. F. Burr, "Reevaluation of X-Ray Atomic Energy Levels," *Rev. Mod. Phys.* **39**, 125 (1967).
2. M. Cardona and L. Ley, Eds., *Photoemission in Solids I: General Principles* (Springer-Verlag, Berlin, 1978). The present table includes several corrections to the values appearing in this reference.
3. J. C. Fuggle and N. Mårtensson, "Core-Level Binding Energies in Metals," *J. Electron Spectrosc. Relat. Phenom.* **21**, 275 (1980).

Table 2-2. *Electron binding energies, in electron volts, for the elements in their natural forms.*

Element	K $1s$	L_I $2s$	L_{II} $2p_{1/2}$	L_{III} $2p_{3/2}$	M_I $3s$	M_{II} $3p_{1/2}$	M_{III} $3p_{3/2}$	M_{IV} $3d_{3/2}$	M_V $3d_{5/2}$	N_I $4s$	N_{II} $4p_{1/2}$	N_{III} $4p_{3/2}$
1 H	16[a]											
2 He	24.6[a]											
3 Li	54.7[a]											
4 Be	111.5[a]											
5 B	188[a]											
6 C	284.2[a]											
7 N	409.9[a]	37.3[a]										
8 O	543.1[a]	41.6[a]										
9 F	696.7[a]											
10 Ne	870.2[a]	48.5[a]	21.7[a]	21.6[a]								
11 Na	1070.8[f]	63.5[f]	30.4[f]	30.5[a]								
12 Mg	1303.0[f]	88.6[a]	49.6[f]	49.2[f]								
13 Al	1558.98[a]	117.8[a]	72.9[a]	72.5[a]								
14 Si	1839	149.7[a,b]	99.8[a]	99.2[a]								
15 P	2149	189[a]	136[a]	135[a]								
16 S	2472	230.9[a,b]	163.6[a]	162.5[a]								
17 Cl	2833	270[a]	202[a]	200[a]								
18 Ar	3205.9[a]	326.3[a]	250.6[a]	248.4[a]	29.3[a]	15.9[a]	15.7[a]					
19 K	3608.4[a]	378.6[a]	297.3[a]	294.6[a]	34.8[a]	18.3[a]	18.3[a]					
20 Ca	4038.5[a]	438.4[f]	349.7[f]	346.2[f]	44.3[f]	25.4[f]	23.4[f]					
21 Sc	4492	498.0[a]	403.6[a]	398.7[a]	51.1[a]	28.3[a]	28.3[a]					
22 Ti	4966	560.9[f]	461.2[f]	453.8[f]	58.7[f]	32.6[f]	32.6[f]					

23 V	5465	626.7[†]	519.8[†]	512.1[†]	66.3[*]	37.2[†]	37.2[†]					
24 Cr	5989	695.7[†]	583.8[†]	574.1[†]	74.1[†]	42.2[†]	42.2[†]					
25 Mn	6539	769.1[†]	649.9[†]	638.7[†]	82.3[†]	47.2[†]	47.2[†]					
26 Fe	7112	844.6[†]	719.9[†]	706.8[†]	91.3[†]	52.7[†]	52.7[†]					
27 Co	7709	925.1[†]	793.3[†]	778.1[†]	101.0[†]	58.9[†]	58.9[†]					
28 Ni	8333	1008.0[†]	870.0[†]	852.7[†]	110.8[†]	68.0[†]	66.2[†]					
29 Cu	8979	1096.7[†]	952.3[†]	932.5[†]	122.5[†]	77.3[†]	75.1[†]					
30 Zn	9659	1196.2[*]	1044.9[*]	1021.8[*]	139.1[*]	91.4[*]	88.6[*]	10.2[*]	10.1[*]			
31 Ga	10367	1299.0[*]b	1143.2[†]	1118.4[†]	159.5[†]	103.5[†]	103.5[†]	18.7[†]	18.7[†]			
32 Ge	11103	1414.6[*]b	1248.1[*]b	1217.0[*]b	180.1[*]	124.9[*]	120.8[*]	29.0[*]	29.0[*]			
33 As	11867	1527.0[*]b	1359.1[*]b	1323.6[*]b	204.7[*]	146.2[*]	141.2[*]	41.7[*]	41.7[*]			
34 Se	12658	1652.0[*]b	1474.3[*]b	1433.9[*]b	229.6[*]	166.5[*]	160.7[*]	55.5[*]	54.6[*]			
35 Br	13474	1782[#]	1596[*]	1550[#]	257[*]	189[*]	182[*]	70[*]	69[*]			
36 Kr	14326	1921	1730.9[*]	1678.4[*]	292.8[*]	222.2[*]	214.4	95.0[*]	92.3[*]	27.5[*]	14.1[*]	14.1[*]
37 Rb	15200	2065	1864	1804	326.7[*]	248.7[*]	239.1[*]	113.0[*]	112[*]	30.5[*]	16.3[*]	15.7[*]
38 Sr	16105	2216	2007	1940	358.7[†]	280.3[†]	270.0[†]	136.0[†]	134.2[†]	38.9[†]	20.3[†]	20.1[†]
39 Y	17035a	2373	2156	2080	392.0[*]b	340.6[*]	298.8[*]	157.7[†]	155.8[†]	63.8[*]	24.4[*]	23.1[*]
40 Zr	17998	2532	2307	2223	430.3[†]	343.5[†]	329.8[†]	181.1[†]	178.8[†]	50.6[†]	28.5[†]	27.7[†]
41 Nb	18986	2698	2465	2371	466.6[†]	376.1[†]	360.6[†]	205.0[†]	202.3[†]	56.4[†]	32.6[†]	30.8[†]
42 Mo	20000	2866	2625	2520	506.3[†]	410.6[†]	394.0[†]	231.1[†]	227.9[†]	63.2[†]	37.6[†]	35.5[†]
43 Tc	21044	3043	2793	2677	544[*]	447.6[*]	417.7[*]	257.6[*]	253.9[*]	69.2[*]	42.3[*]	39.9[*]
44 Ru	22117	3224	2967	2838	586.2[†]	483.3[†]	461.5[†]	284.2[†]	280.0[†]	75.0[†]	46.5[†]	43.2[†]
45 Rh	23220	3412	3146	3004	628.1[†]	521.3[†]	496.5[†]	311.9[†]	307.2[†]	81.4[*]b	50.5[†]	47.3[†]
46 Pd	24350	3604	3330	3173	671.6[†]	559.9[†]	532.3[†]	340.5[†]	335.2[†]	87.1[*]b	55.9[†]a	50.9[†]a
47 Ag	25514	3806	3524	3351	719.0[†]	603.8[†]	573.0[†]	374.0[†]	368.0[†]	97.0[†]	63.7[†]	58.3[†]

Table 2-2. Electron binding energies (continued).

Element	K 1s	L_1 2s	L_{II} $2p_{1/2}$	L_{III} $2p_{3/2}$	M_1 3s	M_{II} $3p_{1/2}$	M_{III} $3p_{3/2}$	M_{IV} $3d_{3/2}$	M_V $3d_{5/2}$	N_1 4s	N_{II} $4p_{1/2}$	N_{III} $4p_{3/2}$
48 Cd	26711	4018	3727	3538	772.0[f]	652.6[f]	618.4[f]	411.9[f]	405.2[f]	109.8[f]	63.9[f,n]	63.9[f,n]
49 In	27940	4238	3938	3730	827.2[f]	703.2[f]	665.3[f]	451.4[f]	443.9[f]	122.9[f]	73.5[f,n]	73.5[f,n]
50 Sn	29200	4465	4156	3929	884.7[f]	756.5[f]	714.6[f]	493.2[f]	484.5[f]	137.1[f]	83.6[f,n]	83.6[f,n]
51 Sb	30491	4698	4380	4132	946[f]	812.7[f]	766.4[f]	537.5[f]	528.2[f]	153.2[f]	93.6[f,n]	93.6[f,n]
52 Te	31814	4939	4612	4341	1006[f]	870.8[f]	820.8[f]	583.4[f]	573.0[f]	169.4[f]	103.3[f,n]	103.3[f,n]
53 I	33169	5188	4852	4557	1072[m]	931[n]	875[n]	631[n]	620[n]	186[n]	123[n]	123[n]
54 Xe	34561	5453	5104	4782	1148.7[m]	1002.1[n]	940.6[n]	689.0[n]	676.4[n]	213.2[n]	146.7	145.5[n]
55 Cs	35985	5714	5359	5012	1211[n,b]	1071[n]	1003[n]	740.5[n]	726.6[n]	232.3[n]	172.4[n]	161.3[n]
56 Ba	37441	5989	5624	5247	1293[n,b]	1137[n,b]	1063[n,b]	795.7[n]	780.5[n]	253.5[n]	192	178.6[n]
57 La	38925	6266	5891	5483	1362[n,b]	1209[n,b]	1128[n,b]	853[n]	836[n]	247.7[n]	205.8	196.0[n]
58 Ce	40443	6548	6164	5723	1436[n,b]	1274[n,b]	1187[n,b]	902.4[n]	883.8[n]	291.0[n]	223.2	206.5[n]
59 Pr	41991	6835	6440	5964	1511	1337	1242	948.3[n]	928.8[n]	304.5	236.3	217.6
60 Nd	43569	7126	6722	6208	1573	1403	1297	1003.3[n]	980.4[n]	319.2[n]	243.3	224.6
61 Pm	45184	7428	7013	6459	~	1403	1357	1052	1027	—	242	242
62 Sm	46834	7737	7312	6716	1723	1541	1419.8	1110.9[n]	1083.4[n]	347.2[n]	265.6	247.4
63 Eu	48519	8052	7617	6977	1800	1614	1481	1158.6[n]	1127.5[n]	360	284	257
64 Gd	50239	8376	7930	7243	1881	1688	1544	1221.9[n]	1189.6[n]	378.6[n]	286	271
65 Tb	51996	8708	8252	7514	1968	1768	1611	1276.9[n]	1241.1[n]	396.0[n]	322.4[n]	284.1[n]
66 Dy	53789	9046	8581	7790	2047	1842	1676	1333	1293.6[n]	414.2[n]	333.5[n]	293.2[n]
67 Ho	55618	9394	8918	8071	2128	1923	1741	1392	1351	432.4[n]	343.5	308.2[n]
68 Er	57486	9751	9264	8358	2208	2006	1812	1453	1409	449.8[n]	366.2	320.2[n]
69 Tm	59390	10116	9617	8648	2307	2090	1885	1515	1468	470.9[n]	385.9[n]	332.6[n]
70 Yb	61332	10486	9978	8944	2398	2173	1950	1576	1528	480.5[n]	388.7[n]	339.7[n]

Table 2-2. Electron binding energies (continued).

Element	$N_{IV}\ 4d_{3/2}$	$N_V\ 4d_{5/2}$	$N_{VI}\ 4f_{5/2}$	$N_{VII}\ 4f_{7/2}$	$O_I\ 5s$	$O_{II}\ 5p_{1/2}$	$O_{III}\ 5p_{3/2}$	$O_{IV}\ 5d_{3/2}$	$O_V\ 5d_{5/2}$	$P_I\ 6s$	$P_{II}\ 6p_{1/2}$	$P_{III}\ 6p_{3/2}$
48 Cd	11.7[†]	10.7[†]										
49 In	17.7[†]	16.4[†]										
50 Sn	24.9[†]	23.9[†]										
51 Sb	33.3[†]	32.1[†]										
52 Te	41.9[†]	40.4[†]										
53 I	50[a]	50[a]										
54 Xe	69.5[a]	67.5[a]	—	—	23.3[a]	13.4[a]	12.1[a]					
55 Cs	79.8[a]	77.5[a]	—	—	22.7	14.2[a]	12.1[a]					
56 Ba	92.6[†]	89.9[†]	—	—	30.3[†]	17.0[†]	14.8[†]					
57 La	105.3[a]	102.5[a]	—	—	34.3[a]	19.3[a]	16.8[a]					
58 Ce	109[a]	—	0.1	0.1	37.8	19.8[a]	17.0[a]					
59 Pr	115.1[a]	115.1[a]	2.0	2.0	37.4	22.3	22.3					
60 Nd	120.5[a]	120.5[a]	1.5	1.5	37.5	21.1	21.1					
61 Pm	120	120	—	—	—	—	—					
62 Sm	129	129	5.2	5.2	37.4	21.3	21.3					
63 Eu	133	133	0	0	32	22	22					
64 Gd	—	127.7[a]	8.6[a]	8.6[a]	36	20	20					
65 Tb	150.5[a]	150.5[a]	7.7[a]	2.4[a]	45.6[a]	28.7[a]	22.6[a]					
66 Dy	153.6[a]	153.6[a]	8.0[a]	4.3[a]	49.9[a]	26.3	26.3					
67 Ho	160[a]	160[a]	8.6[a]	5.2[a]	49.3[a]	30.8[a]	24.1[a]					
68 Er	167.6[a]	167.6[a]	—	4.7[a]	50.6[a]	31.4[a]	24.7[a]					
69 Tm	175.5[a]	175.5[a]	—	4.6	54.7[a]	31.8[a]	25.0[a]					
70 Yb	191.2[a]	182.4[a]	2.5[a]	1.3[a]	53.0[a]	30.3[a]	24.1[a]					

Table 2-2. Electron binding energies (continued).

Element	K 1s	L_1 2s	L_{II} $2p_{1/2}$	L_{III} $2p_{3/2}$	M_I 3s	M_{II} $3p_{1/2}$	M_{III} $3p_{3/2}$	M_{IV} $3d_{3/2}$	M_V $3d_{5/2}$	N_I 4s	N_{II} $4p_{1/2}$	N_{III} $4p_{3/2}$
71 Lu	63314	10870	10349	9244	2491	2264	2024	1639	1589	506.8[a]	412.4[a]	359.2[a]
72 Hf	65351	11271	10739	9561	2601	2365	2107	1716	1662	538[a]	438.2[a]	380.7[a]
73 Ta	67416	11682	11136	9881	2708	2469	2194	1793	1735	563.4[a]	463.4[a]	400.9[a]
74 W	69525	12100	11544	10207	2820	2575	2281	1949	1809	594.1[a]	490.4[a]	423.6[a]
75 Re	71676	12527	11959	10535	2932	2682	2367	1949	1883	625.4[a]	518.7[a]	446.8[a]
76 Os	73871	12968	12385	10871	3049	2792	2457	2031	1960	658.2[a]	549.1[a]	470.7[a]
77 Ir	76111	13419	12824	11215	3174	2909	2551	2116	2040	691.1[a]	577.8[a]	495.8[a]
78 Pt	78395	13880	13273	11564	3296	3027	2645	2202	2122	725.4[a]	609.1[a]	519.4[a]
79 Au	80725	14353	13734	11919	3425	3148	2743	2291	2206	762.1[a]	642.7[a]	546.3[a]
80 Hg	83102	14839	14209	12284	3562	3279	2847	2385	2295	802.2[a]	680.2[a]	576.6[a]
81 Tl	85530	15347	14698	12658	3704	3416	2957	2485	2389	846.2[a]	720.5[a]	609.5[a]
82 Pb	88005	15861	15200	13055	3851	3554	—	3066	2586	891.8[a]	761.9[a]	643.5[a]
83 Bi	90526	16388	15711	13419	3999	3696	3177	2688	2580	939[a]	805.2[a]	678.8[a]
84 Po	93105	16939	16244	13814	4149	3854	3302	2798	2683	995[a]	851[a]	705[a]
85 At	95730	17493	16785	14214	4317	4008	3426	2909	2787	1042[a]	890[a]	740[a]
86 Rn	98404	18049	17337	14619	4482	4159	3538	3022	2892	1097[a]	929[a]	768[a]
87 Fr	101137	18639	17907	15034	4652	4327	3663	3136	3000	1153[a]	980[a]	810[a]
88 Ra	103922	19237	18484	15444	4822	4490	3792	3248	3105	1208[a]	1058[a]	879[a]
89 Ac	106755	19844	19083	15871	5002	4656	3909	3370	3219	1269[a]	1080[a]	899[a]
90 Th	109651	20472	19693	16300	5182	4830	4046	3491	3332	1330[a]	1168[a]	966.4[a]
91 Pa	112601	21105	20314	16733	5367	5001	4174	3611	3442	1387[a]	1224[a]	1007[a]
92 U	115606	21757	20948	17166	5548	5182	4303	3728	3552	1439[a]b	1271[a]b	1043[a]

Table 2-2. *Electron binding energies (continued).*

Element	$N_{IV}\ 4d_{3/2}$	$N_V\ 4d_{5/2}$	$N_{VI}\ 4f_{5/2}$	$N_{VII}\ 4f_{7/2}$	$O_I\ 5s$	$O_{II}\ 5p_{1/2}$	$O_{III}\ 5p_{3/2}$	$O_{IV}\ 5d_{3/2}$	$O_V\ 5d_{5/2}$	$P_I\ 6s$	$P_{II}\ 6p_{1/2}$	$P_{III}\ 6p_{3/2}$
71 Lu	206.1[a]	196.3[a]	8.9[a]	7.5[a]	57.3[a]	33.6[a]	26.7[a]					
72 Hf	220.0[†]	211.5[†]	15.9[a]	14.2[†]	64.2[†]	38[a]	29.9[†]					
73 Ta	237.9[†]	226.4[†]	23.5[†]	21.6[†]	69.7[†]	42.2[a]	32.7[†]					
74 W	[illegible][†]	243.5[†]	33.6[a]	31.4[†]	75.6[†]	45.3[a]b	36.8[†]					
75 Re	273.[illegible]	260.5[†]	42.9[a]	40.5[a]	83[†]	45.6[†]	34.6[a]b					
76 Os	[illegible][†]	278.5[†]	52.0[†]	50.7[†]	33[†]	58[a]	44.5[†]					
77 Ir	311.9[†]	296.3	53.8[†]	60.8[†]	95.2 b	63.0[a]b	48.0[†]					
78 Pt	331.6[†]	314.6[†]	74.5[†]	71.2[†]	101.7[a]b	65.3[a]b	51.7[†]					
79 Au	353.2[†]	335.1[†]	87.6[†]	83.9[†]	107.2[a]b	74.2[†]	57.2[†]					
80 Hg	378.2[†]	358.8[†]	104.0[†]	99.9[†]	127[†]	83.1[†]	64.5[†]	9.6[†]	7.8[†]			
81 Tl	405.7[†]	385.0[†]	122.2[†]	117.8[†]	136.[a]b	94.6[†]	73.5[†]	14.7[†]	12.5[†]			
82 Pb	434.3[†]	412.2[†]	141.7[†]	136.9[†]	147[a]b	106.4[†]	83.3[†]	20.7[†]	18.1[†]			
83 Bi	464.0[†]	440.1[†]	162.3[†]	157.0[†]	159.3[a]b	119.0[†]	92.6[†]	26.9[†]	23.8[†]			
84 Po	500[a]	473[a]	184[a]	184[a]	177[a]	132[a]	104[a]	31[a]	31[a]			
85 At	533[a]	407[a]	210[a]	210[a]	195[a]	148[a]	115[a]	40[a]	40[a]			
86 Rn	567[a]	541[a]	238[a]	238[a]	214[a]	164[a]	127[a]	48[a]	48[a]	26		
87 Fr	603[a]	577[a]	268[a]	268[a]	234[a]	182[a]	140[a]	58[a]	58[a]	34	15	15
88 Ra	636[a]	603[a]	299[a]	299[a]	254[a]	200[a]	153[a]	68[a]	68[a]	44	19	19
89 Ac	675[a]	639[a]	319[a]	319[a]	272[a]	215[a]	167[a]	80[a]	80[a]	—	—	—
90 Th	712.1[†]	675.2[†]	342.4[†]	333.1[†]	291[a]a	229[a]a	182[a]a	92.5[†]	85.4[†]	41.4[†]	24.5[†]	16.6[†]
91 Pa	743[a]	708[a]	371[a]	360[a]	310[a]	232[a]	232[a]	94[a]	94[a]	—	—	—
92 U	778.3[†]	736.2[†]	388.2[a]	377.4[†]	321[a]ab	257[a]ab	192[a]ab	102.8[†]	94.2[†]	43.9[†]	26.8[†]	16.8[†]

2.3 CHARACTERISTIC X-RAY ENERGIES

Jeffrey B. Kortright

In Table 2-3 and Fig. 2-1, characteristic K and L x-ray line energies are given for elements with $3 \leq Z \leq 95$. Only the strongest lines are included: $K\alpha_1$, $K\alpha_2$, $K\beta_1$, $L\alpha_1$, $L\alpha_2$, $L\beta_1$, $L\beta_2$, and $L\gamma_1$. The table presents the energies of these lines for each of the elements, in order of increasing atomic number. Wavelengths, in angstroms, can be obtained from the relation $\lambda = 12.4/E$, where E is in keV. The data in the table were taken from Ref. 1, which should be consulted for a complete listing of all lines. Widths of the $K\alpha$ lines can be found in Ref. 2. Figure 2-1 shows the approximate energies and wavelengths of principal x-ray lines below 40 keV.

REFERENCES

1. J. A. Bearden, "X-Ray Wavelengths," *Rev. Mod. Phys.* 39, 78 (1967).
2. M. O. Krause and J. H. Oliver, "Natural Widths of Atomic K and L Levels, $K\alpha$ X-Ray Lines and Several KLL Auger Lines," *J. Phys. Chem. Ref. Data* 8, 329 (1979).

Table 2-3. Energies, in kilo-electron-volts, of principal x-ray emission lines.

Element	$K\alpha_1$	$K\alpha_2$	$K\beta_1$	$L\alpha_1$	$L\alpha_2$	$L\beta_1$	$L\beta_2$	$L\gamma_1$
3 Li	0.0543							
4 Be	0.1085							
5 B	0.1833							
6 C	0.277							
7 N	0.3924							
8 O	0.5249							
9 F	0.6768							
10 Ne	0.8486	0.8486						
11 Na	1.04078	1.04098	1.0711					
12 Mg	1.25360	1.25360	1.3022					
13 Al	1.48670	1.48627	1.55745					
14 Si	1.73998	1.73938	1.83594					
15 P	2.0137	2.0127	2.1391					
16 S	2.30784	2.30664	2.46404					
17 Cl	2.62239	2.62078	2.8156					
18 Ar	2.95770	2.95563	3.1905					
19 K	3.3138	3.3111	3.5896					
20 Ca	3.69168	3.68809	4.0127	0.3413	0.3413	0.3449		
21 Sc	4.0906	4.0861	4.4605	0.3954	0.3954	0.3996		

Table 2-3. Energies of x-ray emission lines (continued).

Element	$K\alpha_1$	$K\alpha_2$	$K\beta_1$	$L\alpha_1$	$L\alpha_2$	$L\beta_1$	$L\beta_2$	$L\gamma_1$
22 Ti	4.51084	4.50486	4.93181	0.4522	0.4522	0.4584		
23 V	4.95220	4.94464	5.42729	0.5113	0.5113	0.5192		
24 Cr	5.41472	5.405509	5.94671	0.5728	0.5728	0.5828		
25 Mn	5.89875	5.88765	6.49045	0.6374	0.6374	0.6488		
26 Fe	6.40384	6.39084	7.05798	0.7050	0.7050	0.7185		
27 Co	6.93042	6.91530	7.64943	0.7762	0.7762	0.7914		
28 Ni	7.47815	7.46089	8.26466	0.8515	0.8515	0.8688		
29 Cu	8.04778	8.02783	8.90529	0.9297	0.9297	0.9498		
30 Zn	8.63886	8.61578	9.5720	1.0117	1.0117	1.0347		
31 Ga	9.25174	9.22482	10.2642	1.09792	1.09792	1.1248		
32 Ge	9.88642	9.85532	10.9821	1.18800	1.18800	1.2185		
33 As	10.54372	10.50799	11.7267	1.2820	1.2820	1.3170		
34 Se	11.2224	11.1814	12.4959	1.37910	1.37910	1.41923		
35 Br	11.9242	11.8776	13.2914	1.48043	1.48043	1.52590		
36 Kr	12.649	12.598	14.112	1.5860	1.5860	1.6366		
37 Rb	13.3953	13.3358	14.9613	1.69413	1.69256	1.75217		
38 Sr	14.1650	14.0979	15.8357	1.80656	1.80474	1.87172		
39 Y	14.9584	14.8829	16.7378	1.92256	1.92047	1.99584		
40 Zr	15.7751	15.6909	17.6678	2.04236	2.039[illegible]	2.1244	2.2194	2.3027

41 Nb	16.6151	16.5210	18.6225	2.16589	2.1630	2.2574	2.3670	2.4618
42 Mo	17.47934	17.3743	19.6083	2.29316	2.28985	2.39481	2.5183	2.6235
43 Tc	18.3671	18.2508	20.619	2.4240	—	2.5368	—	—
44 Ru	19.2792	19.1504	21.6568	2.55855	2.55431	2.68323	2.8360	2.9645
45 Rh	20.2161	20.0737	22.7236	2.69674	2.69205	2.83441	3.0013	3.1438
46 Pd	21.1771	21.0201	23.8187	2.83861	2.83329	2.99022	3.17179	3.3287
47 Ag	22.16292	21.9903	24.9424	2.98431	2.97821	3.15094	3.34781	3.51959
48 Cd	23.1736	22.9841	26.0955	3.13373	3.12691	3.31657	3.52812	3.71686
49 In	24.2097	24.0020	27.2759	3.2869₈	3.27929	3.48721	3.71381	3.92081
50 Sn	25.2713	25.0440	28.4860	3.44398	3.43542	3.66280	3.90486	4.13112
51 Sb	26.3591	26.1108	29.7256	3.60472	3.59532	3.84357	4.10078	4.34279
52 Te	27.4723	27.2017	30.9957	3.76933	3.7588	4.02958	4.3017	4.5709
53 I	28.6120	28.3172	32.2947	3.93765	3.92604	4.22072	4.5075	4.8009
54 Xe	29.779	29.458	33.624	4.1099	—	—	—	—
55 Cs	30.9728	30.6251	34.9869	4.2865	4.2722	4.6198	4.9359	5.2804
56 Ba	32.1936	31.8171	36.3782	4.46626	4.45090	4.82753	5.1565	5.5311
57 La	33.4418	33.0341	37.8010	4.65097	4.63423	5.0421	5.3835	5.7885
58 Ce	34.7197	34.2789	39.2573	4.8402	4.8230	5.2622	5.6134	6.052
59 Pr	36.0263	35.5502	40.7482	5.0337	5.0135	5.4889	5.850	6.3221
60 Nd	37.3610	36.8474	42.2713	5.2304	5.2077	5.7216	6.0894	6.6021
61 Pm	38.7247	38.1712	43.826	5.4325	5.4078	5.961	6.339	6.892
62 Sm	40.1181	39.5224	45.413	5.6361	5.6090	6.2051	6.586	7.178

Table 2-3. Energies of x-ray emission lines (continued).

Element	$K\alpha_1$	$K\alpha_2$	$K\beta_1$	$L\alpha_1$	$L\alpha_2$	$L\beta_1$	$L\beta_2$	$L\gamma_1$
63 Eu	41.5422	40.9019	47.0379	5.8457	5.8166	6.4564	6.8432	7.4803
64 Gd	42.9962	42.3089	48.691	6.0572	6.0250	6.7132	7.1028	7.7858
65 Tb	44.4816	43.7441	50.382	6.2728	6.2380	6.978	7.3667	8.102
66 Dy	45.9984	45.2078	52.119	6.4932	6.4577	7.2477	7.6357	8.4188
67 Ho	47.5467	46.6997	53.877	6.7198	6.6795	7.5253	7.911	8.747
68 Er	49.1277	48.2211	55.681	6.9487	6.9050	7.8109	8.1890	9.089
69 Tm	50.7416	49.7726	57.517	7.1799	7.1331	8.101	8.468	9.426
70 Yb	52.3889	51.3540	59.37	7.4156	7.3673	8.4018	8.7388	9.7801
71 Lu	54.0698	52.9650	61.283	7.6555	7.6049	8.7090	9.0489	10.1434
72 Hf	55.7902	54.6114	63.234	7.8990	7.8446	9.0227	9.3473	10.5158
73 Ta	57.532	56.277	65.223	8.1461	8.0879	9.3431	9.6518	10.8952
74 W	59.31824	57.9817	67.2443	8.3976	8.3352	9.67235	9.9615	11.2859
75 Re	61.1403	59.7179	69.310	8.6525	8.5862	10.0100	10.2752	11.6854
76 Os	63.0005	61.4867	71.413	8.9117	8.8410	10.3553	10.5985	12.0953
77 Ir	64.8956	63.2867	73.5608	9.1751	9.0995	10.7083	10.9203	12.5126
78 Pt	66.832	65.112	75.748	9.4423	9.3618	11.0707	11.2505	12.9420
79 Au	68.8037	66.9895	77.984	9.7133	9.6280	11.4423	11.5847	13.3817
80 Hg	70.819	68.895	80.253	9.9888	9.8976	11.8226	11.9241	13.8301
81 Tl	72.8715	70.8319	82.576	10.2685	10.1728	12.2133	12.2715	14.2915

82 Pb	74.9694	72.8042	84.936	10.5515	10.4495	12.6137	12.6226	14.7644
83 Bi	77.1079	74.8148	87.343	10.8388	10.73091	13.0235	12.9799	15.2477
84 Po	79.290	76.862	89.80	11.1308	11.0158	13.447	13.3404	15.744
85 At	81.52	78.95	92.30	11.4268	11.3048	13.876	—	16.251
86 Rn	83.78	81.07	94.87	11.7270	11.5979	14.316	—	16.770
87 Fr	86.10	83.23	97.47	12.0313	11.8950	14.770	14.45	17.303
88 Ra	88.47	85.43	100.13	12.3397	12.1962	15.2358	14.8414	17.849
89 Ac	90.884	87.67	102.85	12.6520	12.5008	15.713	—	18.408
90 Th	93.350	89.953	105.609	12.9687	12.8096	16.2022	15.6237	18.9825
91 Pa	95.868	92.287	108.427	13.2907	13.1222	16.702	16.024	19.568
92 U	98.439	94.665	111.300	13.6147	13.4388	17.2200	16.4283	20.1671
93 Np	—	—	—	13.9441	13.7597	17.7502	16.8400	20.7848
94 Pu	—	—	—	14.2786	14.0842	18.2937	17.2553	21.4173
95 Am	—	—	—	14.6172	14.4119	18.8520	17.6765	22.0652

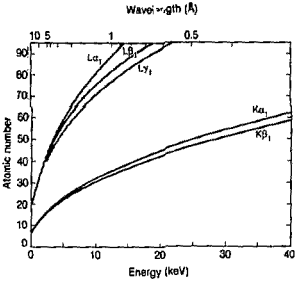

Fig. 2-1. Approximate energies and wavelengths of principal x-ray emission lines below 40 keV.

2.4 FLUORESCENCE YIELDS FOR K AND L SHELLS

Jeffrey B. Kortright

Fluorescence yields for the K and L shells for the elements $5 \leq Z \leq 110$ are plotted in Fig. 2-2; the data are based on Ref. 1. These yields represent the probability of a core hole in the K or L shells being filled by a radiative process, in com-

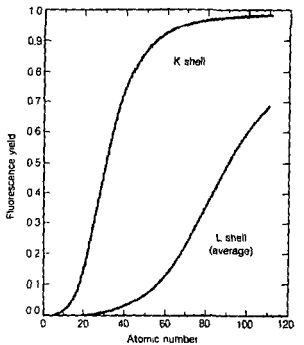

Fig. 2-2. Fluorescence yields for K and L shells for $5 \leq Z \leq 110$. The plotted curve for the L shell represents an average of L_1, L_2, and L_3 effective yields.

petition with nonradiative processes. Auger processes are the only nonradiative processes competing with fluorescence for the K shell and L_3 subshell holes. Auger and Coster-Kronig nonradiative processes complete with fluorescence to fill L_1 and L_2 subshell holes. Only one curve is presented for the three L subshells, repesenting the average of the L_1, L_2, and L_3 effective fluorescence yields in Ref. 1, which differ by less than about 10% over most of the periodic table. See Ref. 1 for more detail on the L subshell rates and the nonradiative rates, and for an appendix containing citations to the theoretical and experimental work upon which Fig. 2-2 is based. Widths of the K and L fluorescence lines can be found in Ref. 2.

REFERENCES

1. M. O. Krause, "Atomic Radiative and Radiationless Yields for K and L Shells," *J. Phys. Chem. Ref. Data* **8**, 307 (1979).
2. M. O. Krause and J. H. Oliver, "Natural Widths of Atomic K and L *J. Phys. Chem. Ref. Data* **8**, 329 (1979).

2.5 PRINCIPAL AUGER ELECTRON ENERGIES

Figure 2-3 has been reproduced by permission of the Physical Electronics Division of Perkin-Elmer, Inc. For each element, dots indicate the energies of principal Auger peaks, the predominant ones represented by the heavier dots. The families of Auger transitions are denoted by labels of the form *WXY*, where *W* is the shell in which the original vacancy occurs, *X* is the shell from which the *W* vacancy is filled, and *Y* is the shell from which the Auger electron is ejected.

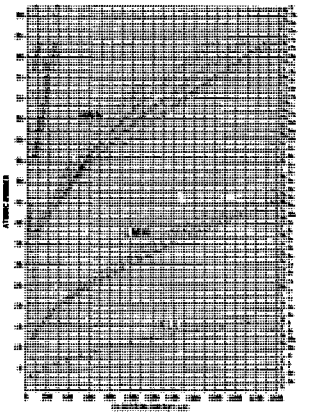

Fig. 7-3. Auger electron energies for the elements. (Reproduced by permission of the Physical Electronics Division of Perkin-Elmer, Inc.)

2.6 ENERGY LEVELS OF HYDROGEN-, HELIUM-, AND NEONLIKE IONS

James H. Scofield

Table 2-4 presents ionization energies for selected few-electron ions with $6 \leq Z \leq 54$. Table 2-5 gives the energies of the resonant $2p$ transitions in hydrogen- and heliumlike ions. Because of the interest in lasers based on neonlike ions in the soft x-ray region, selective transitions for the neonlike ions are presented in Table 2-6. This table includes the two lines for which lasing has been observed in selenium [1], the depopulating transition of the lower lasing level, and two strong lines in the spontaneous spectrum. In addition, Fig. 2-4 shows the $2p^5 3l$ levels for neonlike selenium. The level positions are labeled with a designation of the form $^{2S+1}L_J$ and a jj coupling label.

The energy values in this section have been generated using the relativistic Hartree-Fock code of I. P. Grant and collaborators [2] with a correction term of the form $A + BA(Z - Q)$ added to bring about agreement with the experimental values known for low atomic numbers. Nuclear size effects, radiative corrections, and the Breit interaction accounting for retardation and the magnetic electron-electron interaction are included in the calculations. The hydrogenic values are uncorrected as they come from the code, but to the accuracy given here, they agree with more detailed calculations. The $n = 3$ to $n = 2$ values given in Table 2-6 for the neonlike ions are also uncorrected and show differences at the 2-eV level with experimental values.

REFERENCES

1. D. L. Matthews et al., "Demonstration of a Soft X-Ray Amplifier," *Phys. Rev. Lett.* **54**, 110 (1985).
2. I. P. Grant, B. J. McKenzie, P. H. Norrington, D. F. Mayers, and N. C. Pyper, "An Atomic Multiconfigurational Dirac-Fock Package," *Comput. Phys. Commun.* **21**, 207 (1980).

Table 2-4. *Ionization energies, in electron volts, for selected few-electron ionic species. Each column is labeled with the number of electrons in the ion before ionization and with the symbol for the neutral atom with the same number of electrons.*

Element	1 (H)	2 (He)	3 (Li)	4 (Be)	10 (Ne)	11 (Na)	12 (Mg)
6 C	490.0	392.1	64.49	47.89			
7 N	667.1	552.1	97.89	77.48			
8 O	871.4	739.3	138.11	113.90			
9 F	1103.1	953.9	185.18	157.15			
10 Ne	1362.2	1195.8	239.09	207.28	*21.564*		
11 Na	1648.7	1465.1	299.86	264.21	47.286	5.139	
12 Mg	1962.7	1761.8	367.5	328.0	80.143	15.035	7.646
13 Al	2304.3	2086.0	442.0	398.7	119.99	28.447	18.828
14 Si	2673.2	2437.7	523.4	476.3	166.42	45.12	33.64
15 P	3070	2816.9	611.7	560.8	220.31	65.02	51.50
16 S	3494	3224	707.0	652.1	281.00	88.05	72.39
17 Cl	3946	3658	809.2	750.5	348.5	114.20	96.84
18 Ar	4426	4121	918.4	855.8	422.8	143.46	124.24
19 K	4934	4611	1034.6	968.0	503.9	175.82	154.75
20 Ca	5470	5129	1157.7	1087.3	591.9	211.28	188.38
21 Sc	6034	5675	1288.0	1213.6	686.6	249.84	225.13
22 Ti	6626	6249	1425.3	1346.9	788.2	291.50	264.98
23 V	7246	6851	1569.7	1487.3	896.6	336.3	307.9
24 Cr	7895	7482	1721.2	1634.8	1011.8	384.2	354.0
25 Mn	8572	8141	1879.9	1789.5	1133.8	435.2	403.2
26 Fe	9278	8828	2045.8	1951.3	1262.7	489.3	455.6
27 Co	10012	9544	2218.9	2120.4	1398.3	546.6	511.0
28 Ni	10775	10289	2399.3	2296.7	1540.8	607.0	569.7
29 Cu	11461	10969	2559.1	2455.1	1690.2	670.6	631.4
30 Zn	12389	11865	2782.0	2671.1	1846.4	737.3	696.4
31 Ga	13239	12696	2984.4	2869.4	2009.4	807.3	764.5
32 Ge	14119	13557	3194	3075	2179.3	880.4	835.8
33 As	15029	14448	3412	3288	2356.0	956.8	910.3
34 Se	15968	15367	3637	3509	2539.6	1036.3	988.1
35 Br	16937	16317	3869	3737	2730.1	1119.1	1069.1
36 Kr	17936	17296	4109	3973	2927.4	1205.2	1153.3
37 Rb	18965	18306	4357	4216	3132	1294.5	1240.8
38 Sr	20025	19345	4612	4467	3343	1387.2	1331.5
39 Y	21115	20415	4876	4726	3561	1483.1	1426.6
40 Zr	22237	21516	5147	4993	3786	1582.4	1523.0
41 Nb	23389	22648	5426	5268	4017	1684.9	1623.7
42 Mo	24572	23810	5713	5550	4256	1790.9	1727.8
43 Tc	25787	25004	6008	5841	4502	1900.3	1835.2
44 Ru	27033	26230	6312	6140	4754	2013.0	1946.1
45 Rh	28312	27487	6623	6447	5014	2129.2	2060.3
46 Pd	29623	28776	6943	6762	5282	2248.9	2178.0
47 Ag	30966	30097	7271	7086	5553	2372.0	2299.2
48 Cd	32341	31451	7608	7418	5834	2498.6	2423.9
49 In	33750	32837	7953	7758	6121	2628.8	2552.1
50 Sn	35192	34257	8307	8107	6415	2762.5	2683.0
51 Sb	36668	35710	8670	8463	6717	2899.8	2819.2
52 Te	38177	37196	9041	8832	7025	3041	2958.1
53 I	39721	38718	9421	9207	7340	3185	3101
54 Xe	41300	40271	9810	9591	7663	3334	3247

Table 2-3. *Transition energies, in electron volts, for transitions from the n = 2 states to the n = 1 ground state of H- and He-like ions.*

	Hydrogenlike		Heliumlike	
Element	$2p_{1/2}$	$2p_{3/2}$	$2s\,^3P_1$	$2p\,^3P_2$
5 B	255.17	255.20	202.78	205.57
6 C	367.5	367.5	304.3	307.8
7 N	500.3	500.4	426.3	430.7
8 O	653.5	653.7	568.7	574.0
9 F	827.3	827.6	731.5	737.9
10 Ne	1021.5	1022.0	914.9	922.1
11 Na	1236.3	1237.0	1118.8	1126.9
12 Mg	1471.7	1472.7	1343.2	1352.3
13 Al	1727.7	1729.0	1588.3	1598.4
14 Si	2004.3	2006.1	1853.9	1865.1
15 P	2301.7	2304.0	2140.3	2152.6
16 S	2619.7	2622.7	2447.3	2460.8
17 Cl	2958.5	2962.4	2775.1	2789.8
18 Ar	3318	3323	3124	3140
19 K	3699	3705	3493	3511
20 Ca	4100	4108	3883	3903
21 Sc	4523	4532	4295	4316
22 Ti	4966	4977	4727	4750
23 V	5431	5444	5180	5205
24 Cr	5917	5932	5653	5682
25 Mn	6424	6442	6151	6181
26 Fe	6952	6973	6668	6701
27 Co	7502	7526	7206	7242
28 Ni	8073	8102	7766	7806
29 Cu	8593	8599	8280	8307
30 Zn	9281	9318	8950	8999
31 Ga	9917	9960	9578	9628
32 Ge	10575	10624	10221	10280
33 As	11255	11311	10889	10955
34 Se	11958	12021	11579	11652
35 Br	12682	12753	12292	12372
36 Kr	13429	13509	13026	13114
37 Rb	14199	14288	13783	13880
38 Sr	14990	15090	14562	14669
39 Y	15803	15916	15364	15482
40 Zr	16643	16765	16189	16318
41 Nb	17503	17639	17036	17178
42 Mo	18387	18537	17903	18063
43 Tc	19294	19459	18800	18971
44 Ru	20224	20406	19717	19904
45 Rh	21178	21377	20658	20861
46 Pd	22156	22374	21622	21843
47 Ag	23157	23396	22609	22851
48 Cd	24183	24444	23621	23884
49 In	25232	25518	24657	24942
50 Sn	26308	26617	25717	26027

Table 2-6. Transition energies, in electron volts, for selected transitions in Ne-like ions with 2p vacancies. The transitions for which lasing has been observed are indicated in boldface type.

Element	$3s-2p$ $^3P_1-^1S_0$	$3s-2p$ $^1P_1-^1S_0$	$3d-2p$ $^3D_1-^1S_0$	$3p-3s$ $^3P_2-^3P_1$	$3p-3s$ $^1D_2-^1P_1$	$3d-3p$ $^3P_2-^3D_3$
14 Si	103.06	104.07	126.41	9.849	10.393	12.809
15 P	134.41	135.66	162.77	11.776	12.403	15.365
16 S	169.52	171.06	202.83	13.736	14.416	18.279
17 Cl	208.39	210.28	246.68	15.728	16.435	20.969
18 Ar	251.02	253.35	294.27	17.754	18.474	23.650
19 K	297.38	300.3	345.6	19.814	20.540	26.333
20 Ca	347.5	351.1	400.8	21.915	22.641	29.031
21 Sc	401.3	405.7	459.8	24.058	24.786	31.75
22 Ti	458.8	464.3	522.5	26.251	26.981	34.51
23 V	520.1	526.8	589.1	28.497	29.235	37.31
24 Cr	585.1	593.3	659.5	30.81	31.53	40.15
25 Mn	653.7	663.7	733.8	33.19	33.94	43.06
26 Fe	726.1	738.0	811.8	35.64	36.42	46.03
27 Co	802.2	816.4	893.6	38.19	38.97	49.08
28 Ni	881.9	898.7	979.3	40.82	41.63	52.21
29 Cu	965.3	985.1	1068.8	43.56	44.39	55.43
30 Zn	1052.4	1075.6	1162.1	46.41	47.27	58.76
31 Ga	1143.1	1170.1	1259.2	49.39	50.26	62.20
32 Ge	1237.5	1268.7	1360.3	52.50	53.39	65.76
33 As	1335.5	1371.5	1464.9	55.75	56.67	69.45
34 Se	1437.2	1478.4	1573.4	59.15	60.10	73.29
35 Br	1542.4	1589.5	1685.8	62.72	63.70	77.28
36 Kr	1651.3	1704.8	1802.0	66.47	67.48	81.43
37 Rb	1763.8	1824.4	1899.3	70.41	71.45	85.77
38 Sr	1879.9	1948.2	2021.9	74.56	75.62	90.30
39 Y	1999.6	2076.4	2148.2	78.92	80.01	95.03
40 Zr	2122.8	2208.9	2278.4	83.52	84.64	99.99
41 Nb	2249.5	2345.8	2412.4	88.37	89.51	105.17
42 Mo	2379.9	2487.1	2550.2	93.48	94.65	110.61
43 Tc	2513.7	2632.9	2691.8	98.87	100.06	116.31
44 Ru	2651.1	2783.2	2837.3	104.56	105.77	122.29
45 Rh	2791.9	2938.0	2988.6	110.57	111.80	128.57
46 Pd	2936.3	3097	3140	116.92	118.15	135.17
47 Ag	3084	3262	3297	123.62	124.86	142.10
48 Cd	3235	3430	3457	130.72	131.93	149.38
49 In	3390	3604	3617	138.24	139.39	157.04
50 Sn	3548	3782	3791	146.32	147.27	165.09

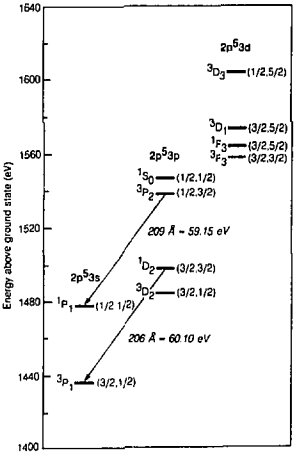

Fig. 2-4. Selected excited energy levels for Ne-like selenium (Z = 34). $1s^2 2s^2 2p^5 3l$; 10 of the 36 levels in this manifold are shown. Transitions for which lasing has been observed are indicated.

2.7 SCATTERING FACTORS AND MASS ABSORPTION COEFFICIENTS

Burton L. Henke

At photon energies between 100 eV and 10 keV, accurate calculations for absorption and scattering in material systems (e.g., filters, mirrors, multilayers, and crystals) can be based on atomic scattering factors $(f_1 + if_2)$ for the constituent atoms. These factors are derived from available experimental photoabsorption data, using the Kramers-Kronig dispersion relations [1,2]:

$$f_1 = Z + C \int_0^\infty \frac{\epsilon^2 \mu_a(\epsilon) d\epsilon}{E^2 - \epsilon^2} \tag{1}$$

and

$$f_2 = \frac{\pi}{2} CE \mu_a(E) , \tag{2}$$

where Z is the total number of electrons; C is a constant equal to $1/\pi r_0 hc$ with r_0 the classical electron radius, h Planck's constant, and c the velocity of light; $\mu_a(\epsilon)$ is the atomic photoabsorption cross section; and E is the incident photon energy. The atomic photoabsorption cross section (in cm^2/atom) is related to the mass absorption coefficient μ (in cm^2/g) by

$$\mu_a = (A/N_A)\mu , \tag{3}$$

where A is the atomic weight and N_A is Avogadro's number.

One may also obtain the complex dielectric constant

$$\epsilon = 1 - \alpha - i\gamma \tag{4}$$

and the index of refraction

$$n = 1 - \delta - i\beta \tag{5}$$

from the scattering factors by using the relations

$$\delta = \frac{\alpha}{2} = Kf_1 \tag{6}$$

and

$$\beta = \frac{\gamma}{2} = Kf_2 , \tag{7}$$

where

$$K = \frac{r_0 \lambda^2}{2\pi} \frac{N_A}{A} \rho \qquad (8)$$

and ρ is the density. The parameters β and δ are called the absorption index and refractive index decrement, respectively.

Figures 2-5 and 2-6 illustrate the variation with atomic number of the mass absorption coefficient for several selected energies, indicating the presence of absorption edges. Near these edges, one expects additional absorption structure, reflecting the molecular and solid states of complex systems. This structure cannot be predicted by calculations that assume atomlike behavior of the system components. Tables 2-7 and 2-8 are a more comprehensive tabulation of the values of the mass absorption coefficient.

Tables 2-9 through 2-12 tabulate the two components of the atomic scattering factor for selected energies and atomic numbers. Values in the tables are recorded in the form 1.42(−)02 to denote the value $1.42 \times 10^{(-)2}$

REFERENCES

1. B. L. Henke, "Low Energy X-Ray Interactions: Photoionization, Scattering, Specular and Bragg Reflection," in D. T. Attwood and B. L. Henke, Eds., *AIP Conference Proceeding No. 75: Low Energy X-Ray Diagnostics* (American Institute of Physics, New York, 1981), p. 146.
2. B. L. Henke, P. Lee, T. J. Tanaka, R. L. Shimabukuro, and B. K. Fujikawa, "Low-Energy X-Ray Interaction Coefficients: Photoabsorption, Scattering, and Reflection," *At. Data Nucl. Data Tables* 27, 1 (1982).

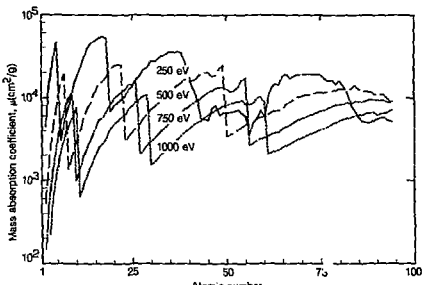

Fig. 2-5. Mass absorption coefficients at energies between 250 and 1000 eV, as functions of atomic number.

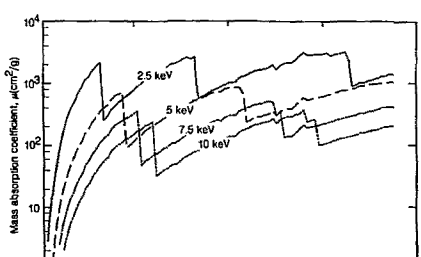

Fig. 2-6. Mass absorption coefficients at energies between 2.5 and 10 keV, as functions of atomic number.

Table 2-7. Mass absorption coefficients for selected values of atomic number Z at energies between 100 and 1000 eV.

	Energy (eV)									
Z	100	200	300	400	500	600	700	800	900	1000
3	1.42 05	2.47 04	7.98 03	3.71 03	1.81 03	1.09 03	6.49 02	4.47 02	3.08 02	2.28 02
6	2.33 04	5.14 03	4.83 04	2.49 04	1.37 04	8.89 03	5.74 03	4.13 03	2.96 03	2.27 03
9	*8.73 04*	*1.88 04*	*7.03 03*	*3.61 03*	*1.97 03*	*1.28 03*	*1.28 04*	*9.91 03*	*7.31 03*	*5.79 03*
12	1.30 05	4.90 04	2.00 04	1.07 04	5.75 03	3.69 03	2.35 03	1.68 03	1.21 03	9.29 02
15	1.02 04	6.90 04	3.45 04	2.02 04	1.16 04	7.65 03	4.97 03	3.62 03	2.61 03	2.02 03
18	1.92 04	8.06 03	4.07 04	2.90 04	1.76 04	1.21 04	8.10 03	6.00 03	4.39 03	3.42 03
21	2.69 04	1.24 04	6.35 03	3.92 03	2.53 04	1.78 04	1.21 04	9.08 03	6.75 03	5.32 03
24	4.58 04	1.79 04	9.00 03	5.53 03	3.41 03	2.39 03	1.66 04	1.26 04	9.50 03	7.56 03
27	6.13 04	2.68 04	1.32 04	7.87 03	4.80 03	3.37 03	2.36 03	1.46 04	1.11 04	9.91 03
30	*7.87 04*	*3.91 04*	*2.00 04*	*1.19 04*	*7.18 03*	*4.93 03*	*3.40 03*	*2.61 03*	*1.96 03*	*1.58 03*
33	4.44 04	4.15 04	2.40 04	1.54 04	9.55 03	6.71 03	4.65 03	3.56 03	2.69 03	2.15 03
36	9.18 03	3.97 04	2.94 04	2.04 04	1.29 04	9.15 03	6.37 03	4.88 03	3.71 03	2.97 03
39	1.30 04	2.15 04	2.92 04	2.50 04	1.63 04	1.18 04	8.32 03	6.42 03	4.91 03	3.95 03
42	8.81 03	5.35 03	2.05 04	2.00 04	1.69 04	1.35 04	1.01 04	8.15 03	6.26 03	5.06 03

K

L_{III}

45	5.41 03	6.66 03	4.26 03	1.93 04	2.02 04	1.68 04	1.29 04	1.01 04	7.78 03	6.31 03
48	4.34 04	6.64 03	5.32 03	4.11 03	2.18 04	1.66 04	1.42 04	1.20 04	9.30 03	7.59 03
51	7.52 04	7.08 03	6.15 03	4.97 03	3.61 03	1.98 04	1.34 04	1.11 04	1.01 04	8.68 03
54	1.23 05	4.61 03	6.75 03	5.69 03	4.42 03	3.48 03	2.24 04	1.25 04	9.55 03	9.38 03
57	2.89 04	3.55 03	6.68 03	6.30 03	4.91 03	3.95 03	3.08 03	2.53 03	1.09 04	8.81 03
60	1.43 04	9.95 03	7.96 03	7.96 03	5.98 03	4.74 03	3.67 03	3.00 03	2.42 03	8.97 03
63	1.73 04	2.30 04	1.13 04	9.48 03	6.99 03	5.48 03	4.21 03	3.45 03	2.78 03	2.33 03
66	3.25 04	2.57 04	1.67 04	1.17 04	8.35 03	6.49 03	4.94 03	4.01 03	3.22 03	2.69 03
69	2.88 04	2.24 04	1.55 04	1.24 04	1.00 04	7.85 03	5.97 03	4.81 03	3.84 03	3.21 03
72	2.10 04	2.12 04	1.65 04	1.28 04	1.06 04	8.86 03	6.76 03	5.46 03	4.38 03	3.66 03
75	1.62 04	1.87 04	1.74 04	1.40 04	1.15 04	9.67 03	7.69 03	6.25 03	5.03 03	4.21 03
78	1.92 04	1.60 04	1.58 04	1.51 04	1.18 04	1.06 04	8.38 03	7.23 03	5.85 03	4.88 03
81	2.31 04	9.62 03	1.50 04	1.49 04	1.26 04	1.05 04	9.29 03	7.79 03	6.63 03	5.64 03
84	4.97 04	6.09 03	1.20 04	1.41 04	1.40 04	1.15 04	9.25 03	8.57 03	7.04 03	6.20 03
87	6.56 04	8.54 03	5.60 03	1.14 04	1.20 04	1.12 04	1.01 04	8.41 03	7.43 03	6.58 03
90	1.30 05	6.15 03	6.99 03	8.84 03	1.07 04	1.03 04	9.95 03	8.63 03	7.21 03	6.16 03

M_V

Table 2-8. Mass absorption coefficients for selected values of atomic number Z as energies between 1 and 10 keV.

Z	Energy (eV) 1000	2000	3000	4000	5000	6000	7000	8000	9000	10000
3	2.28 02	2.50 01	6.54 00	2.49 00	1.18 00	6.46-01	3.88-01	2.49-01	1.69-01	1.19-01
6	2.27 03	3.02 02	9.04 01	3.77 01	1.89 01	1.06 01	6.53 00	4.26 00	2.91 00	2.06 00
9	5.79 03	9.00 02	2.88 02	1.25 02	6.44 01	3.72 01	2.32 01	1.54 01	1.07 01	7.70 00
12	9.29 02	2.03 03	6.75 02	3.00 02	1.58 02	9.26 01	5.88 01	3.96 01	2.79 01	2.04 01
15	2.02 03	3.03 02	1.15 03	5.31 02	2.86 02	1.71 02	1.10 02	7.49 01	5.32 01	3.91 01
18	3.42 03	5.32 02	1.76 02	7.95 02	4.40 02	2.67 02	1.74 02	1.20 02	8.59 01	6.37 01
21	5.32 03	8.84 02	3.00 02	1.36 02	6.57 02	4.12 02	2.74 02	1.90 02	1.37 02	1.02 02
24	7.56 03	1.26 03	4.16 02	1.88 02	1.02 02	5.17 02	3.52 02	2.49 02	1.82 02	1.37 02
27	9.91 03	1.76 03	5.93 02	2.69 02	1.46 02	8.83 01	5.80 01	3.20 02	2.38 02	1.81 02
30	1.58 03	2.39 03	8.28 02	3.83 02	2.09 02	1.27 02	8.30 01	5.71 01	4.09 01	2.37 02
33	2.15 03	3.02 03	1.08 03	5.00 02	2.73 02	1.66 02	1.09 02	7.52 01	5.43 01	4.04 01
36	2.97 03	3.55 03	1.30 03	6.05 02	3.30 02	2.00 02	1.31 02	9.04 01	6.53 01	4.88 01
39	3.95 03	7.42 02	1.61 03	8.00 02	4.41 02	2.69 02	1.77 02	1.22 02	8.85 01	6.64 01
42	5.06 03	9.59 02	2.00 03	9.73 02	5.42 02	3.33 02	2.19 02	1.52 02	1.10 02	8.25 01

45	6.31 03	1.22 03	4.31 02	1.17 03	6.61 02	4.08 02	2.70 02	1.88 02	1.36 02	1.02 02
48	7.59 03	1.51 03	5.10 02	1.05 03	6.96 02	4.33 02	2.87 02	2.01 02	1.46 02	1.09 02
51	8.68 03	1.75 03	6.44 02	3.00 02	8.42 02	5.28 02	3.53 02	2.47 02	1.80 02	1.35 02
54	9.38 03	2.13 03	8.08 02	3.89 02	6.69 02	6.59 02	4.43 02	3.12 02	2.28 02	1.72 02
57	8.81 03	2.55 03	9.93 02	4.86 02	2.67 02	6.81 02	5.26 02	3.73 02	2.74 02	2.07 02
60	8.97 03	2.92 03	1.09 03	5.38 02	3.07 02	1.93 02	5.10 02	4.17 02	3.10 02	2.36 02
63	2.33 03	2.76 03	1.04 03	5.11 02	2.93 02	1.85 02	3.59 02	3.38 02	2.88 02	2.20 02
66	2.69 03	3.47 03	1.38 03	6.75 02	3.85 02	2.43 02	1.64 02	3.25 02	3.23 02	2.85 02
69	3.21 03	4.06 03	1.79 03	8.85 02	5.08 02	3.21 02	2.16 02	1.53 02	3.09 02	3.19 02
72	3.66 03	3.89 03	1.89 03	9.35 02	5.41 02	3.44 02	2.33 02	1.65 02	1.21 02	2.47 02
75	4.21 03	4.32 03	2.11 03	1.05 03	6.04 02	3.81 02	2.57 02	1.82 02	1.35 02	1.02 02
78	4.88 03	1.16 03	2.14 03	1.19 03	6.84 02	4.32 02	2.92 02	2.07 02	1.53 02	1.17 02
81	5.44 03	1.33 03	2.37 03	1.31 03	7.61 02	4.82 02	3.25 02	2.31 02	1.71 02	1.30 02
84	6.20 03	1.53 03	2.28 03	1.39 03	8.39 02	5.34 02	3.62 02	2.58 02	1.91 02	1.46 02
87	6.58 03	1.73 03	7.05 02	1.47 03	9.37 02	5.96 02	4.04 02	2.88 02	2.13 02	1.63 02
90	6.16 03	1.92 03	7.86 02	1.38 03	9.82 02	6.55 02	4.45 02	3.17 02	2.34 02	1.79 02

L_{III}

M_V

2.35

Table 2-9. Values for component f_1 of the atomic scattering factor, for selected values of atomic number Z at energies between 100 and 1000 eV.

Z	Energy (eV) 100	200	300	400	500	600	700	800	900	1000	
3	2.75 00	3.33 00	3.26 00	3.20 00	3.15 00	3.12 00	3.10 00	3.08 00	3.07 00	3.06 00	
6	4.08 00	3.67 00	2.88 00	5.50 00	6.10 00	6.28 00	6.35 00	6.37 00	6.36 00	6.34 00	
9	6.71 00	7.63 00	7.54 00	7.33 00	6.95 00	6.30 00	5.01 00	7.50 00	8.35 00	8.75 00	
12	3.73 00	5.02 01	5.10 01	5.11 01	5.10 01	5.09 01	5.07 01	5.06 01	5.04 01	5.02 01	K
15	2.93 00	7.00 00	1.22 01	1.38 01	1.43 01	1.44 01	1.44 01	1.43 01	1.42 01	1.41 01	
18	6.21 00	4.67 00	7.64 00	1.28 01	1.57 01	1.68 01	1.73 01	1.76 01	1.77 01	1.77 01	
21	8.50 00	9.92 00	8.86 00		1.24 01	1.69 01	1.90 01	1.98 01	2.03 01	2.06 01	
24	1.06 01	1.35 01	1.42 01	1.37 01	1.17 01		1.56 01	1.92 01	2.12 01	2.23 01	
27	9.54 00	1.52 01	1.71 01	1.74 01	1.70 01	1.60 01	1.29 01	7.92 00	1.70 01	2.10 01	
30	5.99 00	1.54 01	1.94 01	2.07 01	2.12 01	2.10 01	2.04 01	1.95 01	1.74 01	1.00 01	L_{III}
33	2.69 00	1.27 01	1.98 01	2.24 01	2.40 01	2.45 01	2.46 01	2.44 01	2.40 01	2.33 01	
36	4.08 00	8.13 00	1.78 01	2.31 01	2.63 01	2.77 01	2.85 01	2.87 01	2.88 01	2.86 01	
39	9.86 00	5.94 00	1.30 01	1.92 01	2.66 01	2.92 01	3.08 01	3.16 01	3.21 01	3.23 01	
42	1.54 01	1.20 01	9.54 00	1.68 01	2.19 01	2.76 01	3.07 01	3.29 01	3.42 01	3.50 01	

45	1.85 01	1.41 01	9.66 00	4.28 00	1.81 01	2.52 01	3.17 01	3.46 01	3.66 01	3.77 01
48	2.11 01	1.64 01	1.44 01	7.60 00	1.55 01	2.29 01	2.92 01	3.47 01	3.82 01	4.02 01
51	2.53 01	1.81 0	1.71 01	1.50 01	1.38 00	1.92 01	2.91 01	3.00 01	3.57 01	3.87 01
54	9.48 00	2.05 01	1.86 01	1.88 01	1.69 01	1.04 01	1.56 01	3.04 01	3.25 01	3.43 01
57	6.84 00	2.53 01	2.20 01	2.36 01	2.45 01	2.41 01	2.11 01	1.16 01	2.21 01	3.05 01
60	1.44 01	3.02 01	2.37 01	2.74 01	2.93 01	3.00 01	2.96 01	2.80 01	2.30 01	1.12 01
63	1.44 01	3.21 01	3.11 01	3.30 01	3.54 01	3.65 01	3.68 01	3.65 01	3.49 01	3.17 01
66	1.18 01	2.47 01	2.66 01	3.33 01	3.55 01	3.68 01	3.78 01	3.80 01	3.76 01	3.65 01
69	1.25 01	1.91 01	2.46 01	2.78 01	3.27 01	3.62 01	3.83 01	3.93 01	3.97 01	3.95 01
72	1.06 01	1.53 01	2.32 01	2.74 01	3.29 01	3.72 01	4.05 01	4.21 01	4.32 01	4.36 01
75	1.55 01	1.46 01	2.29 01	2.90 01	3.35 01	3.85 01	4.37 01	4.62 01	4.80 01	4.91 01
78	1.77 01	1.22 01	1.75 01	2.43 01	3.13 01	3.65 01	4.16 01	4.53 01	4.82 01	4.99 01
81	2.12 01	1.26 01	1.51 01	2.02 01	2.99 01	3.56 01	4.06 01	4.44 01	4.89 01	5.15 01
84	2.47 01	2.01 01	1.11 01	1.80 01	2.76 01	3.57 01	4.03 01	4.54 01	4.99 01	5.24 01
87	1.62 01	2.83 01	1.68 01	1.23 01	2.22 01	2.75 01	3.87 01	4.38 01	4.64 01	5.17 01
90		2.67 01	1.83 01	1.83 01	2.01 01	2.95 01	3.56 01	4.30 01	4.83 01	5.03 01

M_V

Table 2-1B. *Values for component f_1 of the atomic scattering factor for selected values of atomic number Z at energies between 1 and 10 keV.*

Z	Energy (eV) 1000	2000	3000	4000	5000	6000	7000	8000	9000	10000
3	3.06 00	3.02 00	3.01 00	3.01 00	3.00 00	3.00 00	3.00 00	3.00 00	3.00 00	3.00 00
6	6.34 00	6.17 00	6.10 00	6.06 00	6.05 00	6.03 00	6.03 00	6.02 00	6.02 00	6.01 00
9	8.75 00	9.38 00	9.28 00	9.21 00	9.16 00	9.12 00	9.10 00	9.08 00	9.07 00	9.06 00
12	1.02 01	1.21 01	1.24 01	1.24 01	1.23 01	1.23 01	1.22 01	1.22 01	1.22 01	1.21 01
15	1.41 01	1.21 01	1.49 01	1.54 01	1.54 01	1.54 01	1.54 01	1.53 01	1.53 01	1.53 01
18	1.77 01	1.69 01	1.52 01	1.75 01	1.82 01	1.84 01	1.84 01	1.84 01	1.84 01	1.84 01
21	2.06 01	2.05 01	1.99 01	1.89 01	1.96 01	2.08 01	2.12 01	2.14 01	2.14 01	2.15 01
24	2.23 01	2.40 01	2.35 01	2.31 01	2.24 01	1.80 01	2.32 01	2.39 01	2.42 01	2.43 01
27	2.10 01	2.71 01	2.70 01	2.66 01	2.62 01	2.58 01	2.50 01	2.45 01	2.62 01	2.68 01
30	1.00 01	2.97 01	3.02 01	2.99 01	2.96 01	2.93 01	2.90 01	2.86 01	2.78 01	2.75 01
33	2.33 01	3.11 01	3.32 01	3.32 01	3.30 01	3.27 01	3.25 01	3.22 01	3.19 01	3.15 01
36	2.86 01	2.92 01	3.58 01	3.64 01	3.63 01	3.61 01	3.59 01	3.57 01	3.55 01	3.52 01
39	3.23 01	2.48 01	3.71 01	3.91 01	3.94 01	3.93 01	3.92 01	3.90 01	3.88 01	3.86 01
42	3.50 01	3.42 01	3.61 01	4.13 01	4.23 01	4.25 01	4.24 01	4.23 01	4.21 01	4.20 01

K

45	3.77 01	3.90 01	2.44 01	4.24 01	4.48 01	4.54 01	4.55 01	4.55 01	4.54 01	4.53 01
48	4.02 01	4.39 01	4.19 01	4.04 01	4.68 01	4.81 01	4.85 01	4.86 01	4.86 01	4.85 01
51	3.87 01	4.70 01	4.60 01	4.08 01	4.69 01	5.02 01	5.12 01	5.16 01	5.17 01	5.17 01
54	3.43 01	4.93 01	4.94 01	4.75 01	4.31 01	5.08 01	5.33 01	5.42 01	5.46 01	5.48 01
57	3.05 01	5.07 01	5.26 01	5.19 01	4.91 01	4.79 01	5.42 01	5.63 01	5.72 01	5.76 01
60	3.12 01	5.33 01	5.62 01	5.58 01	5.45 01	5.03 01	5.29 01	5.76 01	5.93 01	6.02 01
63	3.17 01	5.72 01	6.04 01	6.03 01	5.96 01	5.82 01	5.11 01	5.74 01	6.12 01	6.25 01
66	3.65 01	5.39 01	6.25 01	6.32 01	6.28 01	6.18 01	5.99 01	5.71 01	5.96 01	6.39 01
69	3.95 01	5.08 01	6.39 01	6.59 01	6.59 01	6.52 01	6.40 01	6.17 01	6.02 01	6.25 01
72	4.36 01	4.64 01	6.58 01	6.90 01	6.94 01	6.91 01	6.84 01	6.72 01	6.48 01	6.43 01
75	4.91 01	3.28 01	6.56 01	7.17 01	7.28 01	7.28 01	7.23 01	7.15 01	7.03 01	6.79 01
78	4.99 01	4.14 01	6.41 01	7.37 01	7.58 01	7.61 01	7.59 01	7.53 01	7.46 01	7.34 01
81	5.15 01	5.34 01	6.11 01	7.45 01	7.83 01	7.92 01	7.93 01	7.89 01	7.84 01	7.76 01
84	5.24 01	6.01 01	5.91 01	7.44 01	8.03 01	8.20 01	8.24 01	8.23 01	8.20 01	8.14 01
87	5.17 01	6.40 01	1.31 01	7.39 01	8.14 01	8.44 01	8.53 01	8.55 01	8.53 01	8.50 01
90	5.03 01	6.77 01	6.29 01	6.93 01	8.13 01	8.63 01	8.80 01	8.86 01	8.87 01	8.85 01

L_{III}

M_V

Table 2-11. Values for component f_2 of the atomic scattering factor, for selected values of atomic number Z, at energies between 100 and 1000 eV.

Z	Energy (eV) 100	200	300	400	500	600	700	800	900	1000
3	2.34 00	8.18-01	3.99-01	2.42-01	1.51-01	1.07-01	7.58-02	5.89-02	4.58-02	3.74-02
6	6.66-01	2.95-01	4.18 00	2.82 00	1.97 00	1.52 00	1.16 00	9.40-01	7.61-01	6.42-01
9	3.95 00	1.71 00	9.62-01	6.46-01	4.48-01	3.44-01	4.09 00	3.57 00	2.98 00	2.59 00
12	7.54 00	5.69 00	3.50 00	2.45 00	1.68 00	1.27 00	9.58-01	7.77-01	6.29-01	5.33-01
15	7.51-01	1.02 01	7.70 00	5.88 00	4.30 00	3.37 00	2.59 00	2.13 00	1.73 00	1.48 00
18	1.82 00	1.54 00	1.17 01	1.09 01	8.44 00	6.84 00	5.44 00	4.55 00	3.75 00	3.22 00
21	2.88 00	2.67 00	2.06 00	1.66 00	1.36 01	1.13 01	9.16 00	7.75 00	6.50 00	5.64 00
24	5.66 00	4.46 00	3.37 00	2.71 00	2.13 00	1.76 00	1.45 01	1.24 01	1.06 01	9.27 00
27	9.39 00	7.55 00	5.60 00	4.37 00	3.39 00	2.82 00	2.33 00	1.63 01	1.40 01	1.38 01
30	1.22 01	1.22 01	9.41 00	7.35 00	5.63 00	4.58 00	3.74 00	3.24 00	2.74 00	2.44 00
33	7.92 00	1.49 01	1.30 01	1.08 01	8.58 00	7.13 00	5.86 00	5.05 00	4.32 00	3.80 00
36	1.83 00	1.59 01	1.78 01	1.61 01	1.29 01	1.09 01	8.98 00	7.75 00	6.65 00	5.87 00
39	2.75 00	9.12 00	1.87 01	2.09 01	1.74 01	1.48 01	1.24 01	1.08 01	9.35 00	8.28 00
42	2.01 00	2.45 00	1.42 01	1.80 01	1.94 01	1.83 01	1.63 01	1.48 01	1.29 01	1.15 01

K

L_{III}

45	1.32 00	3.27 00	3.16 00	1.87 01	2.49 01	2.46 01	2.23 01	1.96 01	1.71 01	1.53 01	
48	1.16 0-	3.57 00	4.30 00	4.35 00	2.93 01	2.65 01	2.69 01	2.56 01	2.24 01	2.01 01	
51	2.18 01	4.12 00	5.39 00	5.69 00	5.27 00	3.42 01	2.74 01	2.57 01	2.64 01	2.49 01	
54	3.85 01	2.90 00	6.38 00	7.03 00	6.96 00	6.48 00	4.95 01	3.12 01	2.69 01	2.91 01	
57	9.53 00	2.35 00	6.69 00	8.23 00	8.18 00	7.78 00	7.19 00	6.67 00	3.24 01	2.89 01	
60	4.92 00	6.86 00	8.28 00	1.08 01	1.03 01	9.71 00	8.90 00	8.20 00	7.49 00	3.05 01	
63	6.27 00	1.67 01	1.24 01	1.36 01	1.27 01	1.18 01	1.08 01	9.94 00	9.06 00	8.37 00	M_y
66	1.26 01	1.99 01	1.95 01	1.79 01	1.63 01	1.50 01	1.35 01	1.24 01	1.12 01	1.03 01	
69	1.16 01	1.81 01	1.89 01	1.98 01	2.03 01	1.88 01	1.69 01	1.54 01	1.39 01	1.28 01	
72	8.93 00	1.81 01	2.13 01	2.15 01	2.28 01	2.25 01	2.03 01	1.85 01	1.68 01	1.54 01	
75	7.16 00	1.66 01	2.33 01	2.45 01	2.57 01	2.56 01	2.41 01	2.21 01	2.01 01	1.85 01	
78	8.93 00	1.49 01	2.22 01	2.78 01	2.77 01	2.93 01	2.75 01	2.68 01	2.44 01	2.25 01	
81	1.12 01	9.40 00	2.21 01	2.87 01	3.09 01	3.03 01	3.19 01	3.02 01	2.90 01	2.72 01	
84	2.48 01	6.11 00	1.81 01	2.78 01	3.53 01	3.44 01	3.26 01	3.42 01	3.17 01	3.07 01	
87	3.48 01	9.10 00	9.00 00	2.39 01	3.20 01	3.54 01	3.77 01	3.56 01	3.55 01	3.46 01	
90	7.19 01	6.82 00	1.17 01	1.93 01	2.98 01	3.38 01	3.88 01	3.80 01	3.59 01	3.37 01	

Table 2-12. Values for component f_2 of the atomic scattering factor, for selected values of atomic number Z at energies between 1 and 10 keV.

Z	Energy (eV) 1000	2000	3000	4000	5000	6000	7000	8000	9000	10000
3	3.74-02	8.25-03	3.24-03	1.64-03	9.77-04	6.40-04	4.48-04	3.29-04	2.51-04	1.96-04
6	6.42-01	1.73-01	7.74-02	4.30-02	2.69-02	1.82-02	1.31-02	9.72-03	7.47-03	5.89-03
9	2.59 00	8.13-01	3.90-01	2.26-01	1.45-01	1.01-01	7.34-02	5.57-02	4.35-02	3.48-02
12	5.33-01	2.34 00	1.17 00	6.92-01	4.55-01	3.21-01	2.38-01	1.83-01	1.45-01	1.18-01
15	1.48 00	4.46-01	2.54 00	1.56 00	1.05 00	7.55-01	5.67-01	4.41-01	3.53-01	2.88-01
18	3.22 00	1.01 00	5.01-01	3.02 00	2.09 00	1.52 00	1.16 00	9.11-01	7.35-01	6.05-01
21	5.64 00	1.89 00	9.61-01	5.80-01	3.91 00	2.64 00	2.05 00	1.63 00	1.32 00	1.09 00
24	9.27 00	3.11 00	1.54 00	9.32-01	6.33-01	3.83 00	3.05 00	2.46 00	2.02 00	1.69 00
27	1.38 01	4.93 00	2.49 00	1.51 00	1.02 00	7.42-01	5.69-01	3.59 00	3.00 00	2.54 00
30	2.44 00	7.44 00	3.86 00	2.38 00	1.63 00	1.19 00	9.03-01	7.11-01	5.73-01	3.69 00
33	3.80 00	1.08 01	5.76 00	3.56 00	2.43 00	1.77 00	1.36 00	1.07 00	8.70-01	7.20-01
36	5.87 00	1.41 01	7.75 00	4.82 00	3.29 00	2.39 00	1.82 00	1.44 00	1.17 00	9.73-01
39	8.28 00	3.14 00	1.06 01	6.76 00	4.67 00	3.42 00	2.62 00	2.07 00	1.68 00	1.40 00
42	1.15 01	4.38 00	1.37 01	8.88 00	6.19 00	4.56 00	3.50 00	2.78 00	2.26 00	1.88 00

K

45	1.53 01	5.99 00	3.17 00	1.15 01	8.08 00	5.99 00	4.62 00	3.68 00	3.00 00	2.50 00
48	2.01 01	8.09 00	4.09 00	1.12 01	9.31 00	6.94 00	5.37 00	4.29 00	3.51 00	2.92 00
51	2.49 01	1.01 01	5.59 00	3.48 00	1.22 01	9.17 00	7.14 00	5.72 00	4.69 00	3.92 00
54	2.91 01	1.33 01	7.57 00	4.86 00	1.04 01	1.23 01	9.69 00	7.80 00	6.41 00	5.37 00
57	2.89 01	1.68 01	9.84 00	6.42 00	4.42 00	1.35 01	1.22 01	9.86 00	8.15 00	6.85 00
60	3.05 01	2.00 01	1.13 01	7.38 00	5.27 00	3.98 00	1.22 01	1.15 01	9.55 00	8.09 00
63	8.37 00	1.99 01	1.13 01	7.39 00	5.29 00	4.00 00	9.07 00	9.77 00	9.36 00	7.95 00
66	1.03 01	2.68 01	1.60 01	1.04 01	7.44 00	5.63 00	4.45 00	1.00 01	1.12 01	1.10 01
69	1.28 01	3.26 01	2.15 01	1.42 01	1.02 01	7.73 00	6.08 00	4.92 00	1.12 01	1.28 01
72	1.54 01	3.30 01	2.40 01	1.59 01	1.15 01	8.76 00	6.93 00	5.61 00	4.62 00	1.05 01
75	1.85 01	3.82 01	2.80 01	1.87 01	1.34 01	1.01 01	7.97 00	6.46 00	5.37 00	4.54 00
78	2.25 01	1.08 01	2.98 01	2.21 01	1.59 01	1.20 01	9.47 00	7.69 00	6.39 00	5.41 00
81	2.72 01	1.30 01	3.46 01	2.54 01	1.... 01	1.40 01	1.11 01	8.97 00	7.46 00	6.32 00
84	3.07 01	1.53 01	3.42 01	2.77 01	2.10 01	1.60 01	1.26 01	1.03 01	8.57 00	7.27 00
87	3.46 01	1.83 01	1.12 01	3.11 01	2.48 01	1.90 01	1.50 01	1.22 01	1.02 01	8.63 00
90	3.37 01	2.12 01	1.30 01	3.05 01	2.71 01	2.17 01	1.72 01	1.40 01	1.16 01	9.87 00

L_{III}

M_V

2.8 TRANSMISSION BANDS OF SELECTED FILTERS

Burton L. Henke

Figures 2-7 and 2-8 show transmission bands for selected practical filter materials between 50 eV and 10 keV. The filter materials and absorption edges are given in Table 2-13, along with the mass thickness m required to give about a 60% maximum transmission. This value of m is equal to $1/(2\mu)$, where μ is the mass absorption coefficient in $cm^2/\mu g$. These figures illustrate only the principal transmission band for each filter. A typical transmission curve for a wider spectral region is shown in Fig. 2-9, and detailed transmission curves for all the filter materials considered here can be found in B. L. Henke and P. A. Jaanimagi, "A Two-Channel, Elliptical Analyzer Spectrograph for Absolute, Time-Resolving/Time-Integrating Spectrometry of Pulsed X-Ray Sources in the 100–10,000 eV Region," *Rev. Sci. Instrum.* **56**, 1537 (1985).

Table 2-13. Absorption edges and mass thicknesses for the filters with transmission characteristics illustrated in Fig. 2-7 and 2-8.

No.	Filter	Edge (eV)	$1/2\mu$ ($\mu g/cm^2$)
1	Beryllium (Be)	Be-K (111)	81
2	Boron nitride (BN)	B-K (188)	68
3	Carbon (C)	C-K (284)	226
	Polypropylene $(CH_2{=}CHCH_3)_x$	C-K (284)	256
	Formvar ($C_5H_7O_2$)	C-K (284)	156
	Mylar ($C_{10}H_8O_4$)	C-K (284)	152
	Kimfol ($C_{16}H_{14}O_3$)	C-K (284)	181
4	Boron nitride (BN)	N-K (400)	66
5	Aluminum oxide (Al_2O_3)	O-K (532)	126
	Silicon dioxide (SiO_2)	O-K (532)	116
	Polyformaldehyde $(CH_2O)_x$	O-K (532)	92
6	Iron (Fe)	Fe-L_3 (707)	234
7	Nickel (Ni)	Ni-L_3 (854)	279
8	Copper (Cu)	Cu-L_3 (933)	318
9	Magnesium (Mg)	Mg-K (1303)	1139
10	Aluminum (Al)	Al-K (1560)	1427
11	Silicon (Si)	Si-K (1840)	1680
12	Saran $(CH_2{=}CCl_2)_x$	Cl-K (2820)	3151
13	Silver (Ag)	Ag-L_3 (3351)	1296
14	Tin (Sn)	Sn-L_3 (3929)	1669
15	Titanium (Ti)	Ti-K (4964)	6010
16	Chromium (Cr)	Cr-K (5989)	7924
17	Iron (Fe)	Fe-K (7111)	9804
18	Nickel (Ni)	Ni-K (8331)	11820
19	Copper (Cu)	Cu-K (8980)	13699

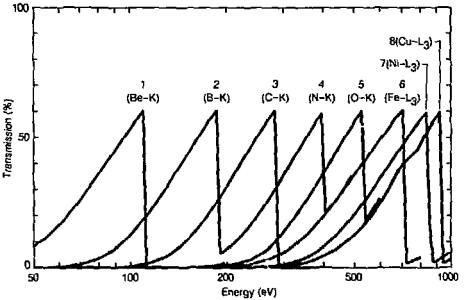

Fig. 2-7. Transmission bands of selected filters (see table) between 50 eV and 1 keV.

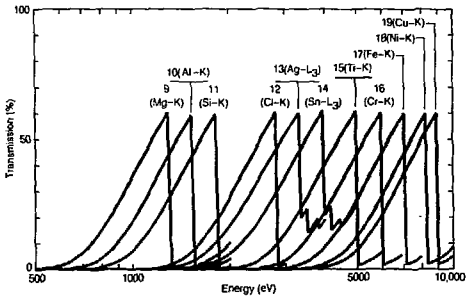

Fig. 2-8. Transmission bands of selected filters (see table) between 500 eV and 10 keV.

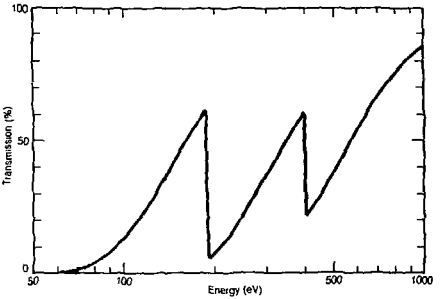

Fig. 2-9. Transmission characteristics for boron nitride between 50 eV and 1 keV.

SECTION 3

SCATTERING PROCESSES

3.1 SCATTERING OF X-RAYS FROM ELECTRONS AND ATOMS

Janos Kirz

A. COHERENT, RAYLEIGH, OR ELASTIC SCATTERING

Scattering from single electrons (Thomson scattering) has a total cross section

$$\sigma_T = 8\pi r_e^2/3 = 6.652 \times 10^{-29}\ \mathrm{m}^2 \ , \qquad (1)$$

where r_e is the classical radius of the electron, $e^2/mc^2 = 2.818 \times 10^{-15}$ meter. The angular distribution for unpolarized incident radiation is proportional to $(1 + \cos^2\theta)$, where θ is the scattering angle. For polarized incident radiation, the cross section vanishes at 90° in the plane of polarization.

Scattering from atoms involves the cooperative effect of all the electrons, and the cross section becomes

$$\sigma_R = \pi r_e^2 \int_{-1}^{1} |f(\theta)|^2 (1 + \cos^2\theta)\, d(\cos\theta) \ , \qquad (2)$$

where $f(\theta)$ is the (complex) atomic scattering factor, tabulated in Section 2.7 of this booklet. Up to about 2 keV, the scattering factor is approximately independent of scattering angle, with a real part that represents the effective number of electrons that participate in the scattering. At higher energies, the scattering factor falls off rapidly with scattering angle. For details see Ref. 1.

B. COMPTON SCATTERING

In relativistic quantum mechanics, the scattering of x-rays by a free electron is given by the Klein-Nishina formula. If we assume unpolarized x-rays and unaligned electrons, this formula can be approximated as follows for x-ray energies below 100 keV:

$$d\sigma_{KN}/d\Omega \cong \frac{r_e^2(1 + \cos^2\theta)}{2[1 + k(1 - \cos\theta)]^2} , \tag{3}$$

where $k = E/mc^2$, the photon energy measured in units of the electron rest energy. The total cross section is approximately

$$\sigma_{KN} \cong 8\pi r_e^2 \frac{(1 + 2k + 1.2k^2)}{3(1 + 2k)^2} . \tag{4}$$

Note that for very low energies ($k \to 0$), we recover the Thomson cross section. The real difference comes when we deal with atoms. In that case, if the scattering leaves the atom in the ground state, we deal with coherent scattering (see above), whereas if the electron is ejected from the atom, the scattering is (incoherent) Compton scattering. At high energies, the total Compton cross section approaches $Z\sigma_{KN}$. At low energies and small scattering angles, however, binding effects are very important, the Compton cross section is significantly reduced, and coherent scattering dominates (see Figs. 3-1 and 3-2). For details see Refs. 1 and 2.

The scattered x-ray suffers an energy loss, which (ignoring binding effects) is given by

$$E'/E = 1/[1 + k(1 - \cos\theta)] \tag{5}$$

or, in terms of the wavelength shift,

$$\lambda' - \lambda = \lambda_c (1 - \cos\theta) , \tag{6}$$

where $\lambda_c = h/mc = 2.426 \times 10^{-12}$ meter. The kinetic energy of the recoil electron is just the energy lost by the photon in this approximation:

$$E_e = E \frac{k(1 - \cos\theta)}{1 + k(1 - \cos\theta)} . \tag{7}$$

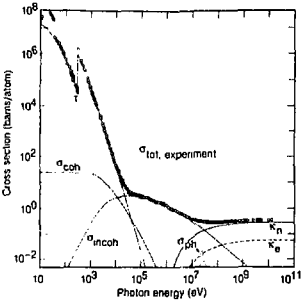

Fig. 3-1. *Total photon cross section σ_{tot} in carbon, as a function of energy, showing the contributions of different processes: τ, atomic photo-effect (electron ejection, photon absorption); σ_{coh}, coherent scattering (Rayleigh scattering—atom neither ionized nor excited); σ_{incoh}, incoherent scattering (Compton scattering off an electron); κ_n, pair production, nuclear field; κ_e, pair production, electron field; σ_{ph}, photonuclear absorption (nuclear absorption, usually followed by emission of a neutron or other particle). (From Ref. 3; figure courtesy of J. H. Hubbell.)*

REFERENCES

1. J. H. Hubbell, W. J. Veigele, E. A. Briggs, R. T. Brown, D. T. Cromer, and R. J. Howerton, "Atomic Form Factors, Incoherent Scattering Functions, and Photon Scattering Cross Sections," *J. Phys. Chem Ref. Data* 4, 471 (1975).

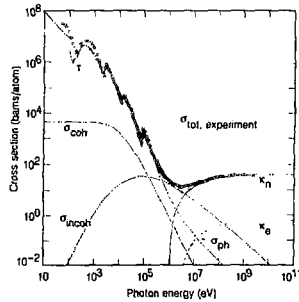

Fig. 3-2. *Total photon cross section σ_{tot} in lead, as a function of energy. See Fig. 3-1. (From Ref. 3; figure courtesy of J. H. Hubbell.)*

2. R. D. Evans, *The Atomic Nucleus* (Krieger, Malabar, FL, 1982); R. D. Evans, "The Compton Effect," in S. Flugge, Ed., *Handbuch der Physik*, vol. 34 (Springer-Verlag, Berlin, 1958), p. 218; W. J. Veigele, P. T. Tracy, and E. M. Henry, "Compton Effect and Electron Binding," *Am. J. Phys.* **34**, 1116 (1966).
3. J. H. Hubbell, H. A. Gimm, I. Øverbø, "Pair, Triplet, and Total Atomic Cross Sections (and Mass Attenuation Coefficients) for 1 MeV–100 GeV Photons in Elements $Z = 1$ to 100," *J. Phys. Chem. Ref. Data* **9**, 1023 (1980).

3.2 LOW-ENERGY ELECTRON RANGES IN MATTER

Piero Pianetta

The electron range is a measure of the straight-line penetration distance of electrons in a solid [1]. Electrons with energies in the kilo-electron volt range, traveling in a solid, are scattered inelastically in collisions with the electrons in the material. For low-Z materials, such as organic insulators, scattering from the valence electrons is the major loss mechanism for incident electron energies from 10 eV to 10 keV. The core levels contribute less than 10% to the electron's energy dissipation for energies between 1 keV and 10 keV [2].

For electron energies below 5 keV, the usual Bethe-Bloch formalism is inadequate for calculating the electron energy loss in a solid, and an approach using the dielectric response of the material is used [3]. The complex dielectric function $\epsilon(k,\omega)$ describes the response of a medium to a given energy transfer $\hbar\omega$ and momentum transfer $\hbar k$. The dielectric function contains contributions from both valence and core electrons. References 4 and 5 describe the steps for calculating $\epsilon(k,\omega)$ for insulators and metals, respectively. For an electron of energy E, the probability of an energy loss ω per unit distance is given by [2]

$$\tau(E,\hbar\omega) = \frac{1}{\pi a_0 E}\int_{k_-}^{k_+}\frac{dk}{k}\,\mathrm{Im}\left[\frac{-1}{\epsilon(k,\omega)}\right], \qquad (1)$$

where $\hbar k_\pm = \sqrt{2m}\,(\sqrt{E} \pm \sqrt{E-\hbar\omega})$ and $a_0 = \hbar^2/me^2$. The quantity $\tau(E,\hbar\omega)$ is also known as the differential inverse mean free path, because by integrating it over all allowed energy transfers, the inelastic mean free path is obtained. Furthermore, an integration of $\hbar\omega\tau(E,\hbar\omega)$ over all allowed energy transfers gives the energy loss per unit path length, or stopping power $S(E)$. The stopping power can then be used to calculate the distance it takes to slow an electron down to a given energy. This distance is called the continuous slowing down approximation range, or CSDA range, because the calculation assumes that the electron slows down continuously from the initial energy E to the final energy, which is usually taken

to be 10 eV [2]. The CSDA range $R_0(E)$ is given by

$$R_0(E) = \int_{10\text{eV}}^{E} \frac{dE'}{S(E')} . \qquad (2)$$

The calculations for inelastic mean free path and stopping power have been carried out down to 10 eV for a number of materials, including SiO_2 [3]; polystyrene [2]; polyethylene [6]; collodion [7]; and silicon, aluminum, nickel, copper, and gold [5]. The CSDA ranges from 15 eV to 6 keV were then calculated for polystyrene, silicon, and gold by integrating Eq. (2) and are shown in Fig. 3-3. These curves can be used with confidence down to 100 eV. However, comparisons of different available calculations with the meager experimental data below 100 eV indicate that errors as large as 100% may occur

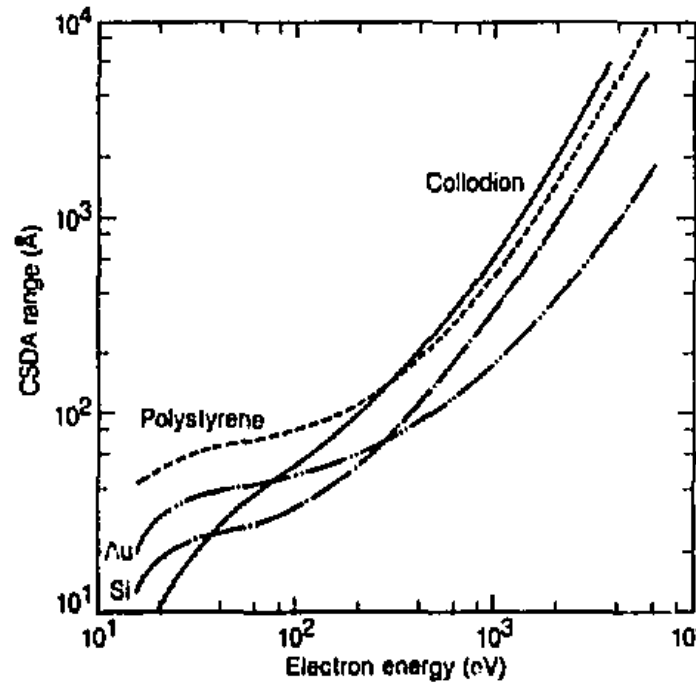

Fig. 3-3. *Plot of the CSDA range, as a function of energy, for gold and silicon [5] and for polystyrene, $(C_8H_8)_n$, with a density of 1.05 g/cm³ [2]. The measured electron range in collodion with a density of 1 g/cm³ is also plotted [7].*

at 10 eV. An example of this is shown in the figure, where experimental range data for collodion are given. It is clear that the agreement between the collodion and polystyrene data starts to become reasonable above 100 eV. The differences below 100 eV could equally well be due to problems with the theory or to the increased difficulty of the measurement. Stopping-power calculations for PMMA have been carried out only from 100 eV, so that the CSDA range as defined above could not be calculated [4]. However, data on effective electron ranges of photoelectrons in PMMA at several energies can be found in Ref. 8.

REFERENCES

1. T. E. Everhart and P. H. Hoff, "Determination of Kilovolt Electron Energy Dissipation vs Penetration Distance in Solid Materials," *J. Appl. Phys.* **42**, 5837 (1971).
2. J. C. Ashley, C. J. Tung, and R. H. Ritchie, "Inelastic Interactions of Electrons with Polystyrene: Calculations of Mean Free Paths, Stopping Powers, and CSDA Ranges," *IEEE Trans. Nucl. Sci.* **NS-26**, 1566 (1978).
3. J. C. Ashley and V. E. Anderson, "Interaction of Low Energy Electrons with Silicon Dioxide," *J. Elect. Spectrosc.* **24**, 127 (1981).
4. J. C. Ashley, "Inelastic Interactions of Low Energy Electrons with Organic Solids: Simple Formulae for Mean Free Paths and Stopping Powers," *IEEE Trans. Nucl. Sci.* **NS-27**, 1454 (1980).
5. J. C. Ashley, C. J. Tung, R. H. Ritchie, and V. E. Anderson, "Calculations of Mean Free Paths and Stopping Powers of Low Energy Electrons (< 10 keV) in Solids Using a Statistical Model," *IEEE Trans. Nucl. Sci.* **NS-23**, 1833 (1976).
6. J. C. Ashley, "Energy Losses and Inelastic Mean Free Path of Low Energy Electrons in Polyethylene," *Radiat. Res.* **90**, 433 (1982).
7. A. Cole, "Absorption of 20 eV to 50 keV Electron Beams in Air and Plastic," *Radiat. Res.* **38**, 7 (1969).
8. R. Feder, E. Spiller, and J. Topalian, "X-Ray Lithography," *Polymer Eng. Sci.* **17**, 385 (1977).

SECTION 4

X-RAY SOURCES

4.1 CHARACTERISTICS OF SYNCHROTRON RADIATION

Kwang-Je Kim

Synchrotron radiation occurs when a charge moving at relativistic speeds follows a curved trajectory. In this section, formulas and supporting graphs are used to quantitatively describe characteristics of this radiation for the cases of circular motion (bending magnets) and sinusoidal motion (periodic magnetic structures).

We will first discuss the ideal case, where the effects due to the angular divergence and the finite size of the electron beam—the emittance effects—can be neglected.

A. BENDING MAGNETS

The angular distribution of radiation emitted by electrons moving through a bending magnet with a circular trajectory in the horizontal plane is given by

$$\frac{d^2\mathcal{F}_B(\omega)}{d\theta d\psi} = \frac{3\alpha}{4\pi^2}\gamma^2\frac{\Delta\omega}{\omega}\frac{I}{e}\gamma^2(1+X^2)^2 \times\left[K_{2/3}^2(\xi)+\frac{X^2}{1+X^2}K_{1/3}^2(\xi)\right], \quad (1)$$

where

$\mathcal{F}_B$ = photon flux (number of photons per second)
θ = observation angle in the horizontal plane
ψ = observation angle in the vertical plane
α = fine-structure constant
γ = electron energy/$m_e c^2$ (m_e = electron mass, c = velocity of light)
ω = angular frequency of photon ($\epsilon = \hbar\omega$ = energy of photon)
I = beam current
e = electron charge = 1.602×10^{-19} coulomb
y = $\omega/\omega_c = \epsilon/\epsilon_c$
ω_c = critical frequency, defined as the frequency that divides the emitted power into equal halves, = $3\gamma^3 c/2\rho$
ρ = radius of instantaneous curvature of the electron trajectory [in practical units, $\rho(m) = 3.3\, E(\text{GeV})/B(T)$]
E = electron beam energy
B = magnetic field strength
ϵ_c = $\hbar\omega_c$ [in practical units, $\epsilon_c(\text{keV}) = 0.665\, E^2\,(\text{GeV})\, B(T)$]
X = $\gamma\psi$
ξ = $y(1 + X^2)^{3/2}/2$

The subscripted Ks are modified Bessel functions of the second kind. In the horizontal direction ($\psi = 0$), Eq. (1) becomes

$$\left.\frac{d^2\mathcal{F}_B}{d\theta d\psi}\right|_{\psi=0} = \frac{3\alpha}{4\pi^2}\gamma^2\frac{\Delta\omega}{\omega}\frac{I}{e}H_2(y), \tag{2}$$

where

$$H_2(y) = y^2 K_{2/3}^2(y/2). \tag{3}$$

In practical units [photons·s^{-1}·mr^{-2}·(0.1% bandwidth)$^{-1}$],

$$\left.\frac{d^2\mathcal{F}_B}{d\theta d\psi}\right|_{\psi=0} = 1.327 \times 10^{13}\, E^2[\text{GeV}]\, I[A]\, H_2(y).$$

The function $H_2(y)$ is shown in Fig 4-1.

The distribution integrated over ψ is given by

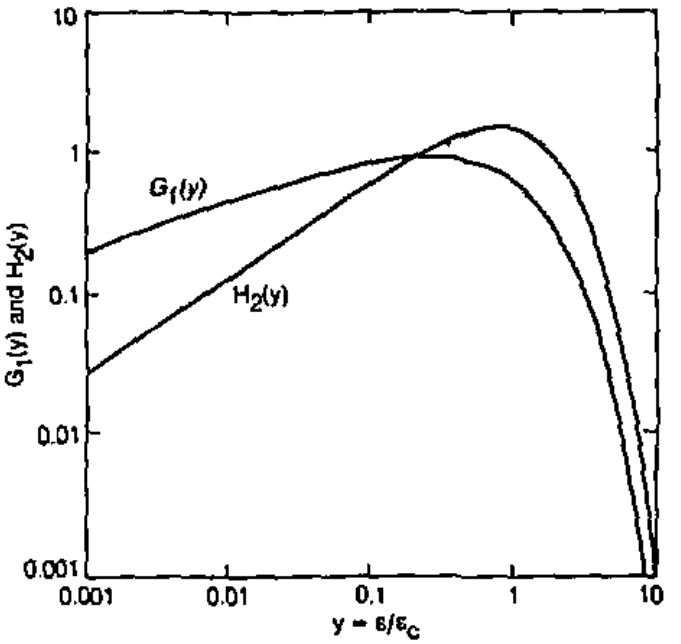

Fig. 4-1. *The functions $G_1(y)$ and $H_2(y)$, where y is the ratio of photon energy to critical photon energy.*

$$\frac{d\mathcal{F}_B}{d\theta} = \frac{\sqrt{3}}{2\pi}\,\alpha\gamma\,\frac{\Delta\omega}{\omega}\,\frac{I}{e}\,G_1(y)\,, \tag{4}$$

where

$$G_1(y) = y\int_y^\infty K_{5/3}(y')dy'\,. \tag{5}$$

In practical units $\left[\text{photons}\cdot\text{s}^{-1}\cdot\text{mr}^{-1}\cdot(0.1\%\ \text{bandwidth})^{-1}\right]$,

$$\frac{d\mathcal{F}_B}{d\theta} = 2.457\times 10^{13}\,E[\text{GeV}]I[A]G_1(y)\,.$$

The function $G_1(y)$ is also plotted in Fig 4-1.

Radiation from a bending magnet is linearly polarized when observed in the bending plane. Out of this plane, the polarization is elliptical and can be decomposed into its horizontal and vertical components. The first and second terms

in the last bracket of Eq. (1) correspond, respectively, to the intensity of the horizontally and vertically polarized radiation. Figure 4-2 gives the normalized intensities of these two components, as functions of emission angle, for different energies. The square root of the ratio of these intensities is the ratio of the major and minor axes of the polarization ellipse. The sense of the electric field rotation reverses as the vertical observation angle changes from positive to negative.

Synchrotron radiation occurs in a narrow cone of nominal angular width $\sim 1/\gamma$. To provide a more specific measure of this angular width, in terms of electron and photon energies, it is convenient to introduce the effective rms half-angle σ_ψ as follows:

$$\frac{d\mathcal{F}_B}{d\theta} \Big/ \frac{d^2\mathcal{F}_B}{d\theta d\psi}\Bigg|_{\psi=0} = \sqrt{2\pi}\,\sigma_\psi , \tag{6}$$

where σ_ψ is given by

$$\sigma_\psi = \frac{2}{\gamma\sqrt{2\pi}}\,C(y) = 0.408\frac{C(y)[\text{mr}]}{E[\text{GeV}]} . \tag{7}$$

The function $C(y)$ is plotted in Fig 4-3. In terms of σ_ψ, Eq. (2) may now be rewritten as

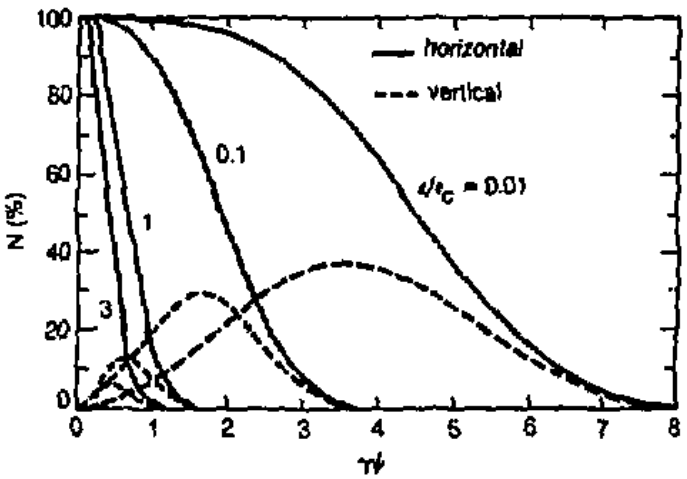

Fig. 4-2. Normalized intensities of horizontal and vertical polarization components, as functions of the vertical observation angle ψ, for different photon energies. (Adapted from Ref. 1.)

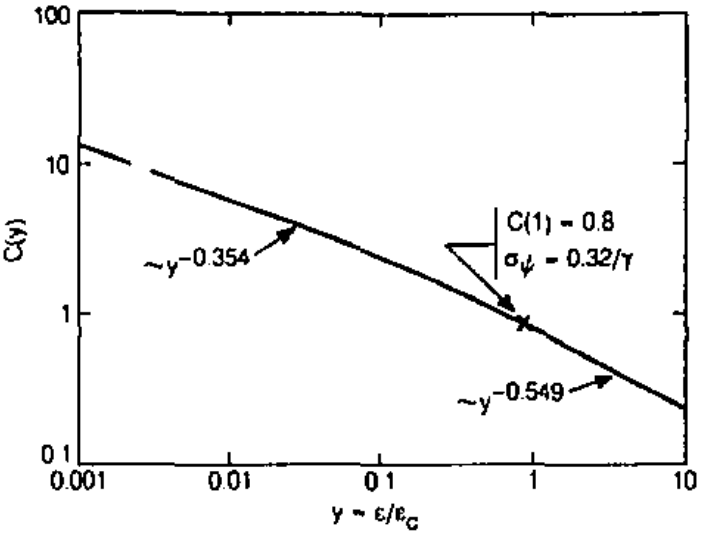

Fig. 4-3. The function $C(y)$. The limiting slopes, for $\epsilon/\epsilon_c \ll 1$ and $\epsilon/\epsilon_c \gg 1$, are indicated.

$$\left.\frac{d^2\mathcal{I}_B}{d\theta d\psi}\right|_{\psi=0} = \frac{d\mathcal{I}_B}{d\theta}\,\frac{1}{\sigma_\psi\sqrt{2\pi}}\,. \tag{2a}$$

B. PERIODIC MAGNETIC STRUCTURES

In a wiggler or an undulator, electrons travel through a periodic magnetic structure. We consider the case where the magnetic field B varies sinusoidally and is in the vertical direction:

$$B(z) = B_0 \cos(2\pi z/\lambda_u)\,, \tag{8}$$

where z is the distance along the wiggler axis, B_0 the peak magnetic field, and λ_u the magnet period. Electron motion is also sinusoidal and lies in the horizontal plane. An important parameter characterizing the electron motion is the deflection parameter K given by

$$K = eB_0\lambda_u/2\pi mc = 0.934\,\lambda_u[\mathrm{cm}]B_0[\mathrm{T}]\,. \tag{9}$$

In terms of K, the maximum angular deflection of the orbit is

$\delta = K/\gamma$. For $K \lesssim 1$, radiation from the various periods can exhibit strong interference phenomena, because the angular excursions of the electrons are within the nominal $1/\gamma$ radiation cone; in this case, the structure is referred to as an undulator. In the case $K \gg 1$, interference effects are less important, and the structure is referred to as a wiggler.

B.1 Wiggler radiation

In a wiggler, K is large (typically $\gtrsim 10$) and radiation from different parts of the electron trajectory adds incoherently. The flux distribution is then given by $2N$ (where N is the number of magnet periods) times the appropriate formula for bending magnets, either Eq. (1) or Eq. (2). However, ρ or B must be taken at the point of the electron's trajectory tangent to the direction of observation. Thus, for a horizontal angle θ,

$$\epsilon_c(\theta) = \epsilon_{c\ \max} \sqrt{1 - (\theta/\delta)^2}\,. \tag{10}$$

where

$$\epsilon_{c\ \max} = 0.665\, E^2[\mathrm{GeV}]\, B_0[\mathrm{T}]\,.$$

When $\psi = 0$, the radiation is linearly polarized in the horizontal plane, as in the case of the bending magnet. As ψ increases, the direction of the polarization changes, but because the elliptical polarization from one half-period of the motion combines with the elliptical polarization (of opposite sense of rotation) from the next, the polarization remains linear.

B.2 Undulator radiation

In an undulator, K is moderate ($\lesssim 1$) and radiation from different periods interferes coherently, thus producing sharp peaks at harmonics of the fundamental ($n = 1$). The wavelength of the fundamental on axis ($\theta = \psi = 0$) is given by

$$\lambda_1 = \frac{(1 + K^2/2)}{2\gamma^2}\,\lambda_u \tag{11}$$

or

$$\lambda_1[\mathrm{A}] = \frac{13.056\,\lambda_u\,[\mathrm{cm}]}{E^2\,[\mathrm{GeV}]}\,(1 + K^2/2)\,.$$

The corresponding energy, in practical units, is

$$\epsilon_1\,[\mathrm{keV}] \approx 0.950\,\frac{E^2[\mathrm{GeV}]}{(1 + K^2/2)\lambda_u\,[\mathrm{cm}]}$$

The relative bandwidth at the nth harmonic is

$$\frac{\Delta\lambda}{\lambda} = \frac{\Delta\omega}{\omega} = \frac{1}{nN} \quad (n = 1,2,3,\ldots). \tag{12}$$

On axis the peak intensity of the nth harmonic is given by

$$\left.\frac{d^2\mathscr{F}_n}{d\theta d\psi}\right|_0 = \alpha N^2\gamma^2\,\frac{\Delta\omega}{\omega}\,\frac{I}{e}\,F_n(K) \quad (n = 1,3,5,\ldots)$$
$$= 0 \qquad\qquad (n = 2,4,6,\ldots), \tag{13}$$

where

$$F_n(K) = \frac{K^2n^2}{(1 + K^2/2)^2}\left\{J_{\frac{n-1}{2}}\left[\frac{nK^2}{4(1 + K^2/2)}\right] - J_{\frac{n+1}{2}}\left[\frac{nK^2}{4(1 + K^2/2)}\right]\right\}^2. \tag{14}$$

Here, the Js are Bessel functions. The function $F_n(K)$ is plotted in Fig 4-4. In practical units [photons · s^{-1} · mr^{-2} · (0.1% bandwidth)$^{-1}$], Eq. (13) becomes

$$\left.\frac{d^2\mathscr{F}_n}{d\theta d\psi}\right|_0 = 1.744 \times 10^{14}\,N^2\,E^2[\mathrm{GeV}]\,I[\mathrm{A}]\,F_n(K).$$

The angular distribution of the nth harmonic is concentrated in a narrow cone whose half-width is given by

$$\sigma_r \simeq \sqrt{\frac{\lambda_n}{L}} = \frac{1}{\gamma}\sqrt{\frac{(1 + K^2/2)}{2Nn}}. \tag{15}$$

Here L is the length of the undulator ($L = N\lambda_u$). Additional rings of radiation of the same frequency also appear at angular distances

$$\theta_{n,\ell} = \frac{1}{\gamma}\sqrt{\frac{\ell}{n}\,(1 + K^2/2)} \quad (\ell = 1,2,3,\ldots). \tag{16}$$

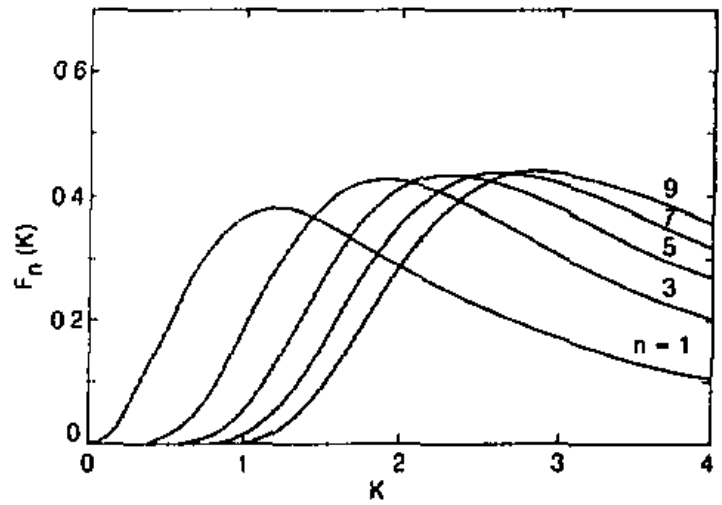

Fig. 4-4. The function $F_n(K)$ for different values of n, where K is the deflection parameter.

The angular structure of undulator radiation is illustrated in Fig. 4-5 for the limiting case of zero beam emittance.

We are usually interested in the central cone. An approximate formula for the flux integrated over the central cone is

$$\mathcal{F}_n = \pi\alpha N \frac{\Delta\omega}{\omega} \frac{I}{e} Q_n(K), \tag{17}$$

or, in units of photons · s^{-1} · (0.1% bandwith)$^{-1}$,

$$\mathcal{F}_n = 1.431 \times 10^{14} N Q_n I[\mathrm{A}].$$

The function $Q_n(K) = (1 + K^2/2)F_n/n$ is plotted in Fig. 4-6. Equation (13) can also be written as

$$\left.\frac{d^2\mathcal{F}_n}{d\theta d\psi}\right|_0 = \frac{\mathcal{F}_n}{2\pi\sigma_{r'}^2}. \tag{13a}$$

Away from the axis, there is also a change in wavelength: The factor $(1 + K^2/2)$ in Eq. (11) must be replaced by $[1 + K^2/2 + \gamma^2(\theta^2 + \psi^2)]$. Because of this wavelength shift with emission angle, the angle-integrated spectrum consists of peaks at λ_n superposed on a continuum. The peak-to-

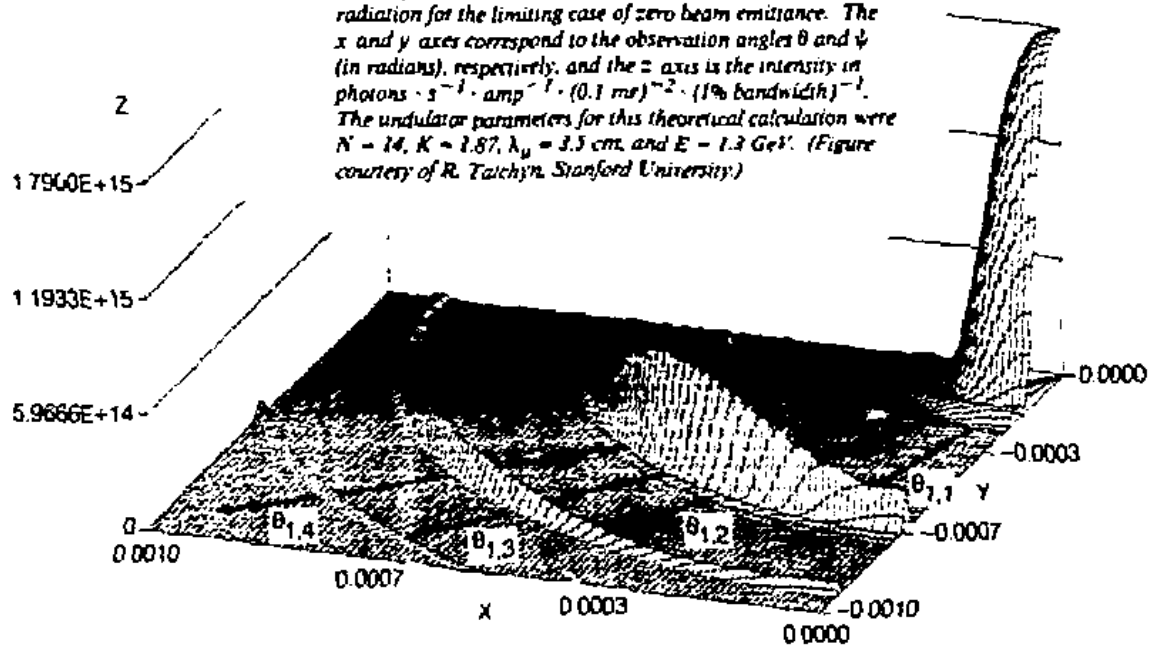

Fig. 4-5. *The angular distribution of fundamental (n = 1) undulator radiation for the limiting case of zero beam emittance. The x and y axes correspond to the observation angles θ and ψ (in radians), respectively, and the z axis is the intensity in photons · s^{-1} · amp^{-1} · (0.1 mr)$^{-2}$ · (1% bandwidth)$^{-1}$. The undulator parameters for this theoretical calculation were N = 14, K = 1.87, λ_u = 3.5 cm, and E = 1.3 GeV. (Figure courtesy of R. Tatchyn, Stanford University.)*

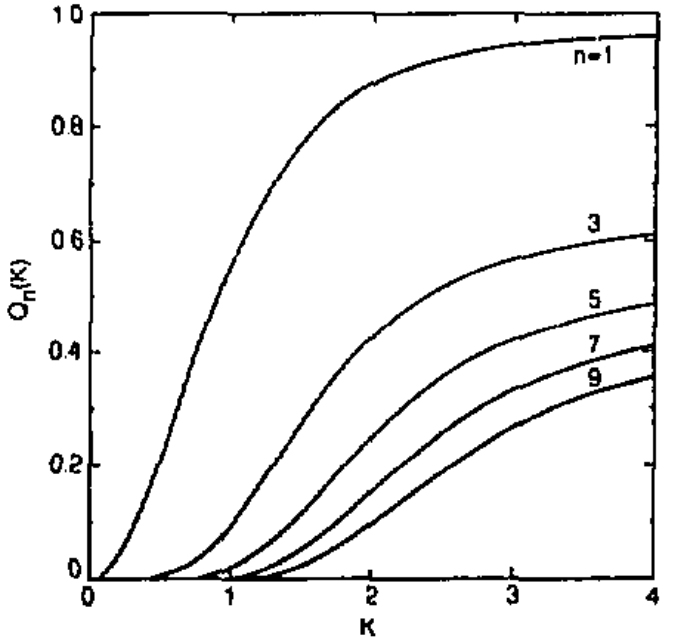

Fig. 4-4. *The function $Q_n(K)$ for different values of n.*

continuum ratio is large for $K \ll 1$, but the continuum increases with K, as one shifts from undulator to wiggler conditions.

B.3 Power

The total power radiated by an undulator or wiggler is

$$P_T = \frac{N}{6} Z_0 I e \frac{2\pi c}{\lambda_u} \gamma^2 K^2 , \tag{18}$$

where $Z_0 = 377$ ohms, or, in practical units,

$$P_T[\mathrm{kW}] = 0.633\, E^2[\mathrm{GeV}] B_0^2[\mathrm{T}] L[\mathrm{m}]\, I[\mathrm{A}] .$$

The angular distribution of the radiated power is

$$\frac{d^2P}{d\theta d\psi} = P_T \frac{21\gamma^2}{16\pi K} G(K) f_K(\gamma\theta, \gamma\psi) , \tag{19}$$

or, in units of $\mathrm{W \cdot mr^{-2}}$,

$$\frac{d^2P}{d\theta d\psi} = 10.84\, B_0[T]E^4[\mathrm{GeV}]I[\mathrm{A}]NG(K)f_K(\gamma\theta,\gamma\psi)\,.$$

The behavior of the angular function $f_K(\gamma\theta,\gamma\psi)$, which is

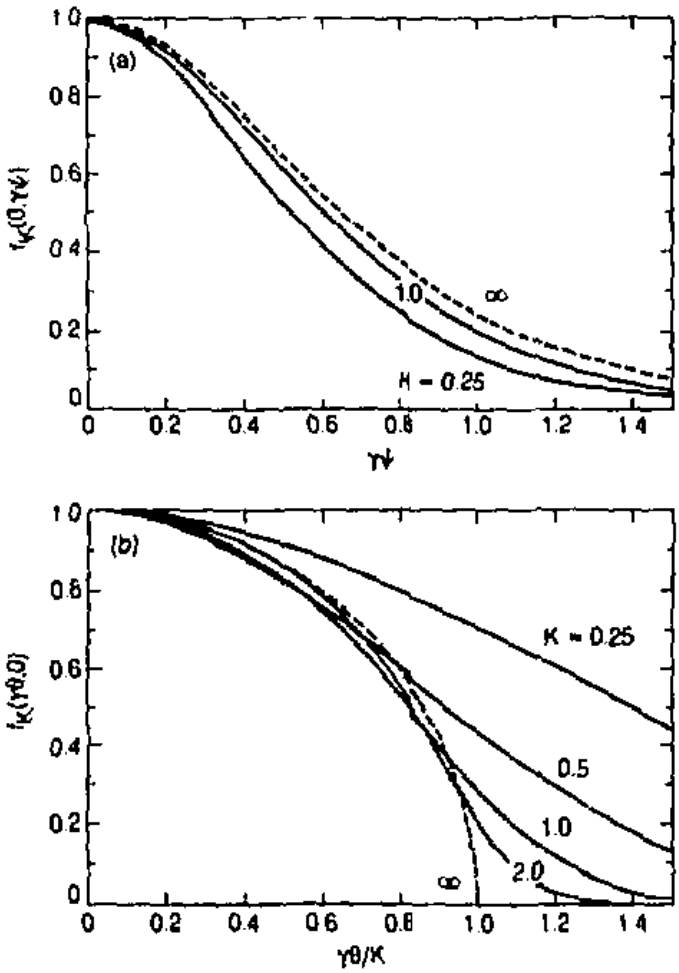

Fig. 4-7. The angular function f_K, for different values of the deflection parameter K, (a) as a function of the vertical observation angle ψ when the horizontal observation angle $\theta = 0$ and (b) as a function of θ when $\psi = 0$.

normalized as $f_K(0,0) = 1$, is shown in Fig. 4-7. The function $G(K)$, shown in Fig. 4-8, quickly approaches unity as K increases from zero.

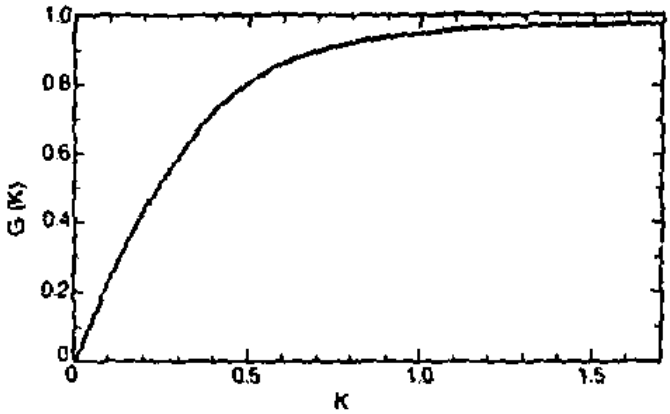

Fig. 4-8. The function $G(K)$.

C. EMITTANCE EFFECTS

Electrons in storage rings are distributed in a finite area of transverse phase space—position × angle. We introduce the rms beam sizes σ_x (horizontal) and σ_y (vertical), and beam divergences $\sigma_{x'}$ (horizontal) and $\sigma_{y'}$ (vertical). The quantities $\epsilon_x = \sigma_x \sigma_{x'}$ and $\epsilon_y = \sigma_y \sigma_{y'}$ are known as the horizontal and vertical emittances, respectively. In general, owing to the finite emittances of real electron beams, the intensity of the radiation observed in the forward direction is less than that given by Eqs. (2a) and (13a). Finite emittances can be taken into account approximately by replacing these equations by

$$\left.\frac{d^2\mathcal{I}_\pi}{d\theta d\psi}\right|_{\psi=0} = \frac{d\mathcal{I}_\pi}{d\theta}\,\frac{1}{\sqrt{2\pi(\sigma_\psi^2 + \sigma_{y'}^2)}} \tag{20}$$

and

$$\left.\frac{d^2\mathcal{I}_\pi}{d\theta d\psi}\right|_0 = \frac{\mathcal{I}_\pi}{2\pi\sqrt{(\sigma_{x'}^2 + \sigma_{x'}^2)(\sigma_{y'}^2 + \sigma_{y'}^2)}} \tag{21}$$

for bends and undulators, respectively. For bending magnets, the electron beam divergence effect is usually negligible in the horizontal plane.

D. SPECTRAL BRIGHTNESS AND TRANSVERSE COHERENCE

For experiments that require a small angular divergence and a small irradiated area, the relevant figure of merit is the beam brightness $\mathscr{B}$, which is the photon flux per unit phase space volume, often given in units of photons · s^{-1} · mr^{-2} · mm^{-2} · (0.1% bandwidth)$^{-1}$. For an undulator, an approximate formula for the peak brightness is

$$\mathscr{B}_n(0,0) = \frac{\mathscr{F}_n}{(2\pi)^2 \sigma_{Tx}\sigma_{Ty}\sigma_{Tx'}\sigma_{Ty'}}, \tag{22}$$

where, for example,

$$\sigma_{Tx} = \sqrt{\sigma_x^2 + \sigma_r^2},$$

$$\sigma_{Tx'} = \sqrt{\sigma_{x'}^2 + \sigma_{r'}^2}, \tag{23}$$

and where the single-electron radiation from an axially extended source of finite wavelength is described by

$$\sigma_r = \frac{1}{4\pi}\sqrt{\lambda L},$$

$$\sigma_{r'} = \sqrt{\lambda/L}. \tag{24}$$

Brightness is shown in Fig. 4-9 for several sources of synchrotron radiation, as well as some conventional x-ray sources.

That portion of the flux that is transversely coherent is given by

$$\mathscr{F}_c = \mathscr{B}_n \left(\frac{\lambda}{2}\right)^2 = \frac{\mathscr{F}_n \lambda^2}{(4\pi)^2 \sigma_{Tx}\sigma_{Ty}\sigma_{Tx'}\sigma_{Ty'}}. \tag{25}$$

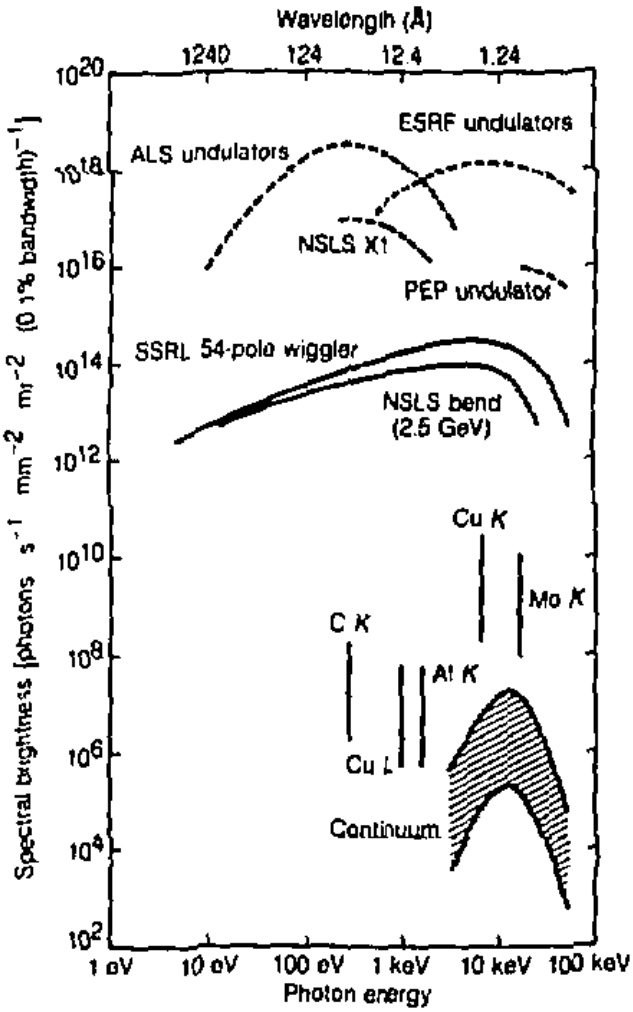

Fig. 4-9. Spectral brightness for several synchrotron radiation sources and conventional x-ray sources. The data for conventional x-ray tubes should be taken as rough estimates only, since brightness depends strongly on such parameters as operating voltage and take-off angle. The indicated two-order-of-magnitude ranges show the approximate variation that can be expected among stationary-anode tubes (lower end of range), rotating-anode tubes (middle), and rotating-anode tubes with microfocusing (upper end of range).

A substantial fraction of undulator flux is thus transversely coherent for a low-emittance beam satisfying $\epsilon_x \epsilon_y \lesssim (\lambda/4\pi)^2$.

E. LONGITUDINAL COHERENCE

Longitudinal coherence is described in terms of a coherence length

$$\ell_c = \lambda^2/\Delta\lambda . \tag{26}$$

For an undulator, the various harmonics have a natural spectral purity of $\Delta\lambda/\lambda = 1/nN$ [see Eq. (12)]; thus, the coherence length is given by

$$\ell_c \simeq nN\lambda , \tag{27}$$

which corresponds to the relativistically contracted length of the undulator. Thus, undulator radiation from low-emittance electron beams $[\epsilon_x \epsilon_y \lesssim (\lambda/4\pi)^2]$ is transversely coherent and is longitudinally coherent within a distance described by E q. (27). In the case of finite beam emittance or finite angular acceptance, the longitudinal coherence is reduced because of the change in wavelength with emission angle. In this sense, undulator radiation is partially coherent. Transverse and longitudinal coherence can be enhanced when necessary by the use of spatial and spectral filtering (i.e., by use of apertures and monochromators, respectively).

REFERENCES

1. G. K. Green, "Spectra and Optics of Synchrotron Radiation," in *Proposal for National Synchrotron Light Source*, Brookhaven National Laboratory, Upton, New York, BNL-50595 (1977).
2. H. Winick, "Properties of Synchrotron Radiation," in H. Winick and S. Doniach Eds., *Synchrotron Radiation Research* (Plenum, New York, 1979), p. 11.
3. S. Krinsky, "Undulators as Sources of Synchrotron Radiation," *IEEE Trans. Nucl. Sci.* **NS-30**, 3078 (1983).
4. D. F. Alferov, Yu. Bashmakov, and E. G. Bessonov, "Undulator Radiation," *Sov. Phys. Tech. Phys.* **18**, 1336 (1974).
5. K.-J. Kim, "Angular Distribution of Undulator Power for an Arbitrary Deflection Parameter *K*," in *Proceedings, International Conference on X-Ray and VUV Synchrotron*

Radiation Instrumentation, to be published in *Nucl. Instrum. Methods Phys. Res.*

6. K.-J. Kim, "Brightness, Coherence, and Propagation Characteristics of Synchrotron Radiation," in *Proceedings, International Conference on X-Ray and VUV Synchrotron Radiation Instrumentation*, to be published in *Nucl. Instrum. Methods Phys. Res.*

4.2 X-RAY TUBES

The spectral brightness of conventional x-ray tubes is compared to that of sources of synchrotron radiation in Fig. 4-9. Detailed data on the emission characteristics of tubes, together with additional references, can be found in the references listed below.

REFERENCES

1. J. V. Gilfrich and L. S. Birks, "Spectral Distribution of X-Ray Tubes for Quantitative X-Ray Fluorescence Analysis," *Anal. Chem.* **40**, 1077 (1968).
2. J. V. Gilfrich, P. G. Burkhalter, R. R. Whitlock, E. S. Warden, and L. S. Birks, "Spectral Distribution of a Thin Window Rhodium Target X-Ray Spectrographic Tube," *Anal. Chem.* **43**, 934 (1971).
3. D. B. Brown and J. V. Gilfrich, "Measurement and Calculation of Absolute X-Ray Intensities," *J. Appl. Phys.* **42**, 4044 (1971).
4. J. V. Gilfrich, "Spectral Distribution of X-Ray Tubes," in J. W. Robinson, Ed., *Handbook of Spectroscopy* (CRC Press, Cleveland, 1974), vol. 1, p. 232.
5. R. Coisson, "X-Ray Sources," in M. Schlinker, M. Fink, J. P. Goedgebuer, C. Malgrange, J. Ch. Vienot, and R. H. Wade, Eds., *Imaging Processes and Coherence in Physics* (Springer-Verlag, Berlin, 1980), p. 51.

4.3 PULSED X-RAY SOURCES

Gary L. Stradling and John C. Riordan

Both laser-generated plasmas and Z-pinch plasmas are commonly used pulsed x-ray sources. In both, x-ray generation is by radiative recombination and atomic inner-shell line emission. The relative contributions of these two processes at a given x-ray energy depends on several physical plasma parameters, including the electron density and energy distribution, the plasma material, and the ionization states. Bremsstrahlung radiation is generally negligible, except in the case of plasmas produced by long-wavelength lasers. In optically thick, high-atomic-number plasmas, the thermal x-ray emission spectrum can be roughly approximated by a black-body spectrum, with some atomic line structure superimposed.

A. LASER PLASMA SOURCES

Laser-generated plasmas are produced by illuminating matter with high-power lasers, focused intensities typically ranging from 10^{12} to 10^{15} W/cm^2. Small systems in which a few tenths of a joule of 1.06-μm light, delivered to an area of about $10^4 \mu m^2$ within a few tens of picoseconds, have proved to be useful x-ray generators, as have larger systems that deliver tens of kilojoules in less than a nanosecond.

Parametric studies have shown that the x-ray emission efficiency, spectral shape, and emission pulse width depend on the illumination conditions, as well as the irradiated material [1]. Shorter (submicron) wavelengths, moderate irradiation intensities ($\sim 10^{14}$ W/cm^2), and high-atomic-number plasmas appear to provide the highest x-ray production efficiency [2]. Figure 4-10 shows some experimental and theoretical results.

The x-ray emission pulse shape depends on both the photon energy of the emitted radiation and the plasma atomic number. Higher photon energies ($\geq$1 keV) and higher atomic numbers yield pulse shapes that conform closely to that of the laser. Lower photon energies ($<$1 keV) and low atomic numbers tend to show pulses wider than the laser pulse. This observation can clearly be understood as the effect of a cooling plasma emitting at progressively lower temperatures. An

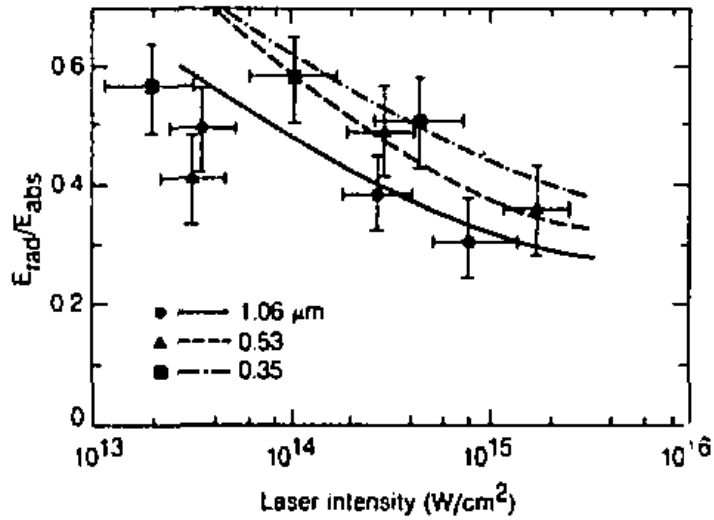

Fig. 4-10. Measured and theoretical x-ray conversion efficiencies as functions of incident intensities, for three laser wavelengths. The curves represent the results of computer simulations. (From Ref. 2.)

example of this spectral dependence of the pulse width is shown in Fig. 4-11.

A crude relationship can be established between the converted incident laser intensity and the x-ray emission characteristics of the plasma by invoking the Stefan-Boltzmann relationship. In units common to laser applications,

$$I_{rad} = 1.03 \times 10^5 \left[\mathrm{W/(cm^2 \cdot eV^4)}\right] \cdot (kT)^4 ,$$

where kT is the black-body temperature in eV. Thus, a black body would radiate as shown in Table 4-1.

Knowledge of the laser intensity and the x-ray conversion efficiency can then be used to obtain an estimate of the region of temperature space the plasma is likely to occupy, assuming that the plasma corresponds to an optically thick black-body emitter.

B. Z-PINCH SOURCES

In a Z-pinch device, the "pinch plasma" is produced by magnetically imploding a cylindrical gas column that fills an electrode gap. The electrodes are connected to a fast capacitor

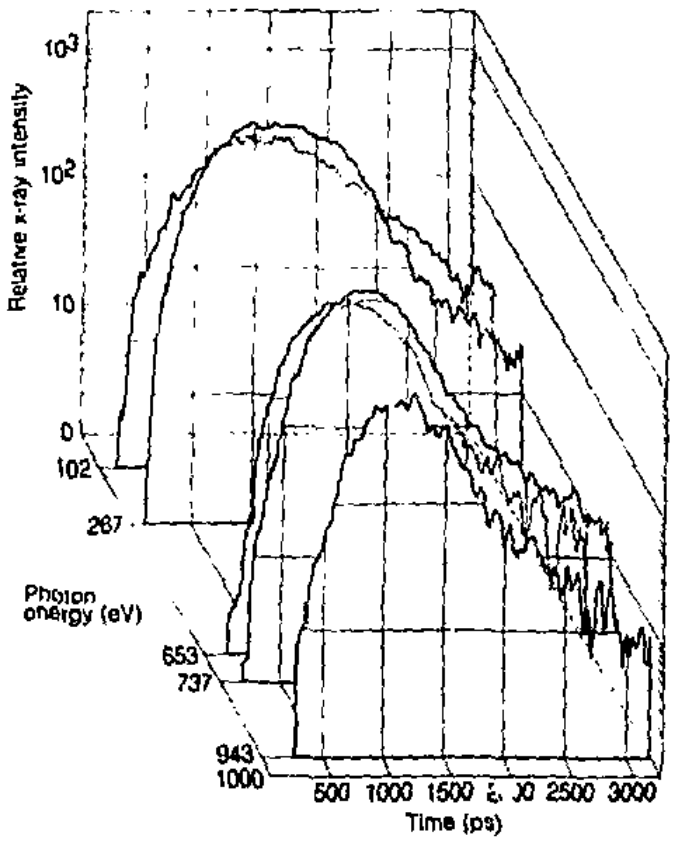

Fig. 4-11. Emission history of a gold plasma generated by a 735-ps, 31-J, 1.06-μm laser pulse incident on a gold slab. The incident power density was 3×10^{14} W/cm^2. The decreasing pulse width with increasing photon energy is apparent. Data were taken with a soft x-ray streak camera in combination with a five-channel layered synthetic microstructure spectrometer with a 10-eV channel width. Relative intensities of the five recorded energy bands were not calibrated. (From Ref. 3.)

Table 4-1. Radiated intensities for several black-body temperatures.

kT (eV)	I_{rad} (W/cm^2)
50	6.4×10^{11}
100	1×10^{13}
150	5.2×10^{13}
200	1.6×10^{14}

bank, which ionizes the gas in several nanoseconds to form a low-temperature plasma sheath. The plasma conducts a large electric current, whose azimuthal magnetic field radially compresses the plasma to create a hot, dense plasma that is an emitter of intense x-rays.

During the implosion, the plasma acquires kinetic energy which is thermalized as the plasma stagnates on axis. This thermal energy is then radiated away in a submicrosecond pulse by bound-bound and free-bound transitions from a wide range of ionization states in the plasma. The resulting spectrum is a quasi-continuum of merged lines and recombination continua, which typically peaks at 100–200 eV and extends beyond 600 eV.

For most applications requiring a small source spot size, the source is viewed along the plasma axis through a hole in the anode. Hot gas debris and energetic electrons are also emitted through the hole and can damage specimens, filters, or windows placed too close to the source. Nonetheless, successful exposures of low-sensitivity photo resists have been made as close as 15 cm to the source, using a baffle array and permanent magnets to divert the debris and electrons. At the other extreme, sensitive materials, such as soft x-ray photographic films, can be exposed tens of meters away in a single

nitrogen, oxygen, neon, argon, and krypton have to optimize the emission of Z-pinch plasmas in different spectral ranges. The radiation spectrum and intensity depend strongly on the working gas, whereas source spot size, pulse width, and jitter do not. Because the soft x-ray yield has a strong inverse dependence on photon energy, the most

intense soft x-radiation ($h\nu \geq 1$ keV) is achieved with a neon plasma [4]. The XUV yield ($h\nu < 1$ keV), on the other hand, generally increases with atomic number because of the greater number of electrons in the radiating shell [4].

The soft x-ray spectrum emitted by a neon plasma consists of *K*-shell lines and recombination continua from both helium-like and hydrogenlike species [4] (see Fig. 4-12). The XUV spectrum emitted by an argon plasma is a quasi-continuum of merged *L*-shell lines and recombination continua from a number of partially ionized argon species [5] (see Fig. 4-13).

REFERENCES

1. W. C. Mead, E. M. Campbell, K. G. Estabrook, R. E. Turner, W. L. Kruer, P. H. Y. Lee, B. Pruett, V. C. Rupert, K. G. Tirsell, G. L. Stradling, F. Ze, C. E. Max, M. D. Rosen, and B. F. Lasinski, "Laser Irradiation of Disk Targets at 0.53 μm Wavelength," *Phys. Fluids* **26**, 2316 (1983).
2. C. D. Hendricks, Ed., *1982 Laser Program Annual Report*, Lawrence Livermore National Laboratory, Livermore, California, UCRL-50021-82 (1983) p. 5-33.
3. G. L. Stradling, D. T. Attwood, and R. L. Kauffman, "A Soft X-Ray Streak Camera," *IEEE J. Quantum Electron.* **QE-19**, 604 (1983).
4. J. S. Pearlman and J. C. Riordan, "Bright Discharge Plasma Sources for X-Ray Lithography," *Proc. SPIE* **537**, in press (1985).
5. J. C. Riordan, J. S. Pearlman, M. Gersten, and J. E Rauch, "Subkilovolt X-Ray Emission from Imploding Wire Plasmas," *AIP Conf. Proc.* **75**, 35 (1981).

Fig. 4-12 *Soft x-ray spectrum and typical pulse shape of a neon plasma source. The lines marked Ne IX are from He-like ions; those marked Ne X are from H-like species*

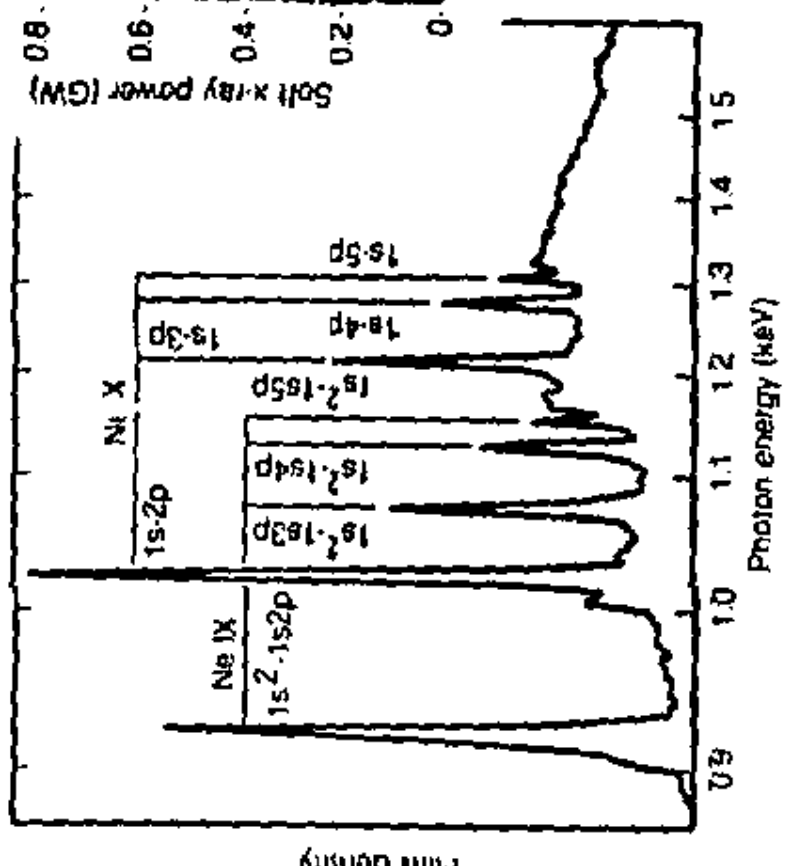

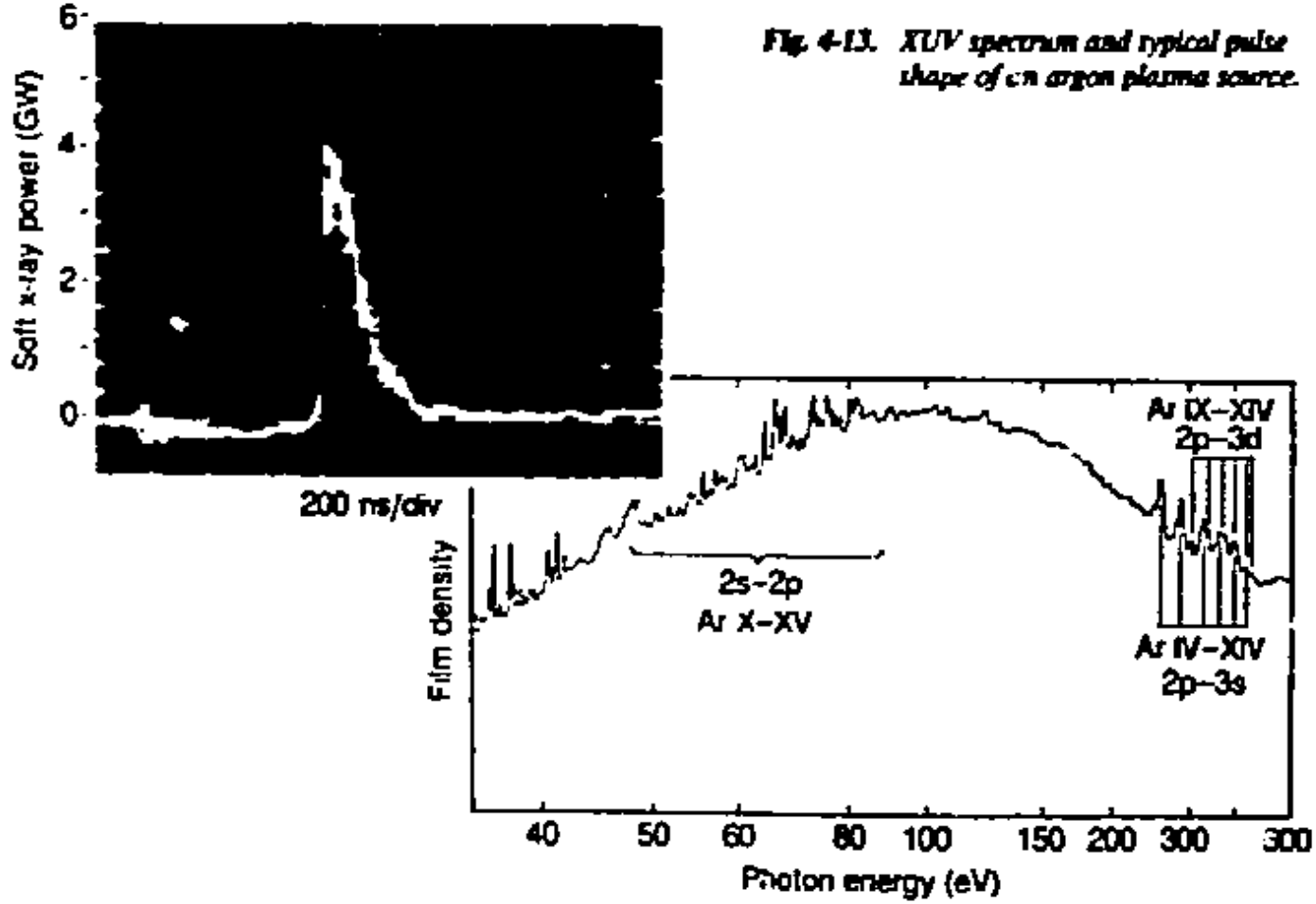

Fig. 4-13. XUV spectrum and typical pulse shape of an argon plasma source.

SECTION 5

OPTICS

5.1 CRYSTAL AND MULTILAYER DISPERSIVE ELEMENTS

James H. Underwood

Short-wavelength electromagnetic radiation (x-rays and extreme ultraviolet light) is commonly analyzed by use of periodic structures, which split the incident beam into a large number N of separate beams. Between any beam i and the beam $i + 1$, the optical path difference is constant. After leaving the periodic structure, the beams are recombined and caused to interfere, whereupon the spectrum of the incident radiation is produced. Dispersion of radiation by a periodic structure is thus formally equivalent to multiple-beam interferometry.

Structures that are periodic across their surface and that produce the N interfering beams by division of the incident wave front are called gratings and are treated in Section 5.3. Here, we consider crystals and multilayer structures, which produce the N interfering beams by division of the incident amplitude.

The spectrum of the incident radiation is dispersed in angle according to the Bragg equation:

$$n\lambda = 2d \sin\theta$$

where n is an integer representing the order of the reflection, λ is the wavelength of the incident radiation, d is the repeat

period of the multilayer or crystal structure, and θ is the angle of glancing incidence (the complement of the conventional optical angle of incidence).

Multilayer structures fall into four separate categories: naturally occurring crystals (i.e., minerals), artificially grown crystals, Langmuir-Blodgett multilayer films, and sputtered or evaporated multilayers.

A. CRYSTALS AND LANGMUIR-BLODGETT FILMS

For a crystal, d is the lattice spacing, the perpendicular distance between the successive planes of atoms contributing to the reflection. These planes are designated by their Miller indices [(hkl) or, in the case of crystals belonging to the hexagonal group, $(hkil)$].

Langmuir-Blodgett multilayer films are made from the heavy-metal (lead, barium, etc.) salts of the aliphatic carboxylic ("fatty") acids $C_nH_{2n}O_2$. These films are laid down on a substrate in successive monolayers, with the metal atoms on one side of the monolayer and the fatty acid chain on the other. The films are first laid on the surface of water as a condensed monolayer under a constant surface pressure, then transferred to the substrate in a dipping process, which builds up the multilayer structure layer by layer. The orientation of the molecules alternates with each successive monolayer, so that d, the repeat period of the structure, is twice the length of the fatty acid chain. Multilayers of this kind can be built with the salts of lauric (dodecanoic) acid (12 carbon atoms, $2d = 70$ Å) through melissic (triacontanoic) acid (30 carbon atoms, $2d = 160$ Å). In general, salts of the naturally occurring acids (those with an even number of carbon atoms) can be layered in this way, whereas those that must be made synthetically cannot.

For $2d$ values greater than about 25 Å, the choice of natural crystals is very limited, and those available (such as prochlorite) are likely to be small and of poor quality. Using vacuum deposition techniques, it is now possible to make artificial layered structures with periods (d) of 15 Å and greater. These sputtered or evaporated multilayers, discussed below, can be used as dispersing elements in the gap between the hydrogen (or "acid") phthalates, such as KAP ($2d = 26$ Å), and lead laurate ($2d = 70$ Å). Together with the Langmuir-Blodgett structures, these devices form a bridge

between the region where crystals are useful and the UV region of conventional multilayer technology.

Table 5-1, which begins on p. 5-7, is an expansion and revision of the one compiled by E. P. Bertin [1]. The crystals and multilayers are arranged in order of increasing $2d$ spacing.

Column 1 is the serial number of the crystal or multilayer in the table.

Column 2 gives common and chemical names and commonly used letter symbols, if any. Only the lead salts are listed for the Langmuir-Blodgett multilayers. The barium or other divalent metal salt usually has a similar $2d$ spacing to the lead salt, but a lower diffracted intensity.

Column 3 gives the Miller indices [(hkl), or $(hkil)$ for hexagonal crystals)] of the diffracting planes parallel to the surface of the dispersive element. A question mark (?) indicates that the crystal is developmental and that the indices have not been ascertained. An asterisk following the indices indicates that, when reference is made to this crystal in the literature without specification of (hkl) or $2d$, it is likely to be this "cut" that is meant. LBF denotes a Langmuir-Blodgett film.

Column 4 gives the value of $2d$ in angstroms. The value of $2d$ also represents the longest wavelength that the structure can diffract.

Column 5 gives the chemical formula for the crystal substance. For organic compounds, the formula is given in a form that indicates the molecular structure.

Column 6 gives the wavelength region lying in the 2θ interval between 10° and 140°. The analyzer should be used outside these limits in special cases only.

Column 7 gives remarks on the principal applications of the analyzer and its limitations. Relative intensities are indicated where known or appropriate.

B. SPUTTERED OR EVAPORATED MULTILAYER MIRRORS AND DISPERSIVE ELEMENTS

Multilayer x-ray reflectors can also be made by vacuum deposition. These structures are made up of ultrathin layers of two different materials, usually elemental, which are laid down on the substrate by alternately exposing it to sources (either sputtering or evaporation sources) of two different vapors. By careful control of deposition conditions, layers as thin as 7.5 Å can be laid down.

Normally a sputtered or evaporated multilayer reflector is made up of layers of a material A with thickness t_A and having a high value of δ (the refractive index decrement, see Sec. 2.7) alternating with "spacer" layers of a material B with thickness t_B and having as low a value of δ as possible in the wavelength region of interest. For example, the use of tungsten (or a similar refractory heavy metal, such as molybdenum or tungsten-rhenium alloy), with carbon as the spacer, has been found to be effective over a wide range of the x-ray and soft x-ray spectrum.

When the layers are strictly periodic in depth, as described above, the relation between the reflected wavelength and the glancing angle θ is again given by the Bragg relation, where d is now the period $t_A + t_B$. It should be noted that in the soft x-ray region, where values of both δ and β (the absorption index, see Sec. 2.7) may be relatively high, the Bragg equation should be corrected for the effects of refraction and absorption. This is best accomplished using a program designed to compute the reflectivity of multilayers; many programs designed for carrying out such calculations for visible-light interference coatings will work for the x-ray and extreme UV case without modification. Such programs are also required to calculate the reflectivity of structures that are not periodic in depth, but rather graded in some way to widen the bandpass, increase reflectivity for a fixed number of layers, etc.

Since the number of possible material combinations is quite large, being limited mainly by considerations of material compatibility and "depositability," only some examples of the performance of these multilayers can be given here. In Fig. 5-1, we present the calculated normal-incidence peak reflectivity of idealized multilayer coatings of material combinations having the optimum optical constants. The number of layer pairs required to achieve this reflectivity is also plotted on the same scale. In Fig. 5-2, the Bragg reflection characteristics of sputtered or evaporated multilayer structures of tungsten and carbon are presented. For tabulations of the parameters plotted in Fig. 5-2 and for details on how they were calculated, see Ref. 2.

REFERENCES

1. E. P. Bertin, "Crystals and Multilayer Langmuir-Blodgett Films Used as Analyzers in Wavelength-Dispersive X-Ray

Spectrometers," in J. W. Robinson, Ed., *Handbook of Spectroscopy* (CRC Press, Cleveland, 1974), vol. 1, p. 238.
2. B. L. Henke, P. Lee, T. J. Tanaka, R. L. Shimabukuro, and B. K. Fujikawa, "Low-Energy X-Ray Interaction Coefficients: Photoabsorption, Scattering, and Reflection," *At. Data Nucl. Data Tables* 27, 1 (1982).
3. A. Rosenbluth, *Reflecting Properties of X-Ray Multilayer Devices*, Ph.D. thesis, University of Rochester (1983).

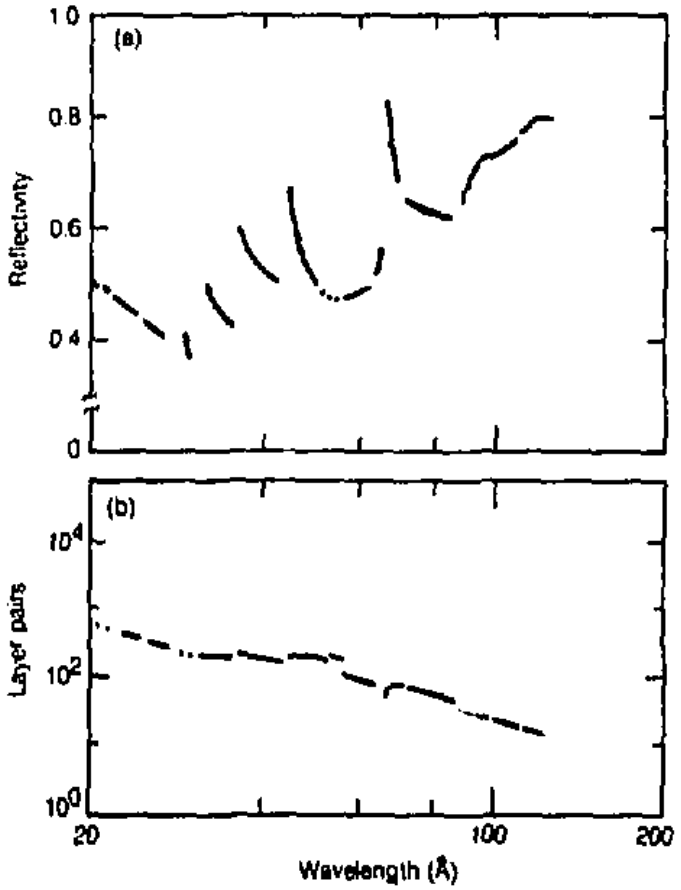

Fig. 5-1. *(a) Calculated normal-incidence peak reflectivities of idealized multilayer coatings of optimum material combinations and (b) the required number of layer pairs. (Computations from Ref. 3.)*

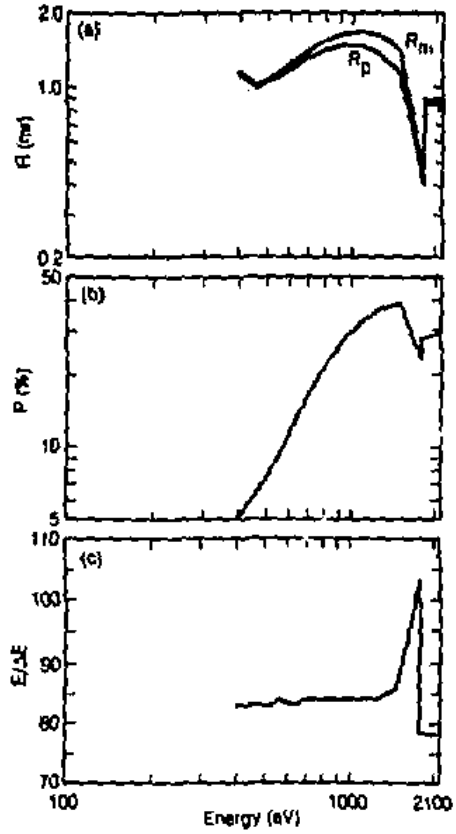

Fig. 5-2. *Bragg reflection characteristics, plotted as functions of energy, for a sputtered or evaporated tungsten-carbon multilayer. The number of tungsten-carbon double layers was taken as 100, the 2d spacing as 40 Å, and the fractional thickness Γ of the tungsten layer as 0.4 ($t_W = \Gamma d$). (a) Integrated reflection efficiency calculated with a relation derived for a mosaic crystal model (R_m) and by integrating a modified Darwin-Prins relation (R_p). Numerical integration limits were $\pm 5\omega$, where ω is the diffraction width at half maximum. (b) Percentage reflectivity P at the peak, as given by the modified Darwin-Prins relation. (c) Resolving power of the analyzer, $E/\Delta E$, where ΔE is the equivalent energy diffraction width. (From Ref. 2.)*

Table 5-1. *Selected data for crystals and Langmuir-Blodgett multilayer films used as dispersive elements in x-ray spectrometers and monochromators.*

No.	Crystal	Miller indices	2d (Å)	Chemical formula	Useful wavelength region (Å)	Applications, remarks
1	α-Quartz, silicon dioxide	$(50\bar{5}2)$	1.624	SiO_2	0.142–1.55	Shortest 2d of any practical crystal. Good for high-Z K-lines excited by 100-kV generators.
2	Lithium fluoride	(422)	1.652	LiF	0.144–1.58	Better than quartz $(50\bar{5}2)$ for the same applications.
3	Corundum, aluminum oxide	(146)	1.660	Al_2O_3	0.145–1.58	Same applications as quartz $(50\bar{5}2)$.
4	Lithium fluoride	(420)	1.801	LiF	0.157–1.72	Similar to LiF (422).
5	Calcite, calcium carbonate	(633)	2.02	$CaCO_3$	0.176–1.95	
6	α-Quartz, silicon dioxide	$(22\bar{4}3)$	2.024	SiO_2	0.177–1.96	
7	α-Quartz, silicon dioxide	$(31\bar{4}0)$	2.3604	SiO_2	0.205–2.25	Transmission-crystal optics.
8	α-Quartz, silicon dioxide	$(22\bar{4}0)$	2.451	SiO_2	0.213–2.37	
9	Topaz, hydrated aluminum fluorosilicate	(303)[a]	2.712	$Al_2(F,OH)_2SiO_4$	0.236–2.59	Improves dispersion for V-Ni K-lines and rare earth L-lines.
10	Corundum, aluminum oxide, sapphire, alumina	(030)	2.748	Al_2O_3	0.240–2.62	Diffracted intensity ~ 2–4X topaz (303) and quartz (203) with the same or better resolution.

Table 5-1. *Selected data for crystals and Langmuir-Blodgett multilayer films (continued).*

No.	Crystal	Miller indices	2*d* (Å)	Chemical formula	Useful wavelength region (Å)	Applications, remarks
11	α-Quartz, silicon dioxide	$(20\bar{2}3)$	2.749	SiO_2	0.240–2.62	Same applications as topaz (303) and LiF (220).
12	Topaz	(006)	2.795	$Al_2(F,OH)_2SiO_4$	0.244–2.67	
13	Lithium fluoride	(220)	2.848	LiF	0.248–2.72	Same applications as topaz (303) and quartz $(20\bar{2}3)$, with 2–4X their diffracted intensity. Diffracted intensity ~ 0.4–0.8X LiF (200).
14	Mica, muscovite	(331)	3.00	$K_2O \cdot 3Al_2O_3 \cdot 6SiO_2 \cdot 2H_2O$	0.262–2.86	Transmission-crystal optics (Cauchois, DuMond type).
15	Calcite, calcium carbonate	(422)	3.034	$CaCO_3$	0.264–2.93	
16	α-Quartz, silicon dioxide	$(21\bar{3}1)$	3.082	SiO_2	0.269–2.94	
17	α-Quartz, silicon dioxide	$(11\bar{2}2)$	3.636	SiO_2	0.317–3.47	
18	Silicon	(220)	3.840343	Si	0.335–3.66	Lattice period known to high accuracy.
19	Fluorite, calcium fluoride	(220)	3.862	CaF_2	0.337–3.68	
20	Germanium	(220)	4.00	Ge	0.349–3.82	
21	Lithium fluoride	(200)*	4.027	LiF	0.351–3.84	Best general crystal for K *K*- to Lr *L*-lines. Highest intensity for

						largest number of elements of any crystal. Combines high intensity and high dispersion.
22	Aluminum	(200)	4.048	Al	0.353 - 3.86	Curved, especially doubly curved, optics.
23	α-Quartz, silicon dioxide	$(20\bar{2}0)$	4.246	SiO_2	0.370–4.11	"Prism" cut.
24	α-Quartz, silicon dioxide	$(10\bar{1}2)$	4.564	SiO_2	0.398–4.35	Used in prototype Laue multichannel spectrometer.
25	Topaz	(200)	4.638	$Al_2(F,OH)_2SiO_4$	0.405–4.43	
26	Aluminum	(111)	4.676	Al	0.408–4.46	Curved, especially doubly curved, optics.
27	α-Quartz, silicon dioxide	$(11\bar{2}0)$	4.912	SiO_2	0.428–4.75	
28	Gypsum, calcium sulfate dihydrate	(002)	4.990	$CaSO_4 \cdot 2H_2O$	0.435–4.76	Efflorescent: loses water in vacuum to become Plaster of Paris.
29	Rock salt, sodium chloride	(200)	5.641	NaCl	0.492–5.38	S Kα and Cl Kα in light matrices. Like LiF (200), good general crystal for S K to La L.
30	Calcite, calcium carbonate	(200)	6.071	$CaCO_3$	0.529–5.79	Very precise wavelength measurements. *Extremely high* degree of crystal perfection with resultant sharp lines. Replaced NaCl (200) as standard for the x-unit. Large pieces can be obtained.
31	Ammonium dihydrogen phosphate (ADP)	(112)	6.14	$NH_4H_2PO_4$	0.535–5.86	

Table 5-1. *Selected data for crystals and Langmuir-Blodgett multilayer films (continued).*

No.	Crystal	Miller indices	2d (Å)	Chemical formula	Useful wavelength region (Å)	Applications, remarks
32	Silicon	(111)[9]	6.271	Si	0.547–5.98	Very rugged and stable general-purpose crystal. High degree of perfection obtainable.
33	Sylvine, potassium chloride	(200)	6.292	KCl	0.549–6.00	
34	Fluorite, calcium fluoride	(111)	6.306	CaF_2	0.550–6.02	Very weak second order, strong third order.
35	Germanium	(111)[9]	6.532	Ge	0.570–6.23	Eliminates second order. Useful for intermediate- and low-Z elements where Ge $K\alpha$ emission is eliminated by pulse-height selection.
36	Potassium bromide	(200)	6.584	KBr	0.574–6.29	
37	α-Quartz, silicon dioxide	$(10\bar{1}1)$	6.687	SiO_2	0.583–6.38	P $K\alpha$ in low-Z matrices, especially in calcium. Intensity for P–K K-lines greater than EDDT, but less than PET.
38	Graphite	(002)	6.708	C	0.585–6.40	P, S, Cl K-lines. P $K\alpha$ intensity >5X EDDT. Relatively poor resolution, but high integrated reflectivity.
39	Ammonium hydrogen citrate	(?)	7.38	$C(OH)(COOH)(CH_2COONH_4)_2$	0.644–7.04	

40	Indium antimonide	(111)	7.4806	InSb	0.632–7.23	Important for *K*-edge of Si.
41	Ammonium dihydrogen phosphate (ADP)	(200)	7.5	$NH_4H_2PO_4$	0.654–7.16	Higher intensity than EDDT.
42	Topaz	(002)	8.374	$Al_2(F,OH)_2SiO_4$	0.730–7.99	
43	*α*-Quartz, silicon dioxide	$(10\bar{1}0)^a$	8.512	SiO_2	0.742–8.12	Same applications as EDDT and PET; higher resolution, but lower intensity.
44	Pentaerythritol (PET)	(002)	8.742	$C(CH_2OH)_4$	0.762–8.34	Al, Si, P, S, Cl *K*α. Intensities ~1.5–2× EDDT, ~2.5× KHP. Good general crystal for Al–Sc *K*α. Low background. Soft; deteriorates with age and exposure to x-rays. Must be stored in desiccator.
45	Ammonium tartrate	(?)	8.80	$(CHOH)_2(COONH_4)_2$	0.767–8.4	
46	Ethylenediamine-d-tartrate (EDDT, EDdT, EDT)	(020)	8.808	$NH_2-CH_2-CH_2-NH_2$ $COOH-(CHOH)_2-COOH$	0.768–8.40	Same applications as PET, but lower intensity, substantially lower thermal expansion coefficient. Rugged and stable.
47	Ammonium dihydrogen phosphate (ADP)	$(101)^a$	10.640	$NH_4H_2PO_4$	0.928–10.15	Mg *K*α. Same applications as PET, EDDT, but lower intensity.
48	Na β-alumina	(0004)	11.24	$NaAl_{11}O_{17}$	0.980–10.87	
49	Oxalic acid dihydrate	(001)	11.92	$(COOH)_2\ 2H_2O$	1.04–11.37	
50	Sorbitol hexacetate (SHA)	(110)	13.98	$CHOH-CO-CH_3$ $(COH-CO-CH_3)_4$ $CHOH-CO-CH_3$	1.22–13.34	Applications similar to ADP (101) and gypsum (020). H^{3+} resolution; stable in vacuum. Available in small pieces only.

Table 5-1. *Selected data for crystals and Langmuir-Blodgett multilayer films (continued).*

No.	Crystal	Miller indices	2d (Å)	Chemical formula	Useful wavelength region (Å)	Applications, remarks
51	Rock sugar, sucrose	(001)	15.12	$C_{12}H_{22}O_{11}$	1.32–14.42	
52	Gypsum, calcium sulfate dihydrate	(020)[a]	15.185	$CaSO_4 \cdot 2H_2O$	1.32–14.49	Na Kα. Inferior to KHP, RHP, and beryl. Poor in vacuum (efflorescent).
53	Beryl	(10$\bar{1}$0)[a]	15.954	$3BeO \cdot Al_2O_3 \cdot 6SiO_2$	1.39–15.22	*Difficult to obtain. Good* specimens have $I_d/I_\lambda \sim$ 2500–3000 at 12 Å. 2d may vary among specimens.
54	Bismuth titanate	(040)	16.40	$Bi_4(TiO_3)_3$	1.43–15.65	
55	Itaconic acid, methylenebutanedioic acid	(020)	18.30	$CH_2C(COOH)CH_2COOH$	1.61–17.65	
56	Mica, muscovite	(002)[a]	19.84	$K_2O \cdot 3Al_2O_3 \cdot 6SiO_2 \cdot 2H_2O$	1.73–18.93	Easy to obtain. Easily bent; good for curved-crystal spectrometers, spectrographs. Cleavage plane. Higher orders may be strong.
57	Silver acetate	(001)	20.0	CH_3COOAg	1.74–19.08	
58	Rock sugar, sucrose	(100)	20.32	$C_{12}H_{22}O_{11}$	1.75–19.19	
59	Na β-alumina	(0002)	22.49	$NaAl_{11}O_{17}$	1.96–21.74	
60	Thallium hydrogen phthalate (THP, TlHP, TAP,[a] TlAP[b])	(100)	25.9	$TlHC_8H_4O_4$	2.26–24.7	Same applications as RHP, RHP.

61	Rubidium hydrogen phthalate (RHP, RbHP, RAP,[a] RbAP[b])	(100)	26.121	$RbHC_8H_4O_4$	2.28–24.92	*Diffracted intensity* ~3X KHP for Na, Mg, Al $K\alpha$ and Cu $L\alpha_1$, ~4X KHP for F $K\alpha$, ~8X KHP for O $K\alpha$.
62	Potassium hydrogen phthalate (KHP, KAP[b])	(100)	26.632	$KHC_8H_4O_4$	2.32–25.41	Good general crystal for all low-Z elements down to O
63	Clinochlore (hydrated Mg Al Fe silicate aluminate)	(001)	28.39		2.48–27.09	O $K\alpha$ intensity ~4X KHP but only ~0.2X Pb stearate. Difficult to obtain good specimens.
64	Pennidite (similar to clinochlore)	(001)	28.4		2.48–27.1	Same applications as clinochlore.
65	Potassium hydrogen cyclohexane-1,2-dicarboxylate	(?)	31.2	$KHC_{10}H_{14}O_4$	2.72–29.76	High resolution; good crystallinity.
66	Tetradecanoamide	(?)	~54	$CH_3(CH_2)_{12}CONH_2$	4.71–51.5	Ultralong-wavelength region down to C $K\alpha$.
67	Hexadecyl hydrogen maleate (HHM)	(?)	58.0	$CH_3(CH_2)_{15}OOC-CH{=}CH-COOH$	5.06–55.3	Ultralong-wavelength region down to C $K\alpha$
68	Octadecyl hydrogen maleate (OHM)	(?)	63.3	$CH_3(CH_2)_{17}OOC-CH{=}CH-COOH$	5.54–60.6	Ultralong wavelength region down to C $K\alpha$.
69	Lead laurate, lead dodecanoate	LBF	~70	$[CH_3(CH_2)_{10}COO]_2Pb$	6.10–66.8	Ultralong-wavelength region down to B $K\alpha$
70	Behenyl hydrogen maleate (BHM)	(?)	~74	$CH_3(CH_2)_{21}OOC-CH{=}CH-COOH$	6.45–70.6	Ultralong-wavelength region down to B $K\alpha$.
71	Lead myristate, lead tetradecanoate (LTD)	LBF	80.5	$[CH_3(CH_2)_{12}COO]_2Pb$	7.03–76.8	Ultralong-wavelength region down to B $K\alpha$

Table 5-1. Selected data for crystals and Langmuir-Blodgett multilayer films (continued).

No.	Crystal	Miller indices	2d (Å)	Chemical formula	Useful wavelength region (Å)	Applications, remarks
72	Dioctadecyl terephthalate (OTO)	(?)	~84		7.32–80.1	Ultralong-wavelength region down to B $K\alpha$.
73	Lead palmitate, lead hexadecanoate	LBF	~90	$[CH_3(CH_2)_{14}COO]_2Pb$	7.85–85.9	Ultralong-wavelength region down to B $K\alpha$.
74	Dioctadecyl adipate (OAO)	(?)	~94	$(CH_2)_4[COO(CH_2)_{17}CH_3]_2$	8.20–89.7	Ultralong-wavelength region down to B $K\alpha$.
75	Octadecyl hydrogen succinate (OHS)	(?)	~97	$CH_3(CH_2)_{17}OOC-CH_2CH_2COOH$	8.46–92.5	Ultralong-wavelength region down to B $K\alpha$.
76	Lead stearate decanoate, lead octadecanoate decanoate (LSD[b],LODF)	LBF	~100	$CH_3(CH_2)_{16}COOPbOOC(CH_2)_8CH_3$	8.72–95.4	Ultralong-wavelength region down to B $K\alpha$.[1] Diffracted intensity ~2X Pb stearate at wavelengths < 44 Å.
77	Lead stearate, lead octadecanoate (LODF)	LBF	100.4	$[CH_3(CH_2)_{16}COO]_2Pb$	8.75–95.8	Ultralong-wavelength region down to B $K\alpha$. LOD/KHP intensity ratios slightly <1 for

						Al $K\alpha$, ~1 for Mg $K\alpha$, ~1.5 for Na $K\alpha$, ~2.5 for F $K\alpha$.
78	*Lead arachidate, lead* eicosanoate	LBF	~110	$[CH_3(CH_2)_{18}COO]_2Pb$	9.6–105	Ultralong-wavelength region down to B $K\alpha$.
79	Lead behenate, lead docosanoate	LBF	~120	$[CH_3(CH_2)_{20}COO]_2Pb$	10.5–114	Ultralong-wavelength region down to Be $K\alpha$.
80	Lead lignocerate, lead carnaubate, lead tetracosanoate (LTE)	LBF	~126	$[CH_3(CH_2)_{22}COO]_2Pb$	11.4–124	Ultralong-wavelength region down to Be $K\alpha$.
81	*Lead cerotate, lead* hexacosanoate	LBF	~140	$[CH_3(CH_2)_{24}COO]_2Pb$	12.2–134	Ultralong-wavelength region down to Be $K\alpha$.
82	Lead melissate, *lead* triacontanoate (LTC)	LBF	~156	$[CH_3(CH_2)_{28}COO]_2Pb$	14.0–156	Ultralong-wavelength region down to Be $K\alpha$.

[a]See text.

[b]For rubidium or potassium *acid* phthalate, which is not preferred nomenclature.

[c]Not to be confused with the hallucinogenic drug *lysergic acid diethylamide*.

[d]The symbol LOD is used for both lead octadecanoate (stearate) and lead octadecanoate dioctanoate.

5.2 SPECULAR REFLECTIVITIES FOR GRAZING-INCIDENCE MIRRORS

Burton L. Henke

Figures 5-3 through 5-10 give reflectivities for eight grazing-incidence x-ray mirrors, calculated from the scattering factors tabulated in Section 2.7. The calculations, which are summarized in B. L. Henke, P. Lee, T. J. Tanaka, R. L. Shimabukuro, and B. K. Fujikawa, "Low-Energy X-Ray Interaction Coefficients: Photoabsorption, Scattering, and Reflection," *At. Data Nucl. Data Tables* 27, 1 (1982), assume unpolarized incident radiation and perfectly smooth mirror surfaces.

The calculations are also based on the assumption that, in the low-energy x-ray region, the atoms within a condensed system act independently as scattering dipoles. The total atomic dipole moment per unit electric field amplitude is thus proportional to the average atomic scattering factor for the medium. Results for grazing angles from 10 to 785 mr at energies between 100 and 1740 eV are given in the reference cited above.

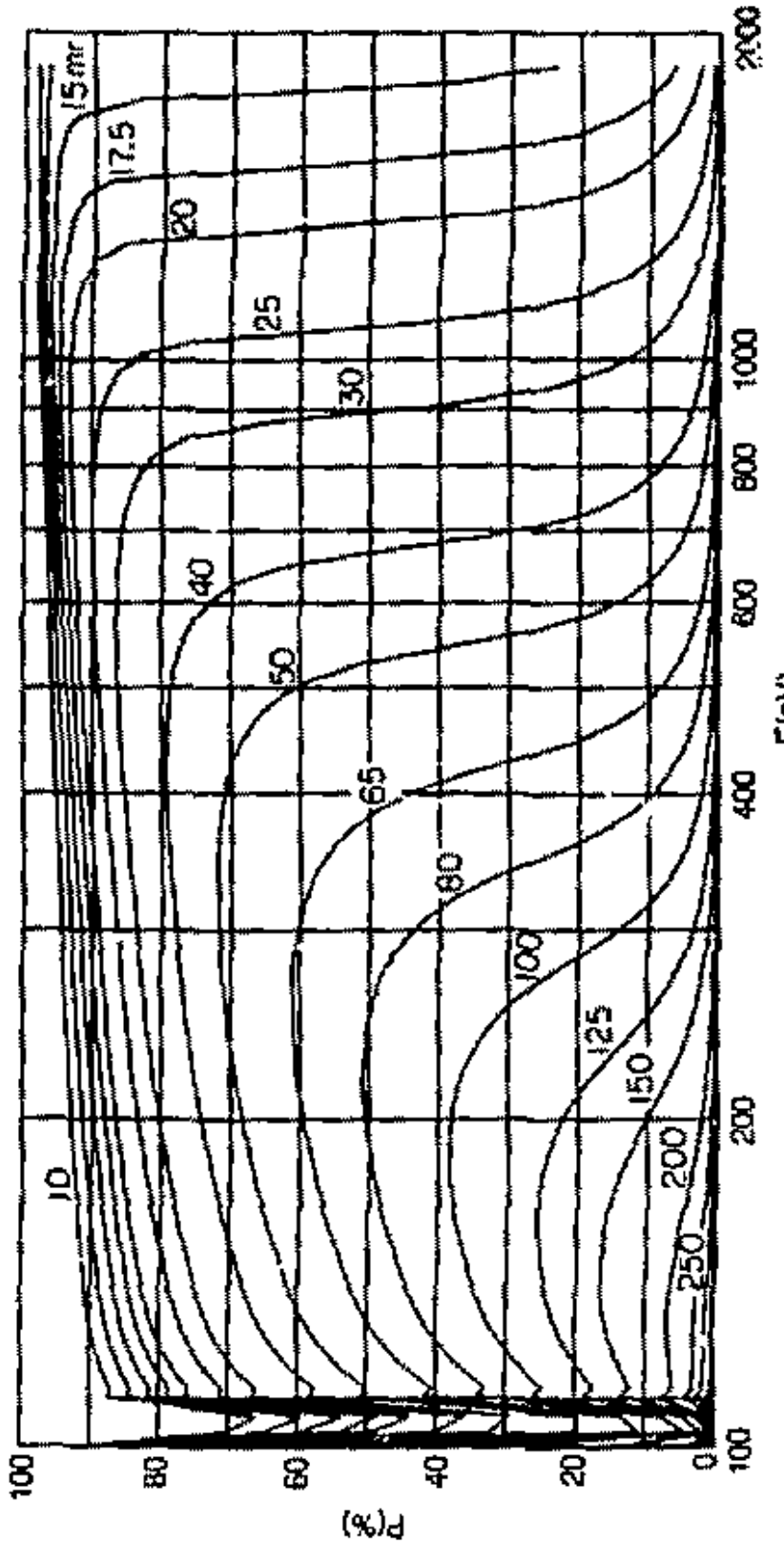

Fig. 5-1. Specular reflectivity for beryllium, assuming a mirror density of 1.85 g · cm⁻³.

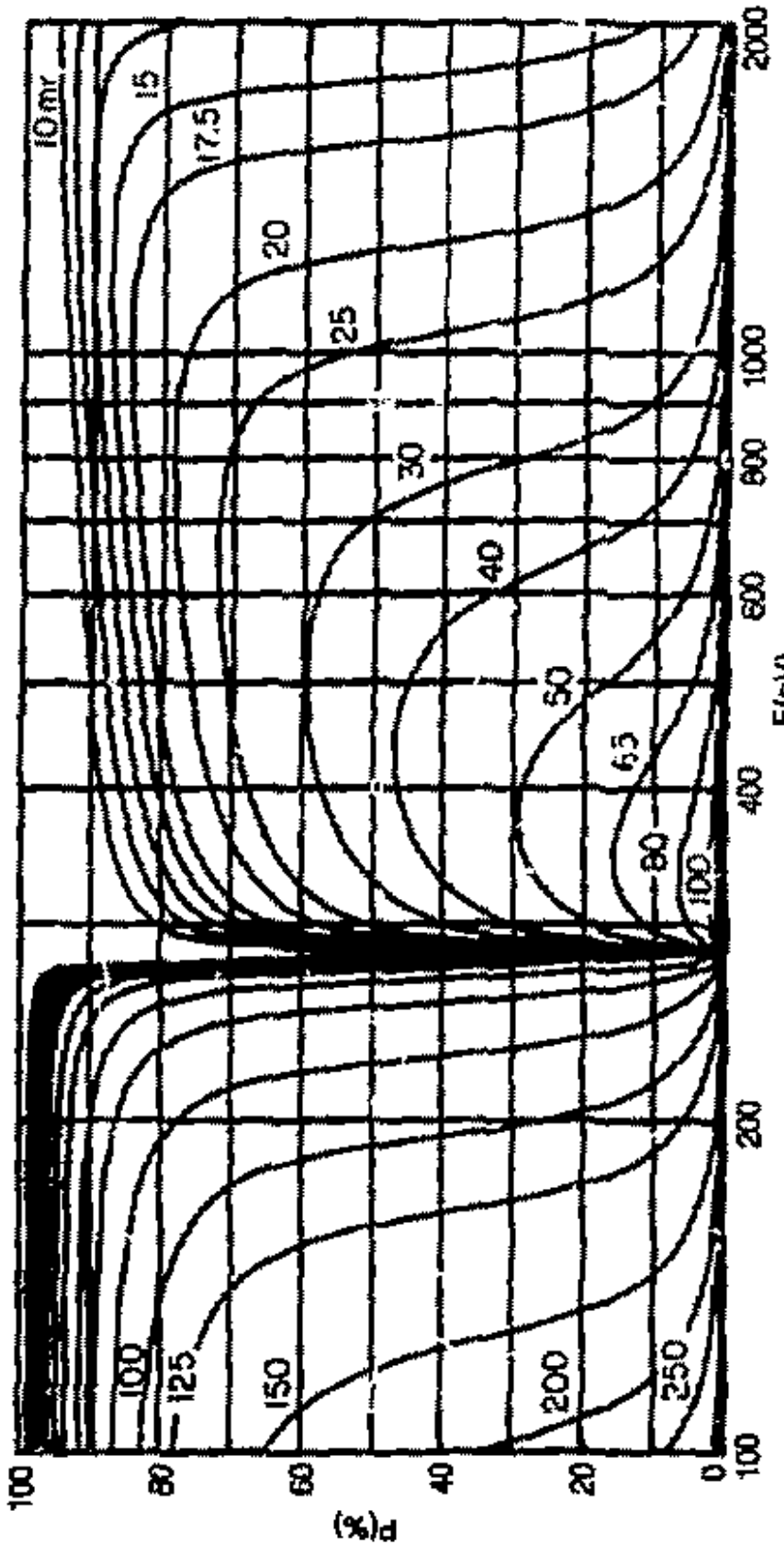

Fig. 5-4 *Specular reflectivity for carbon, assuming a mirror density of 2.20 g · cm^{-3}.*

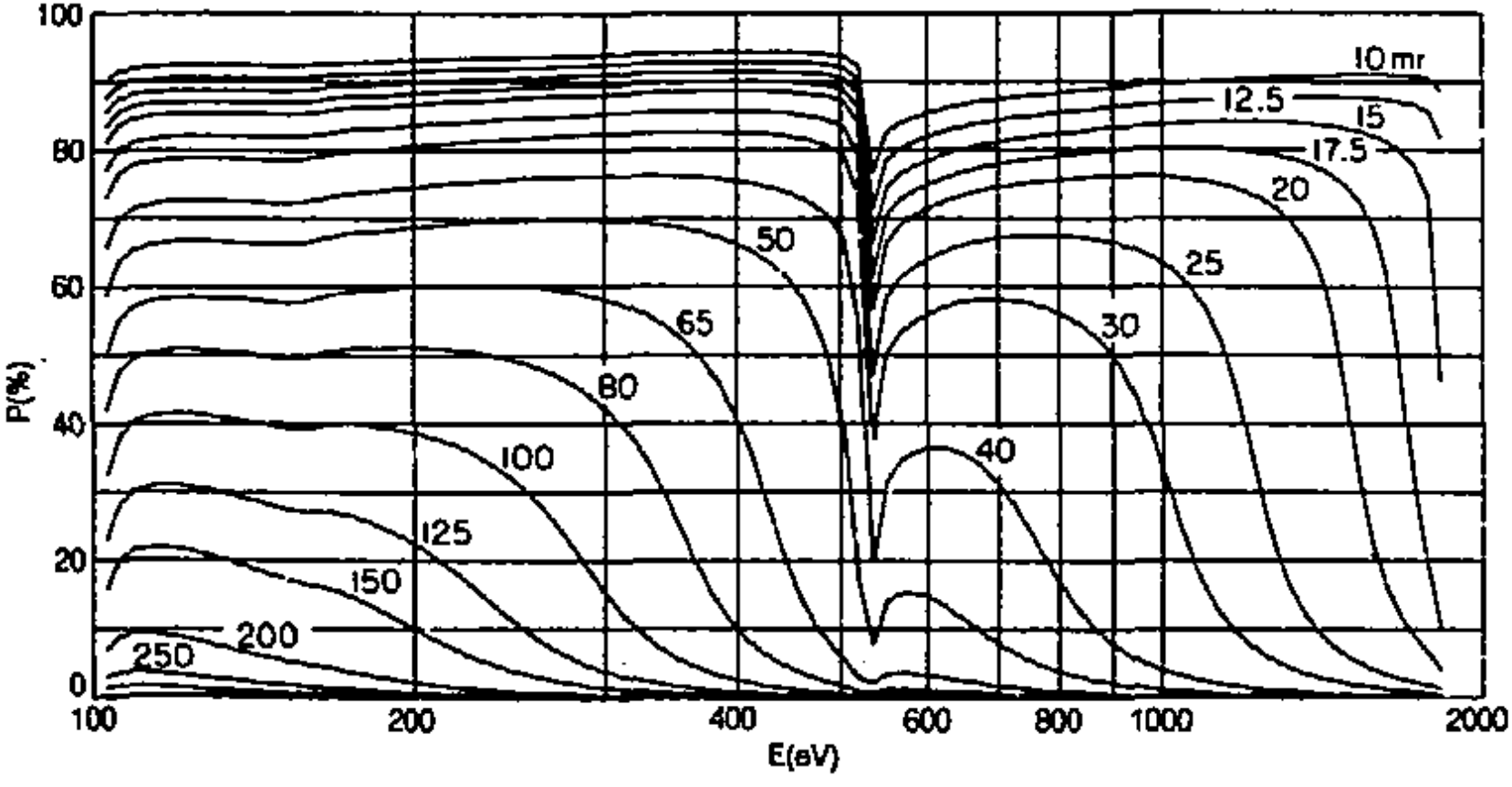

Fig. 5-5. Specular reflectivity for fused quartz, assuming a mirror density of 2.20 g · cm $^{-3}$.

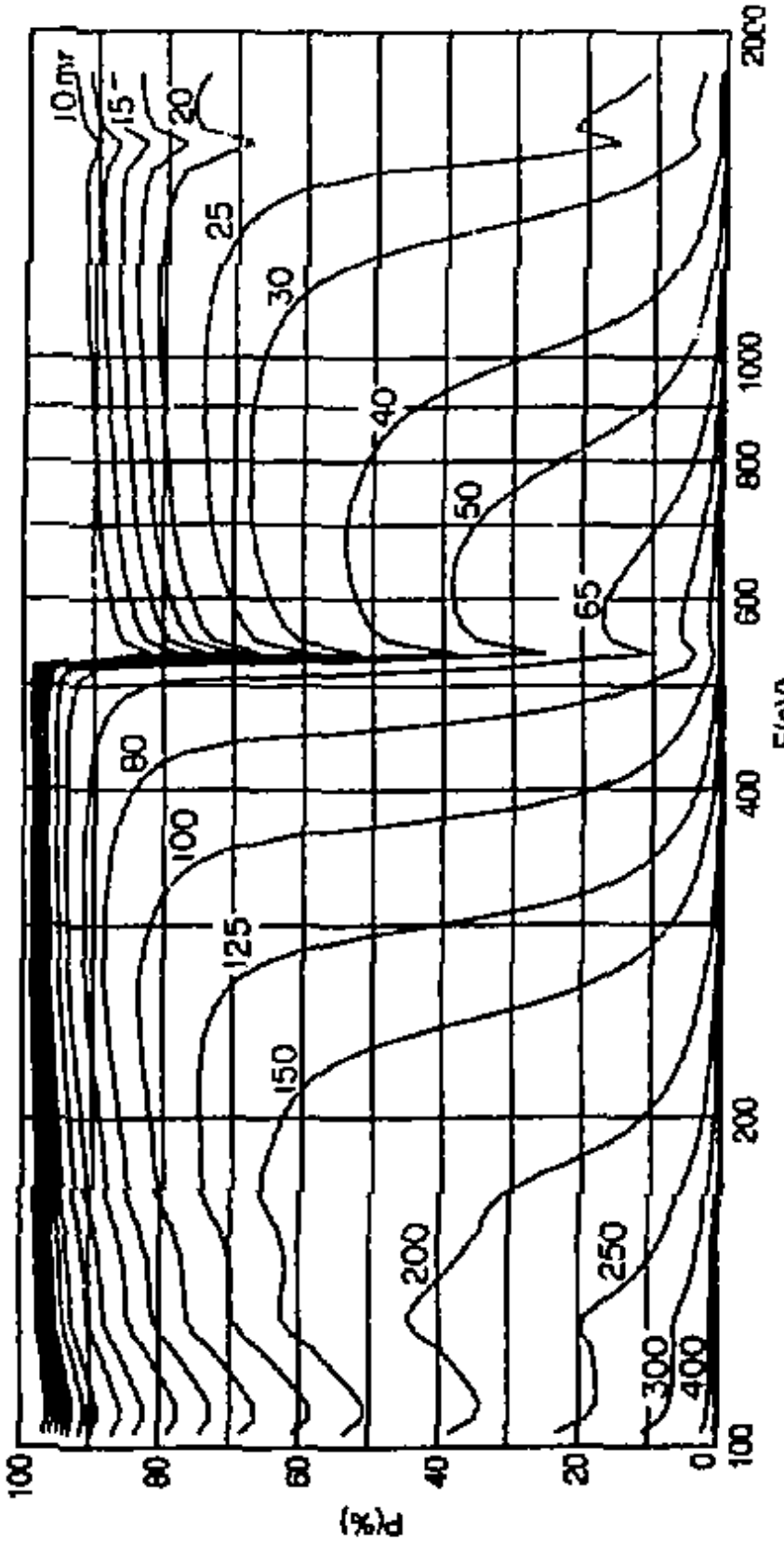

Fig. 5-6. Specular reflectivity for aluminum oxide, assuming a mirror density of 3.96 g · cm⁻³.

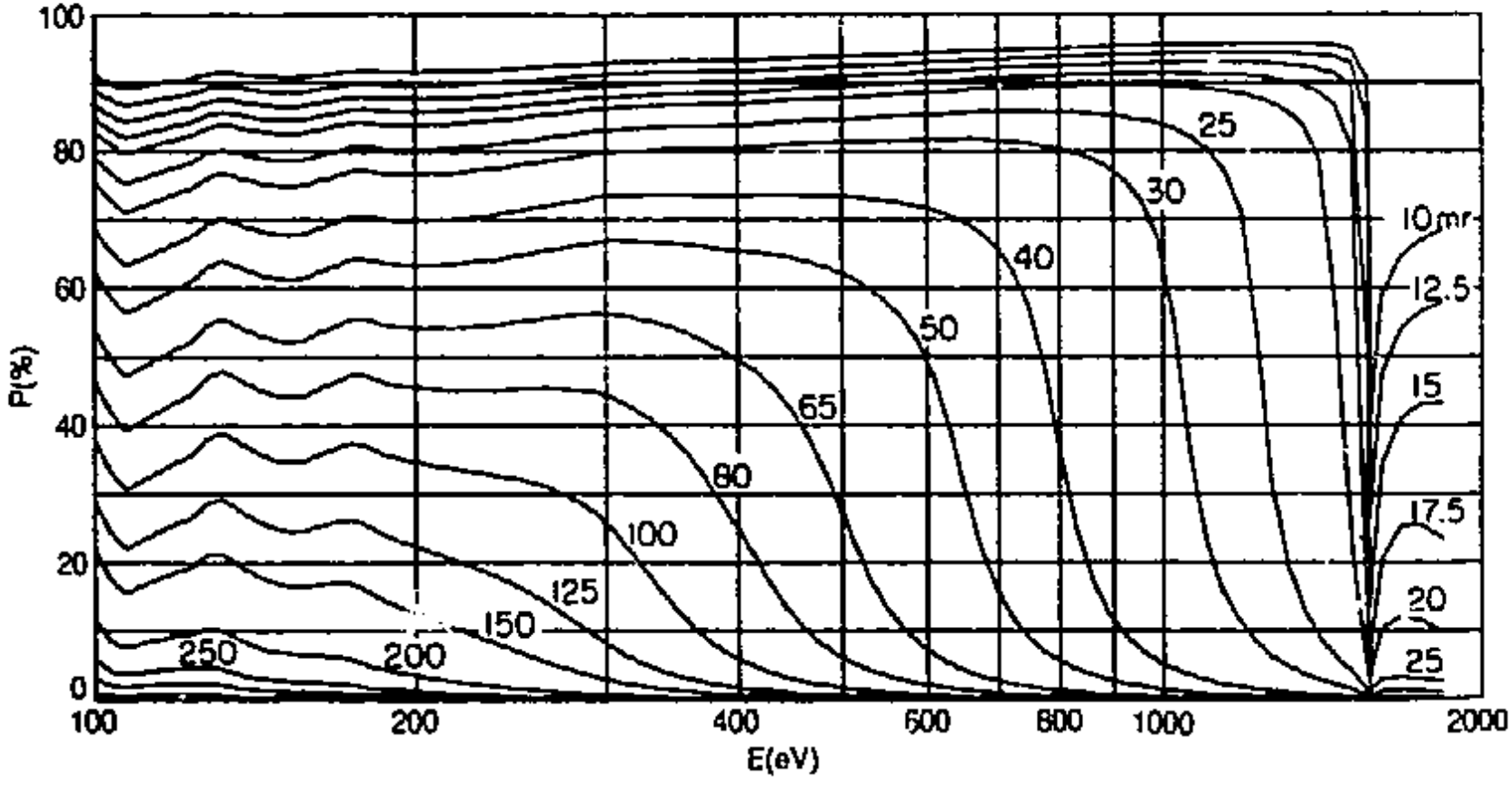

Fig. 5-7. Specular reflectivity for aluminum, assuming a mirror density of 2.70 g · cm $^{-3}$.

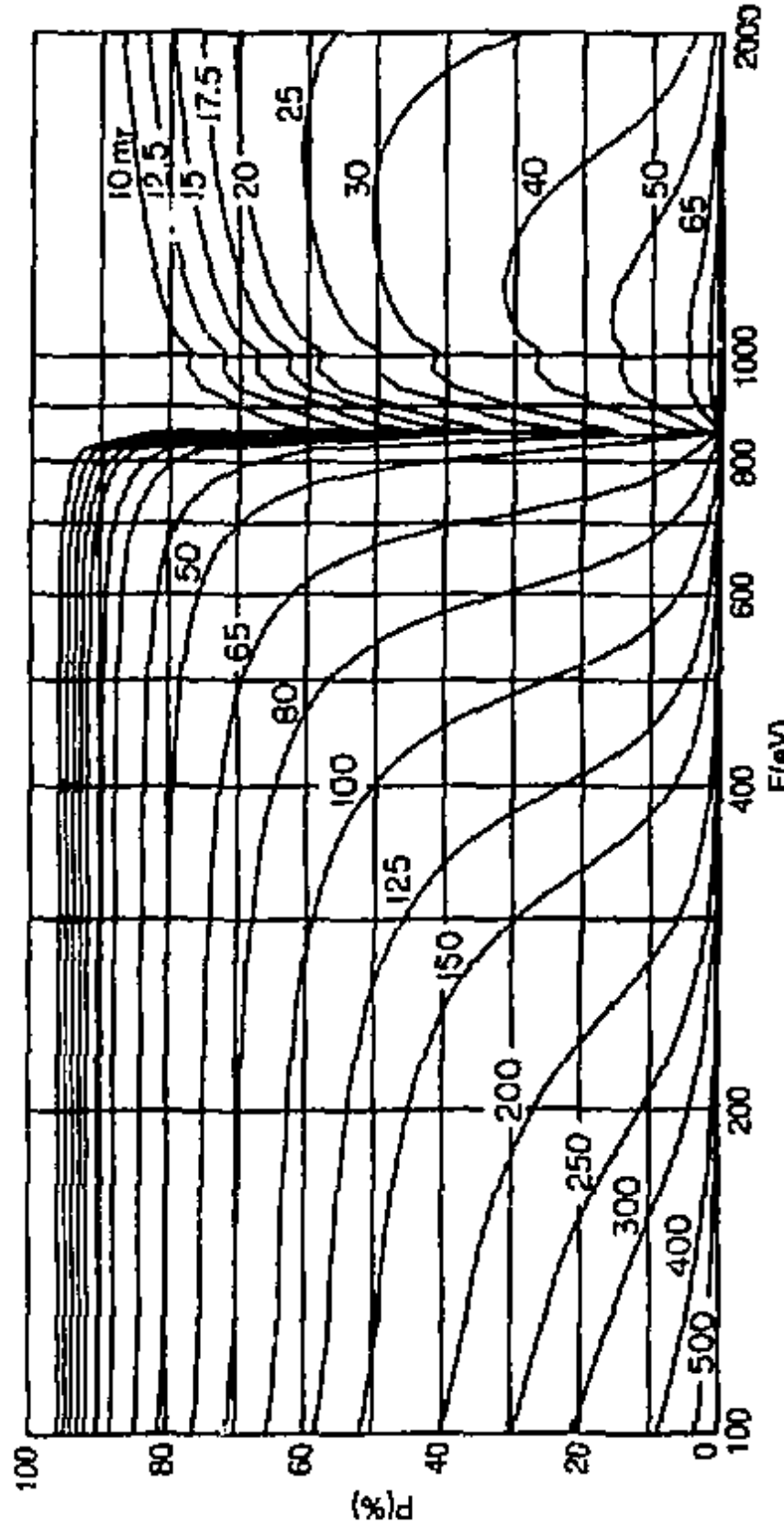

Fig. 5-8. Specular reflectivity for nickel, assuming a mirror density of 8.90 g · cm⁻³.

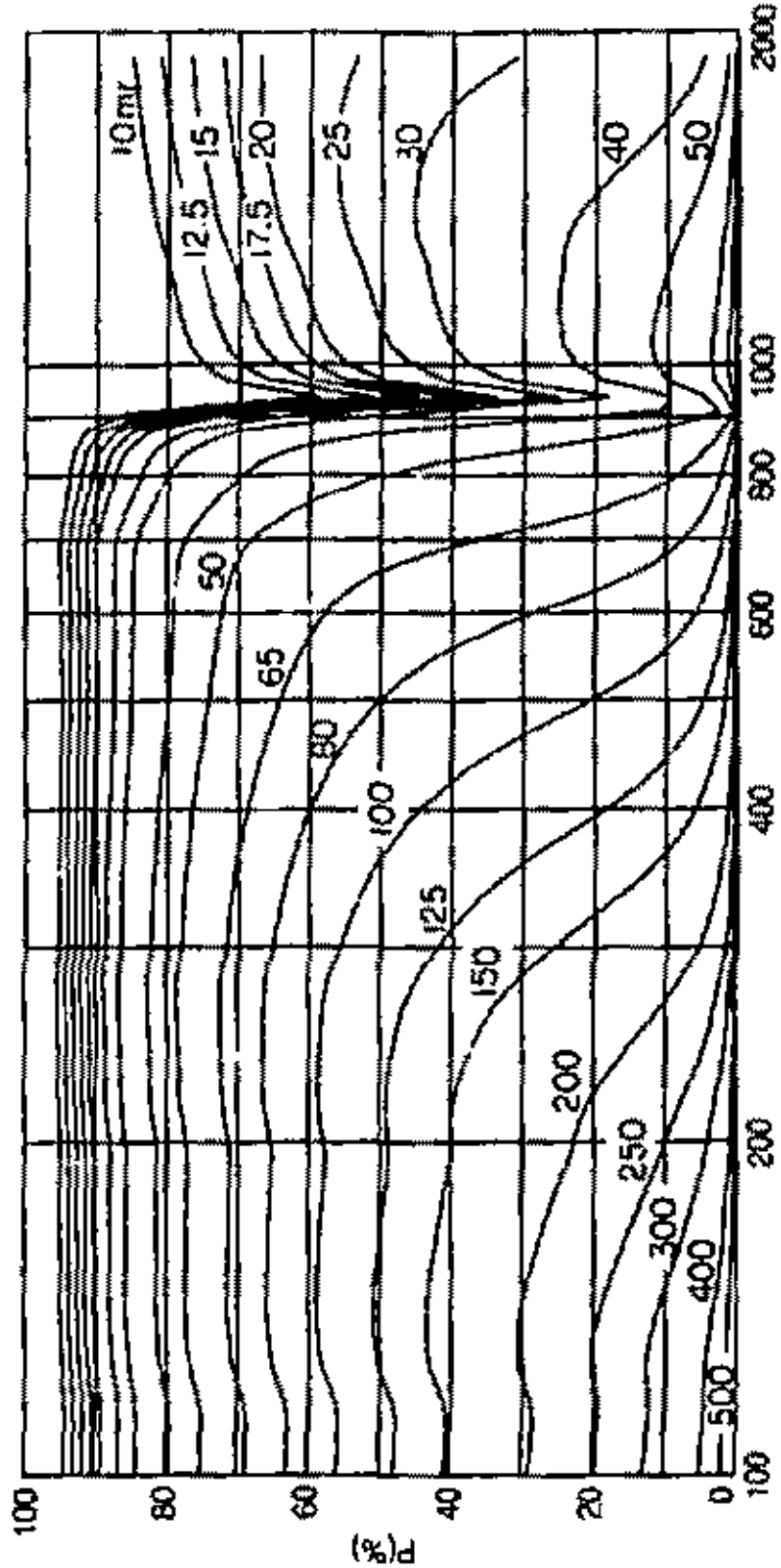

Fig. 5-9. Specular reflectivity for copper, assuming a mirror density of 8.96 g · cm^{-3}.

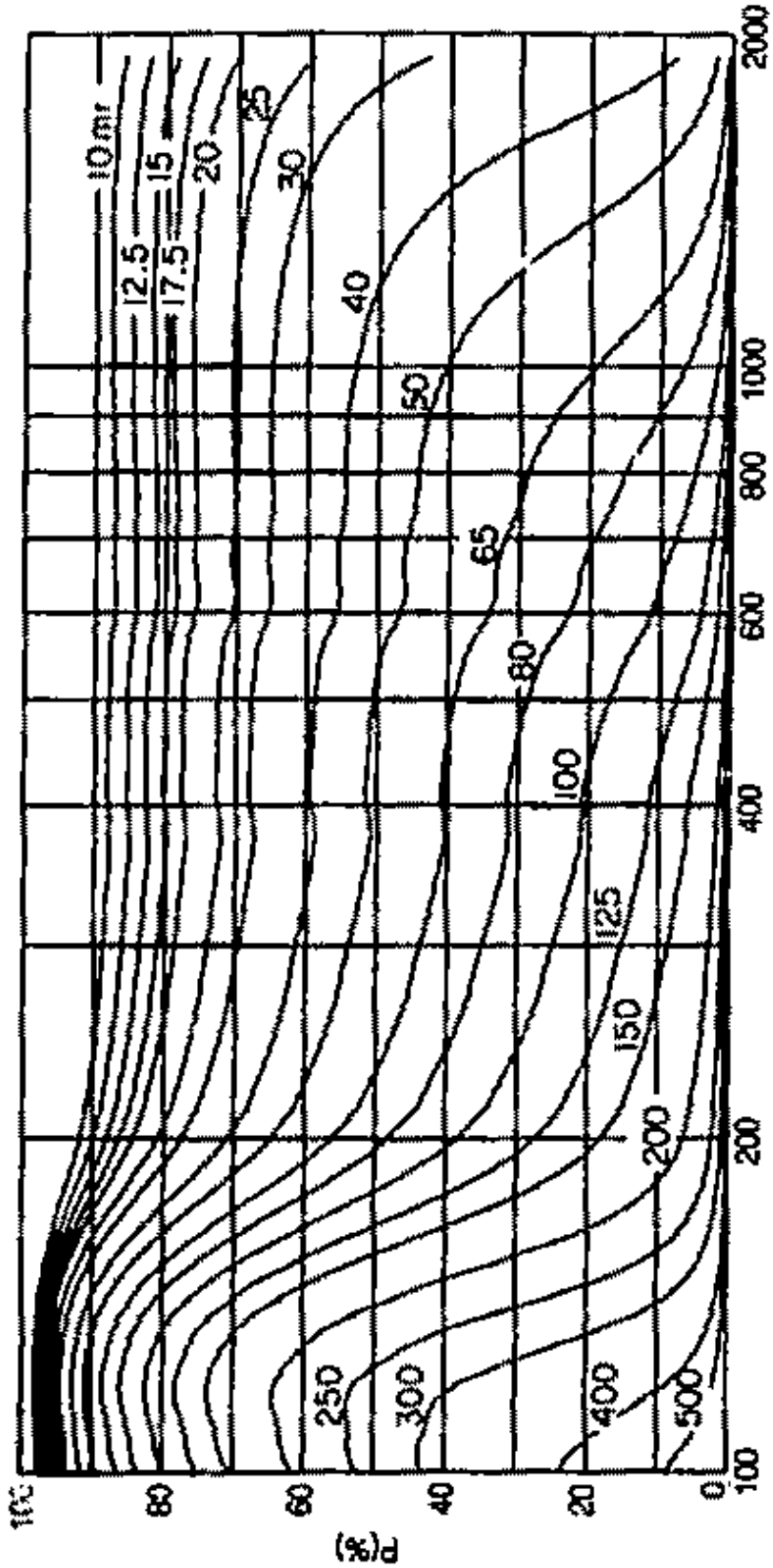

Fig. 5-18. Specular reflectivity for gold, assuming a mirror density of 19.3 g · cm^{-3}.

5.3 GRATINGS AND MONOCHROMATORS

Malcolm R. Howells

A. DIFFRACTION PROPERTIES

A.1 Notation and sign convention

If we adopt the notation of Fig. 5-11, α and β have opposite signs if they are on opposite sides of the normal.

A.2 Grating equation

The basic grating equation may be written

$$m\lambda = d(\sin\alpha + \sin\beta) \ . \tag{1}$$

The angles α and β are both arbitrary, so it is possible to impose various conditions relating them. If this is done, then for each λ, there will be a unique α and β. The following conditions are used:

(i) On-blaze condition:

$$\alpha + \beta = 2\theta_B \ , \tag{2}$$

where θ_B is the blaze angle (the angle of the sawtooth; see Table 5-2). The grating equation is then

$$m\lambda = 2d \sin\theta_B \cos(\beta + \theta_B) \ . \tag{3}$$

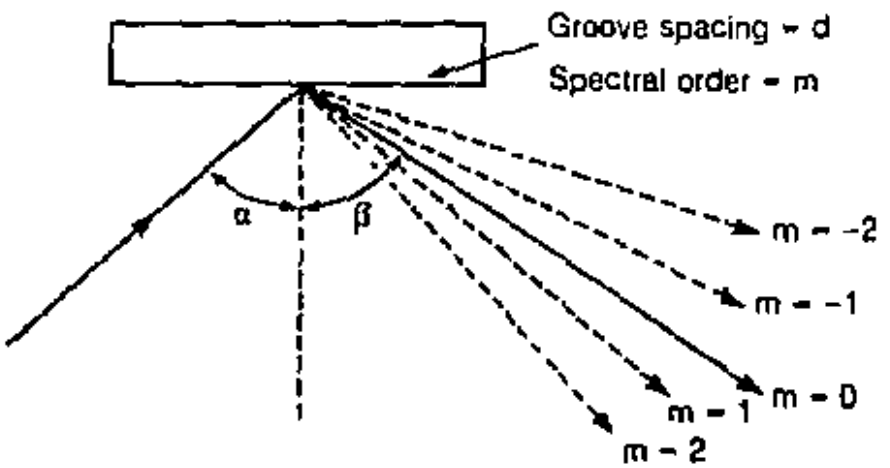

Fig. 5-11. Illustration of notational conventions.

(ii) Fixed in and out directions:

$$\alpha - \beta = 2\theta \ , \tag{4}$$

where 2θ is the (constant) included angle. The grating equation is then

$$m\lambda = 2d \cos\theta \sin(\theta + \beta) \ . \tag{5}$$

In this case, the wavelength scan ends when α or β reaches 90°, which occurs at the horizon wavelength $\lambda_H = 2d \cos^2\theta$.

(iii) Constant incidence angle: Equation (1) gives β directly.

(iv) Constant focal distance (of a plane grating):

$$\frac{\cos^2\alpha}{\cos^2\beta} = K \left(= -\frac{r}{r'} \ ; \ \text{see later}\right) \ , \tag{6}$$

leading to a grating equation

$$\left(\frac{m\lambda}{d} - \sin\beta\right)^2 = 1 - K(1 - \sin^2\beta) \ . \tag{7}$$

Equations (3), (5), and (7) can readily be inverted to give β (and thence α) for any λ. Examples of the above α-β relationships are as follows:

(i) Hunter et al. double plane-grating monochromator (PGM) [1], Kunz et al. PGM [2].

(ii) Mijake et al. [3], West et al. [4], Howells et al. [5], Eberhardt et al. (Flipper) [6] PGMs; all grazing-incidence toroidal-grating monochromators (TGMs) [7], Seya-Namioka [8,9], most aberration-reduced holographic, spherical-grating devices.

(iii) Essentially all spectrographs, Grasshopper monochromator [10].

(iv) Petersen (SX700) [11], Brown et al. (UMO) [12].

B. FOCUSING PROPERTIES

Gratings have complex focusing properties that vary according to the substrate shape and the pattern of grooves on the surface. An important special case is a Rowland grating, which is the intersection of the substrate surface with a set of parallel equispaced planes. The calculation of focusing properties is traditionally carried out by the use of analytical formulas for the optical path function F. Such formulas use a power series

development in the aperture coordinates, with each term of the series representing a recognizable geometrical optical aberration. Here, we consider only a toroidal Rowland grating illuminated by a point source in the symmetry plane [13]; see Fig. 5-12.

We then have

$$F = F_{00} + wF_{01} + \tfrac{1}{2} w^2 F_{20} + \tfrac{1}{2} \ell^2 F_{02} + \tfrac{1}{2} w^3 F_{30} + \tfrac{1}{2} w\ell^2 F_{12} + \tfrac{1}{8} w^4 F_{40} + \cdots \quad (8)$$

$$F_{00} = r + r' \quad (8a)$$

$$F_{01} = \frac{m\lambda}{d} - \sin\alpha - \sin\beta \quad \text{(Grating equation)} \quad (8b)$$

$$F_{20} = \sum T \quad \text{Defocus} \quad (8c)$$

$$F_{02} = \sum S \quad \text{Astigmatism} \quad (8d)$$

$$F_{30} = \sum \frac{\sin\alpha}{r} T \quad \text{Coma} \quad (8e)$$

$$F_{12} = \sum \frac{\sin\alpha}{r} S \quad \text{Astigmatic coma} \quad (8f)$$

$$F_{40} = \sum \left(\frac{4\sin^2\alpha}{r^2} T - \frac{T^2}{r} + \frac{S}{R^2} \right) \quad \text{Spherical aberration} \quad (8g)$$

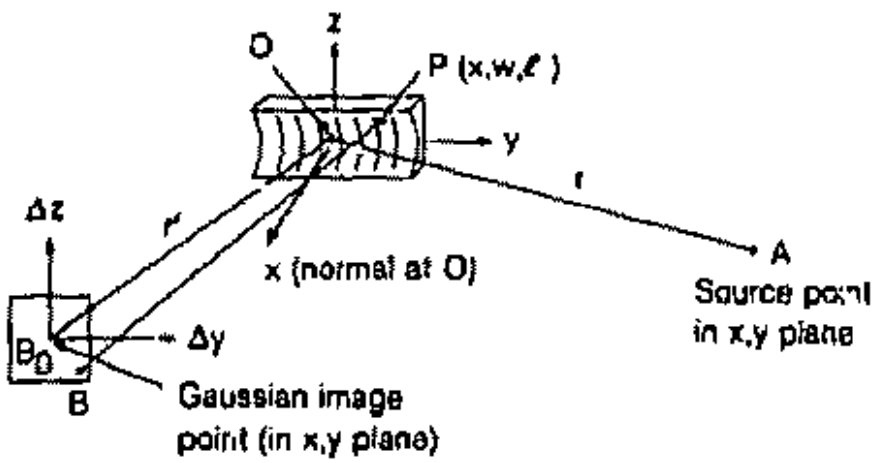

Fig. 5-12. Geometry and notation for a toroidal Rowland grating illuminated by a point source in the symmetry plane.

where

$$T = \frac{\cos^2 \alpha}{r} - \frac{\cos \alpha}{R} \quad ,$$

$$S = \frac{1}{r} - \frac{\cos \alpha}{\rho} \quad ,$$

and the Σ implies that a second expression must be added that is identical to the first, except for the replacements $r \rightarrow r'$ and $\alpha \rightarrow \beta$.

The condition for focus is $F_{20} = 0$. This can be achieved by setting $r = R \cos \alpha$ and $r' = R \cos \beta$, which implies that A and B_0 are on the Rowland circle with diameter R. This is the normal choice for spectrographs but is not convenient for constant-deviation monochromators. For TGMs, r and r' are chosen so that $F_{20} = 0$ for two wavelengths within the working region.

The importance of the optical path function is that it enables the transverse ray aberrations Δy_{ij} and Δz_{ij} to be calculated for each aberration. These are measured from the Gaussian (paraxial) image point $B_0(r', \beta, 0)$ given by the grating equation and the focusing condition ($F_{20} = 0$).

The transverse ray aberrations are then given by

$$\Delta y_{ij} = \frac{r'}{\cos \beta} \frac{\partial F_{ij}}{\partial w} \tag{9a}$$

and

$$\Delta z_{ij} = r' \frac{\partial F_{ij}}{\partial \ell} \quad . \tag{9b}$$

The final result for the ray position is given by

$$\Delta y = \sum_{ij} \Delta y_{ij} \tag{10a}$$

and

$$\Delta z = \sum_{ij} \Delta z_{ij} \quad . \tag{10b}$$

C. DISPERSION PROPERTIES

C.1 Angular dispersion

Angular dispersion is given by

$$\left\{ \frac{\partial \lambda}{\partial \beta} \right\}_{\alpha} = \frac{d \cos \beta}{m} \quad . \tag{11}$$

C.2 Reciprocal linear dispersion

Reciprocal linear dispersion is given by

$$\left(\frac{\partial\lambda}{\partial q}\right)_{\alpha} = \frac{d\cos\beta}{mr'} = \frac{10^{-3}\,d[\text{Å}]\cos\beta}{mr'[\text{m}]}\ \text{Å/mm}\ , \quad (12)$$

where q is measured in the symmetry plane perpendicular to the outgoing ray. For the Rowland circle case, $r' = R\cos\beta$ in Eq. (12)

C.3 Magnification

Magnification is given by

$$M(\lambda) = \frac{\cos\alpha}{\cos\beta}\,\frac{r'}{r} \quad (13)$$

D. RESOLUTION PROPERTIES

The following are the main contributions to the final resolution. The actual resolution is the vector sum.

(i) Entrance slit (width S_1):

$$\Delta\lambda_{S1} = \frac{S_1 d\cos\alpha}{mr}\ . \quad (14)$$

(ii) Exit slit (width S_2):

$$\Delta\lambda_{S2} = \frac{S_2 d\cos\beta}{mr'}\ . \quad (15)$$

(iii) Diffraction:

$$\Delta\lambda_D = \lambda/mN\ , \quad (16)$$

where N is the number of participating grooves.

(iv) Aberrations (due to perfect optics):

$$\Delta\lambda_A = \frac{\Delta y d\cos\beta}{mr'} = \frac{d}{m}\left(\frac{\partial F}{\partial y}\right)\ . \quad (17)$$

(v) System spread function (due to imperfect optics):

$$\Delta\lambda_{LSF} = \frac{wd\cos\beta}{mr'}\ , \quad (18)$$

where w is the width of the system line spread function.

E. EFFICIENCY

The calculation of diffraction grating efficiencies is, in general, highly complex [14]; however, some simplification is possible in the soft x-ray region. In Table 5-2, we give scalar theory formulas for the absolute efficiency E_λ, which should be approximately valid if (a) the reflectance R_λ is independent of polarization, (b) groove shadowing is negligible, and (c) the projected groove spacing satisfies the inequality $d \cos \alpha > 5\lambda$.

In the table, $\delta = 2\pi h(\cos \alpha + \cos \beta)/\lambda$, where h is the peak-to-valley amplitude of the grating profile and m is the spectral order defined in Fig. 5-11. The equation $\delta = Q$ can be solved to find $(\lambda/d)_{peak}$ as a function of h, α, d, and m as follows:

$$\left(\frac{\lambda}{d}\right)_{peak} = \frac{2m \sin \alpha + \dfrac{Qd \cos \alpha}{\pi h}}{\dfrac{Q^2 d^2}{4\pi^2 h^2} + m^2} \tag{19}$$

Table 5-2. Scalar theory formulas for grating efficiency.

	Lamella	Sinusoidal (holographic)	Blazed
Waveform	square wave	sine wave	sawtooth
E_λ/R_λ	$\left(\frac{2}{m\pi}\right)^2 \sin^2\left(\frac{\delta}{2}\right)$	$J_m^2\frac{\delta}{2}$	$\operatorname{sinc}^2\left(\lvert m\rvert\pi - \frac{\delta}{2}\right)$
Valid for m =	$\pm 1,3,5,\ldots$	± 1	$\pm 1,2,3,\ldots$
δ at peak efficiency (Q)	$m\pi$	3.68	$2m\pi$
Peak value of E_λ/R_λ (%)	40	34	100

REFERENCES

1. W. R. Hunter, R. T. Williams, J. C. Rife, J. P. Kirkland, and M. N. Kabler, "A Grating/Crystal Monochromator for the Spectral Range 5 eV to 5 keV," *Nucl. Instrum. Methods* **195**, 141 (1982), and W. R. Hunter, "Aberrations of Grazing Incidence Systems and Their Reduction or Toleration," *Proc. SPIE* **315**, 19 (1981).
2. H. Dietrich and C. Kunz, "A Grazing Incidence Vacuum Ultraviolet Monochromator with Fixed Exit Slit," *Rev.*

Sci. Instrum. **43**, 434 (1972), and C. Kunz, R. Haensel, and B. Sonntag, "Grazing-Incidence Vacuum-Ultraviolet Monochromator with Fixed Exit Slit for Use with Distant Sources," *J. Opt. Soc. Am.* **58**, 1415 (1968).

3. K. P. Miyake, R. Kato, and H. Yamashita, "A New Mounting for Soft X-Ray Monochromator for Synchrotron Orbital Radiation," *Sci. Light* **18**, 39 (1969).
4. J. B. West, K. Codling, and G. V. Marr, "A Grazing Incidence Monochromator for Use with Synchrotron Radiation," *J. Phys. E* **7**, 137 (1974).
5. M. R. Howells, D. Norman, G. P. Williams, and J. B. West, "A Grazing Incidence Monochromator for Synchrotron Radiation," *J. Phys E* **11**, 199 (1978), and M. R. Howells, "Plane Grating Monochromators for Synchrotron Radiation," *Nucl. Instrum. Methods* **177**, 127 (1980).
6. W. Eberhardt, G. Kalkoffen, and C. Kunz, "Grazing Incidence Monochromator Flipper," *Nucl. Instrum. Methods* **152**, 81 (1978).
7. R. P. Madden and D. L. Ederer, "Stigmatic Grazing-Incidence Monochromator for Synchrotrons" (abstract), *J. Opt. Soc. Am.* **62**, 722 (1972), and D. Lepere, "Monochromators with Single Axis Rotation and Holographic Gratings on Toroidal Blanks for the Vacuum Ultraviolet" (in French), *Nouvelle Revue Optique* **6**, 173 (1975).
8. M. Seya, *Sci. Light* **2**, 8 (1952), and T. Namioka, *Sci. Light* **3**, 15 (1954).
9. For a review, see T. Namioka, M. Seya, and H. Noda, "Design and Performance of Holographic Concave Gratings," *Jpn. J. Appl. Phys.* **15**, 1181 (1976).
10. F. C. Brown, R. Z. Bachrach, and N. Lien, "The SSRL Ultrahigh Vacuum Grazing Incidence Monochromator: Design Considerations and Operating Experience," *Nucl. Instr. Methods* **152**, 73 (1978).
11. H. Petersen, "*The Plane Grating and Elliptical Mirror*: A New Optical Configuration for Monochromators," *Opt. Commun.* **40**, 402 (1982).
12. F. C. Brown and S. L. Hulbert, "A High Resolution Monochromator for Undulator Radiation," *Nucl. Instrum. Methods Phys. Res.* **222**, 42 (1984).
13. H. Haber, "The Toric Grating," *J. Opt. Soc. Am.* **40**, 153 (1950). *The general theory of the grating* [H. Noda, T. Namioka, and M. Seya, "Geometrical Theory of the Grating," *J. Opt. Soc. Am.* **64**, 1031 (1974)] is applicable to the

toroid with a_{ij} values as follows: $a_{20} = 1/(2R)$, $a_{02} = 1/(2\rho)$, $a_{40} = 1/(8R^2)$, $a_{22} = 1/(4R^2\rho)$, $a_{04} = 1/(8\rho^3)$, all other $a_{ij} = 0$ for $i + j \leq 4$.

14. R. Petit, Ed., *Electromagnetic Theory of Gratings*, Topics in Current Physics, vol. 22, (Springer-Verlag, Berlin, 1980), and A. Franks, K. Lindsey, J. M. Bennett, R. J. Speer, D. Turner, and D. J. Hunt, "The Theory, Manufacture, Structure and Performance of N.P.L. X-Ray Gratings," *Philos. Trans. Roy. Soc. London A* 277, 503 (1975).

5.4 ZONE PLATES

Janos Kirz

Zone plates are circular diffraction gratings. In its simplest form, a transmission Fresnel zone plate for use with incident plane waves consists of alternate transparent and opaque rings. The radii of the zone edges are given by

$$r_n^2 = nf\lambda + n^2\lambda^2/4 \ , \tag{1}$$

where n is the zone number (opaque and transparent zones counted separately) and f is the focal length in first order. The zone plate can be used as a thin lens to focus monochromatic incident radiation, or, due to the inverse relationship between focal length and wavelength, it can be used as a dispersive element. If used as a lens, the thin-lens formula applies:

$$1/s + 1/s' = 1/f \ , \tag{2}$$

where s and s' are object and image distances, respectively. Diffraction-limited resolution of the zone plate is given by

$$\Delta \approx 1.22\, \delta r_N \approx 1.22\, r_N/2N \ , \tag{3}$$

where r_N is the radius of the zone plate, N is the total number of zones, and δr_N is the width of the outermost zone. In higher orders, the resolution improves in proportion to the order number.

The efficiency of the simple zone plate in first order is ideally π^{-2}, or about 10%. The remainder of the radiation is absorbed (50%) or diffracted in other orders—zero order (25%), negative orders (12.5%), and higher positive orders (2.5%). If opaque zones are replaced by transparent but phase-shifting zones, efficiencies can be substantially improved. See, for example, R. Tatchyn, P. L. Csonka, and I. Lindau, "Outline of a Variational Formulation of Zone-Plate Theory," *J. Opt. Soc. Am. B* **1**, 806 (1984).

SECTION 6

X-RAY DETECTORS

Albert C. Thompson

A wide variety of x-ray detectors are available, some providing only measurements of count rate or total flux, others measuring the energy, position, and/or incidence time of each x-ray [1]. In Table 6-1, typical values for useful energy range, energy resolution, dead time per event, and maximum count rate capability are given for common x-ray detectors. For special applications, these specifications can often be substantially improved.

Table 6-1. *Properties of common x-ray detectors.*

Detector	Energy range (keV)	ΔE (FWHM)/E at 5.9 keV (%)	Dead time/event (μs)	Maximum count rate (s^{-1})
Geiger counter	3–50	none	200	10^4
Gas ionization in current mode	0.2–50	n/a	n/a	10^{11} [a]
Gas proportional	0.2–50	15	0.2	10^5
Multiwire proportional chamber	3–50	20	0.2	10^5/anode wire
Scintillation [NaI(Tl)]	3–10,000	40	0.25	10^6
Semiconductor [Si(Li)]	1–60	3	4–30	5×10^4
Semiconductor (Ge)	1–10,000	3	4–30	5×10^4

[a] Maximum count rate is limited by space-charge effects to around 10^{11} photons/s per cm^3.

New instruments currently being developed using semiconductor technology will have substantially improved count rate capabilities, position resolutions, and/or energy resolutions, and will, therefore, be especially useful with the intense x-ray sources that are becoming available at synchrotron facilities.

A. GAS IONIZATION DETECTORS

One of the simplest x-ray detectors is the gas ionization chamber. Such detectors are commonly used with a low-noise current amplifier to measure x-ray flux rather than to count individual photons. A common detector geometry consists of a rectangular gas-tight container with thin entrance and exit windows and a flowing gas supply. Inside the detector are two parallel plates across which a potential is applied to produce an electric field of about 100 V/cm. X-rays are photoelectrically absorbed to produce fast photoelectrons and either Auger electrons or fluorescence photons. The energetic electrons produce additional electron-ion pairs by inelastic collisions, and the photons either escape or are photoelectrically absorbed. The voltage applied across the chamber sweeps the electrons and ions apart, and they are collected at the plates.

The average energy required to produce an electron-ion pair in several common gases is given in Table 6-2. The number of x-rays stopping in the detector can be calculated from the active volume of the chamber, the gas pressure, and the x-ray absorption cross sections for the gas used. Figure 6-1 shows, for different gases at normal pressure, the efficiency of a 15-cm-long ion chamber as a function of energy.

Table 6-2. Average energy required to produce an electron-hole pair in several gases.

Element	Energy (eV)
Helium	27.8
Neon	27.4
Argon	24.4
Krypton	22.8
Xenon	20.8

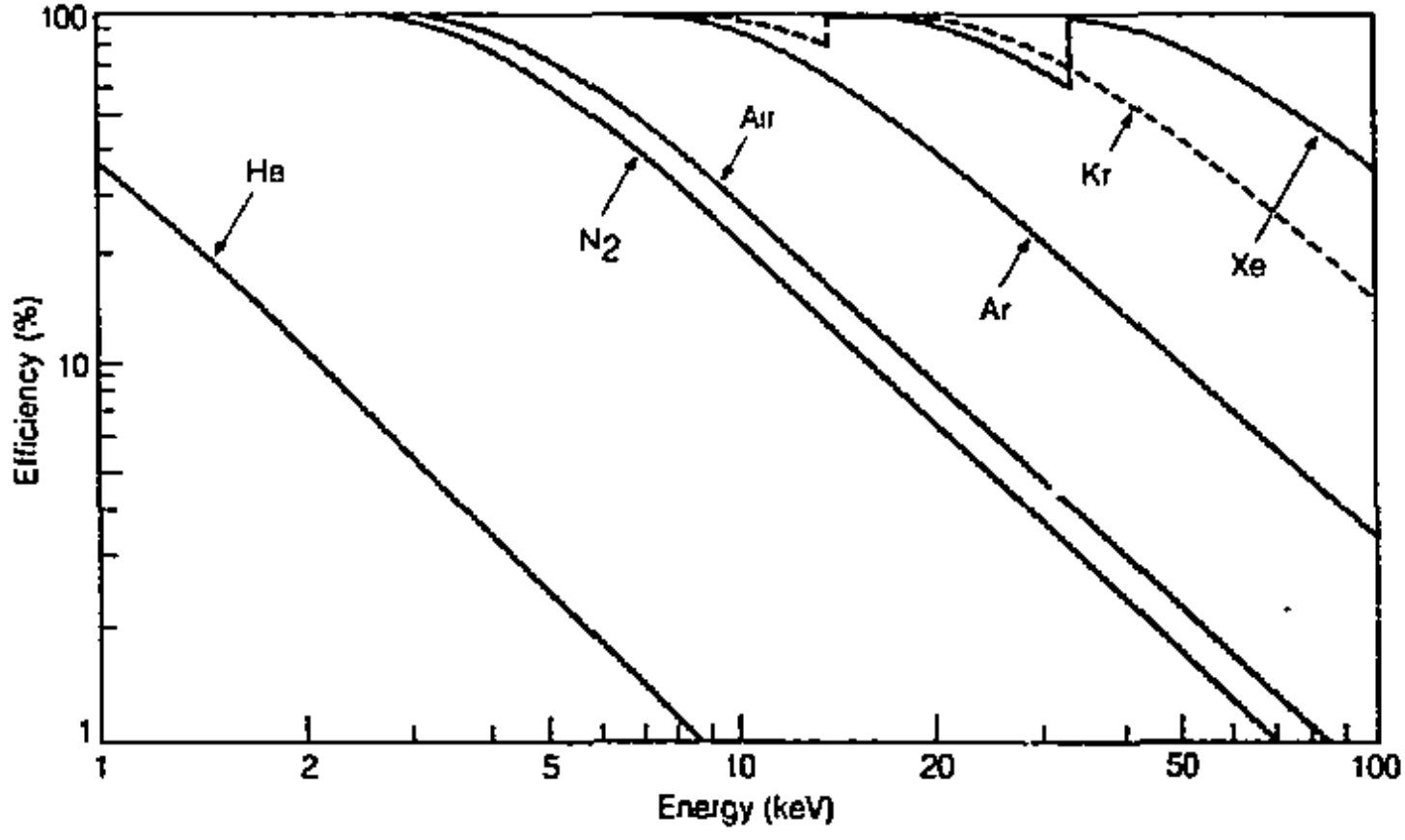

Fig. 6-1. *Efficiency of a 15-cm-long gas ionization chamber as a function of energy, for different gases at normal pressure.*

B. GAS PROPORTIONAL COUNTERS

Gas proportional detectors comprise a small-diameter anode wire in an enclosed cylindrical gas volume. A high voltage is applied, so that the field around the wire is above 25 kV/cm. These detectors are usually used to count single photon events.

If operated in an avalanche mode, such detectors are called Geiger counters and give very large pulses for each stopping x-ray. In this mode, they are filled with a noble gas to which a small amount of halogen is added to quench the gas after each pulse. A major limitation of this mode of operation is the large dead time (about 200 μs) for each event.

The normal mode of operation of gas proportional counters is at a lower voltage, so that the detector gain is linear. In this mode, the output is coupled to a low-noise preamplifier to give usable pulses. The pulse height resolution of the detector (about 20% at 6 keV) can be used for some energy discrimination, and the output counting rate can be as high as 10^6 counts per second.

C. MULTIWIRE PROPORTIONAL CHAMBERS

Multiwire proportional chambers are widely used as position-sensitive detectors of both photons and charged particles [2–4]. They use a grid of fine wires spaced about 2 mm apart as the anode plane in a gas proportional chamber. Many different read-out techniques are used to measure the event positions [5,6]; four examples are amplifier per wire, analog charge division, time digitization using a delay line, and drift-time systems. The spatial resolution from the anode plane is usually the anode wire spacing (typically 1–5 mm). Two-dimensional read-out can be achieved if the cathode plane is also segmented and read out. A spatial resolution of around 80 μm can be achieved for the cathode read-out plane.

D. SCINTILLATION DETECTORS

Scintillation detectors use either a photomultiplier tube or a photodiode to detect the optical photons produced in special materials when an x-ray is stopped. The scintillator material can be either organic scintillators, single crystals of thallium-activated sodium iodide [commonly referred to as NaI(Tl)], or single crystals of bismuth germanate (BGO). Since the light output is low (about 200–300 eV is required for each optical

photon), the energy resolution is low. Organic scintillators have very poor energy resolution, whereas the NaI(Tl) and BGO crystals have an energy resolution of about 40% at 10 keV. These detectors are often used for measuring the stopping time of x-rays. They can have a time resolution of better than 1 ns and a count rate capability up to 10^5 photons per second.

Gas scintillation detectors combine the operation of a gas ionization chamber and a photon detector to give improved performance [7]. Electrons generated from photon or charged-particle interactions in a gas (usually pure xenon or argon with 1% xenon) are accelerated in a high-field (~3 kV/cm) region, where they produce UV scintillation light. This light is usually wave-shifted and then detected by a photomultiplier. These detectors have an energy resolution about two to three times better than a conventional proportional chamber.

E. SEMICONDUCTOR DETECTORS

A semiconductor detector is basically a very large, reverse biased n^+-i-p^+ diode. When the diode is reverse biased, an intrinsic region with an electric field across it is created. When an incident photon interacts in this region, tracks of electron-hole pairs are produced. In the presence of the electric field, these pairs separate and rapidly drift to the detector contacts. The average energy required to generate an electron-hole pair at 77 K is 3.6 eV for silicon and 2.98 eV for germanium. To keep the leakage current low, the detector must be of very high purity. To fabricate silicon detectors, lithium is generally drifted through the device at elevated temperature with a field on. The lithium compensates the p-type impurities in the device to give a large active region in the detector with intrinsic conductivity. Germanium crystals do not now require lithium drifting, because they can be directly purified by zone refining to the required purity ($<10^{10}$ electrically active impurities/cm^3). These detectors are usually cooled to liquid nitrogen temperature (77 K) to reduce the thermal leakage current. They are usually used in a single-photon-counting mode to exploit their excellent energy resolution (typically 175 eV at 5.9 keV). The count rate capability is limited to less than 5×10^4 per second.

Lithium-drifted silicon and planar germanium detectors are

widely used for energy-dispersive analysis. The efficiency of 3- and 5-mm-thick Si(Li) and 5-mm-thick germanium detectors, as a function of energy, is illustrated in Fig. 6-2. Si(Li) detectors are often used to measure nondestructively the elemental composition of samples. Germanium detectors are generally not used below 20 keV because of the interference from peaks due to the escape of the germanium K fluorescence photon. Large germanium detectors are widely used for γ-ray spectroscopy.

F. OTHER X-RAY DETECTORS

Many instruments (especially spectrographs) use photographic film as the detector. Film is an excellent detector in experiments requiring a total-flux detector with high spatial resolution. The major limitation of film is the need for processing. If carefully calibrated with a microdensitometer, film can be used for quantitative analysis of x-ray intensity. To enhance the detection efficiency of film, a fluorescent screen is often placed next to it. Special films are available to give improved efficiency, contrast, or resolution; for initial alignment of instruments, Polaroid film is often used.

A variety of imaging systems can be used to image x-rays electronically [8]. For medical imaging, an image converter is widely used to provide real-time imaging. These detectors use a cesium iodide scintillator with a photocathode screen deposited on it to produce electrons from incident x-rays. The electrons are then accelerated and imaged onto a phosphor screen, which is viewed, in turn, by a video camera. Linear photodiode arrays and CCD detectors are available to give excellent position information with fast read-out. Large, one-dimensional photodiode arrays coupled to a scintillator are also used for x-ray detectors. Two-dimensional x-ray CCD detectors are becoming available with 512 × 512 pixels, each pixel measuring 13 μm × 13 μm. These detectors are currently undergoing rapid development and will find many applications both for detecting low-energy x-rays directly and for use with x-ray image intensifiers.

For high-speed imaging of plasmas and other intense x-ray sources, x-ray streak cameras have also been developed [9].

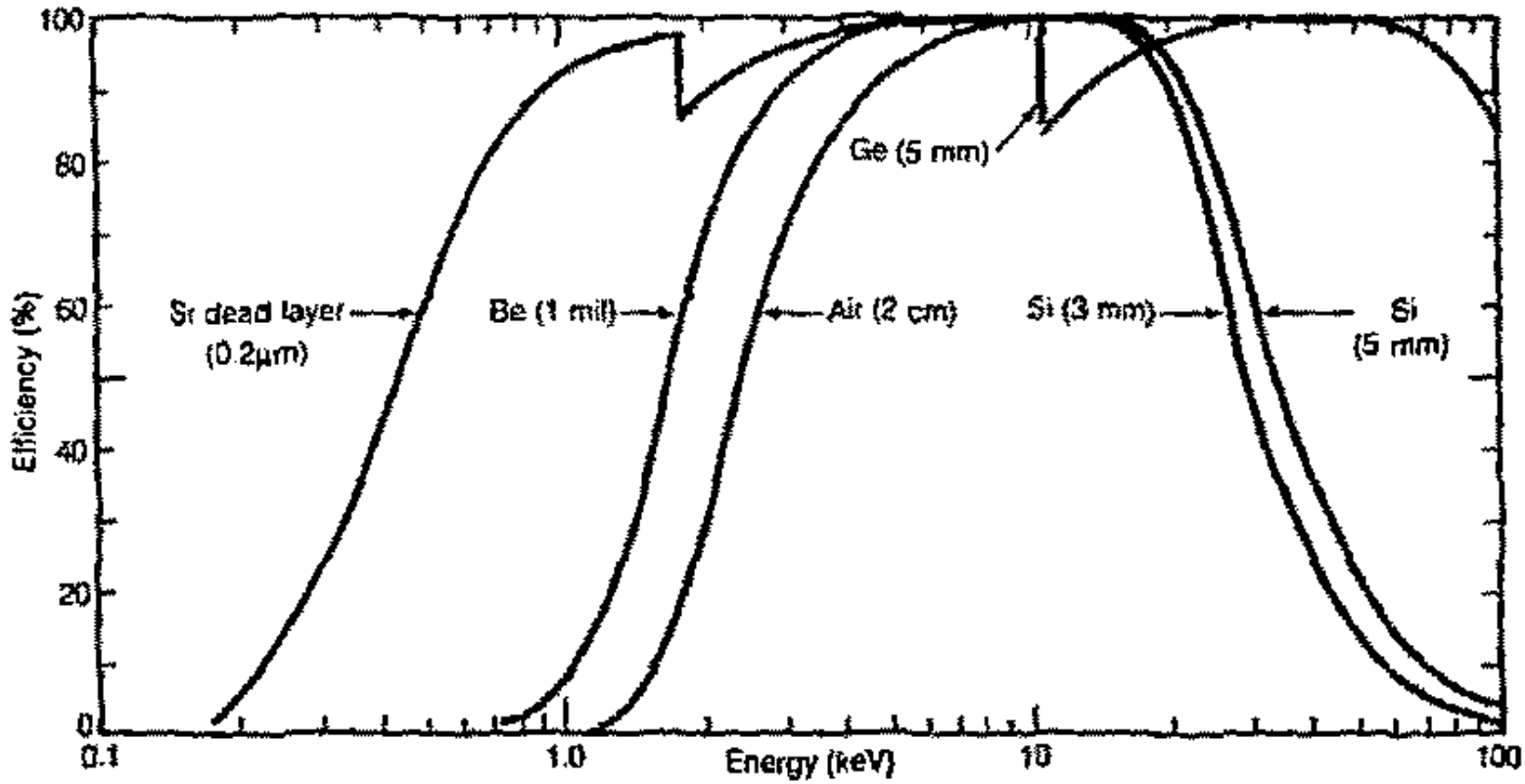

Fig. 6-2. *Detection efficiency as a function of energy for semiconductor crystals. The thickness of the detector crystal limits the detection of high-energy photons; absorption by air, beryllium windows, and the dead layer of silicon crystals limits efficiency at low energies.*

REFERENCES

1. J. G. Timothy and R. P. Madden, "Photon Detectors for the Ultraviolet and X-Ray Region," in E. Koch, Ed., *Handbook on Synchrotron Radiation* (North-Holland, Amsterdam, 1983), vol. 1A, p. 315.
2. A .H. Walenta, "State-of-the-Art and Application of Wire Chambers," *Nucl. Instrum. Methods* 217, 65 (1983).
3. J. E. Bateman, J. F. Connolly, R. Stephenson, G. J. R. Tappern, and A. C. Flesher, "The Development of MWPC-Based Systems for Imaging X-Rays, Gamma Rays and Charged Particles in Applications in Medicine, Materials Science and Biochemistry," *Nucl. Instrum. Methods* 217, 77 (1983).
4. G. Charpak, "Some Prospects with Gaseous Detectors," *Nucl. Instrum. Methods* 176, 9 (1980).
5. G. Charpak, F. Sauli, and R. Kahn, "On Some Factors Controlling High-Accuracy Measurements of X-Ray Quanta Positions with Multiwire Proportional Chambers," *Nucl. Instrum. Methods* 152, 185 (1978).
6. G. C. Smith, "High Accuracy Gaseous X-Ray Detectors," *Nucl. Instrum. Methods Phys. Res.* 222, 230 (1984).
7. M. R. Sims, A. Peacock, and B. G. Taylor, "The Gas Scintillation Proportional Counter," *Nucl. Instrum. Methods Phys. Res.* 221, 168 (1984).
8. S. M. Gruner, J. R. Milch, and G. T. Reynolds, "Survey of Two-Dimensional Electro-Optical Detectors," *Nucl. Instrum. Methods* 195, 287 (1982).
9. V. Rehn, "Time Resolved Spectroscopy in Synchrotron Radiation," *Nucl. Instrum. Methods* 177, 193 (1980).

SECTION 7

SYNCHROTRON RADIATION FACILITIES

Herman Winick

Table 7-1 lists storage ring synchrotron radiation facilities now in operation or under construction, together with typical electron beam energies and characteristic photon energies. The characteristic energy is defined as

$$\epsilon_c\ [\text{keV}] = 2.218\ E^3/R = 0.665\ BE^2\ ,$$

where E is in GeV, R (the bending radius) is in meters, and B is in tesla. Additional information has recently been compiled in Refs. 1 and 2. Following the table, names and addresses are given for the current directors of these and other facilities.

REFERENCES

1. H. Winick and R. E. Watson, "Worldwide Census of Synchrotron Radiation Facilities," *Nucl. Instrum. Methods Phys. Res.* 222, 373 (1984).
2. D. E. Eastman and Y. Farge, Eds., *Handbook on Synchrotron Radiation* (North-Holland, Amsterdam, 1983), vol. 1A, p. 33.

Table 7-1. Storage rings used as synchrotron radiation sources. E is the typical electron beam energy and ϵ_c is the characteristic photon energy of bending-magnet radiation.

Location	Ring (lab)	E (GeV)	ϵ_c (keV)	Notes[a]
China				
Beijing	BEPC (IHEP)	2.2–2.8	3.8 (2.6 GeV)	C, Par
Hefei	HESYRL (USTC)	0.8	0.43	C, Ded
England				
Daresbury	SRS	2.0	3.2	O, Ded
France				
Orsay	ACO (LURE)	0.54	0.33	O, Ded
	DCI (LURE)	1.8	3.4	O, PDed
	SuperACO (LURE)	0.8	0.62	C, Ded
Germany				
Hamburg	DORIS (DESY)	3.7–5.2	23 (5 GeV)	O, PDed
W. Berlin	BESSY	0.8	0.63	O, Ded
	COSY	0.56	-	C, Ded
Italy				
Frascati	ADONE	1.5	1.5	O, PDed
Japan				
Tsukuba	Photon Factory (KEK)	2.5	4.1	O, Ded
	Accumulator (KEK)	6–8	33 (7 GeV)	O, PDed
	TRISTAN (KEK)	30	243	C, Par
	TERAS (ETL)	0.66	0.24	O, Ded
Tokyo	SOR-Ring (ISSP)	0.4	0.13	O, Ded
Okazaki	UVSOR (IMS)	0.6	0.32	O, Ded
Sweden				
Lund	Max (LTH)	0.56	0.30	C, Ded
Taiwan				
Hsinchu	TSL (SRRC)	1.0	-	C, Ded
USA				
Gaithersburg, MD	SURF (NBS)	0.284	0.06	O, Ded
Ithaca, NY	CESR (CHESS)	5.5	11.3	O, Par
Stanford, CA	SPEAR (SSRL)	3–4	4.7 (3 GeV)	O, PDed
	SXRL (SSRL)	1.0	-	C, PDed
	PEP (SSRL)	15.0	-	C, Par
Stoughton, WI	Tantalus (SRC)	0.24	0.05	O, Ded
	Aladdin (SRC)	1.0	1.03	O, Ded
Upton, NY	NSLS I (BNL)	0.75	0.50	O, Ded
	NSLS II (BNL)	2.5	5.0	O, Ded
USSR				
Kurkhov	N-100 (KPI)	0.10	0.04	O, Ded
Moscow (Kurchatov)	PLANIA I	0.45	0.20	C, Ded
Novosibirsk	VEPP-2M (INP)	0.67	0.34	O, PDed
	VEPP-3 (INP)	2.2	4.3	O, PDed
	VEPP-4 (INP)	7	46	O, Par

[a] O = Operational, C = Under construction, Ded = Dedicated, PDed = Partly dedicated, Par = Parasitic

Dr. Xie Jialin, Director
BEPC
IHEP Academia Sinica
P.O. Box 918
Beijing
The People's Republic of China

Dr. Bao Zhong-Mou, Director
HESYRL
Univ. Science & Technology
Hefei, Anhui
The People's Republic of China

Dr. D. J. Thompson, Director
Synchrotron Radiation Source
Daresbury Laboratory
Warrington WA4 4AD
Lancashire, England

Dr. Yves Petroff, Director
LURE
Batiment 200
91405 Orsay
France
Tel: 941 82-70
Telex: LALORS 690 369 F

Dr. G. Materlik, Director
HASYLAB at the DESY
Notkestr. 85
2000 Hamburg 52
West Germany
Tel: 040/89 98-0
Telex: 2 15 124 desy d

Dr. Ernst Koch, Director
BESSY
Lentzeallee 100
1000 Berlin 33
West Germany
Tel: 82 00 40

Dr. R. Natoli, Director for
Synchrotron Radiation
Frascati
Via E. Fermi, 13
00044 Frascati
Italy
Tel: 94031
Telex: 614122 INFN LNF

Dr. Jun-ichi Chikawa, Director
Photon Factory, KEK
Oho-Machi, Tsukuba/Gun
Ibaraki/Ken 300-32
Japan

Dr. Takio Tomimasu, Director
TERAS
Electrotechnical Lab
1-1-4, Umezono, Sakura-mura
Nihari-gun, Ibaraki
Japan

Dr. Takehiko Ishii, Director
Synchrotrun Radiation Laboratory
SRL-ISSP
3-2-1 Midoricho, Tanashi
Tokyo 188
Japan
Tel: (0424) 61-4131
Telex: ISSP UT J32469

Dr. Hiroo Inokuchi, Director
UVSOR
Institute of Molecular Science
Myodaiji, Okasaki 444
Japan

Dr. B. Forkman, Director
MAX
University of Lund
Professorsgatan 3
SA-22363 Lund
Sweden

Dr. L. C. Yuan, Chairman
Board of Directors
Synchrotron Radiation Research Center
8F, No. 6, Roosevelt Rd., Sec. 1
Taipei, Taiwan 107
Republic of China

Dr. R. Madden, Director
SURF
National Bureau of Standards
Physics A257
Washington, DC 20234
Tel: (301) 921-2031

Dr. B. W. Batterman, Director
CHESS
Cornell University
Ithaca, NY 14853
Tel: (607) 256-5161

Dr. A. Bienenstock, Director
Stanford Synchrotron Radiation Laboratory (SSRL)
P.O. Box 4349, Bin 69
Stanford, CA 94305
Tel: (415) 854-3300, ext. 3155

Dr. John Madey, Director
Stanford X-ray Radiation Laboratory (SXRL)
High Energy Physics Laboratory
Stanford University
Stanford, CA 94305
Tel: (415) 497-3034

Dr. David Huber, Director
Synchrotron Radiation Center
3725 Schneider Drive
Stoughton, WI 53589
Tel: (608) 873-6651

Dr. M. Knotek, Chairman
NSLS
Brookhaven National Laboratory
Associated Universities, Inc.

Upton, NY 11973
Tel: (516) 282-3735

Dr. Igor A. Grishaev
Director for Synchrotron Radiation
Karkhov Physico-Tek. Institute
Academicheskaga 1
310108 Karkhov
USSR

Dr. Boris Rybakoff
Director for Synchrotron Radiation
Kurchatov Institute
Kurchatov Square
123182 Moscow
USSR

Dr. G. Kulipanov
Director for Synchrotron Radiation
Institute of Nuclear Physics
Novosibirsk
USSR

Dr. S. R. Gowariker
Director for Synchrotron Radiation
Central Scientific Instruments Organization
Sector 30, Chandigarh-160020
India

Dr. Roberto Lobo
Director for Synchrotron Radiation
Inst. de Fisica/Sao Carlos
C.P. 369
13.560 Sao Carlos SP
Brazil

SECTION 8

MISCELLANEOUS

8.1 PROBABILITY AND STATISTICS

A. PROBABILITY DISTRIBUTIONS AND CONFIDENCE LEVELS

We give here properties of three commonly used probability distributions: normal (or Gaussian), chi-squared (χ^2), and Poisson. We *warn* the reader that there is no universal convention for the term "confidence level"; thus, explicit definitions that correspond to common usage are given for each distribution. It is explained below how confidence levels for all three distributions may be extracted from Fig. 8-1.

A.1 Normal distribution

The normal distribution with mean $\bar{x}$ and standard deviation σ (variance σ^2) is

$$P(x)dx = \frac{1}{\sigma\sqrt{2\pi}}\, e^{-(x-\bar{x})^2/2\sigma^2} dx \,. \tag{1}$$

The *confidence level* associated with an observed deviation δ from the mean is the probability that $|x-\bar{x}| > \delta$, i.e.,

$$\mathrm{CL} = 2 \int_{\bar{x}+\delta}^{\infty} dx\, P(x) \,, \tag{2}$$

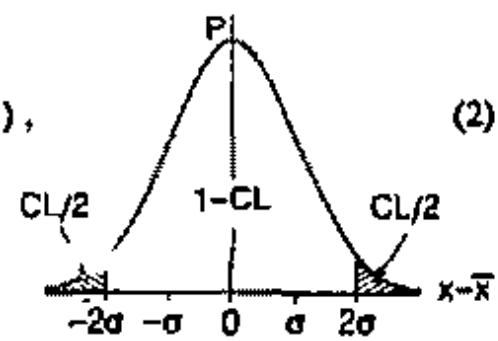

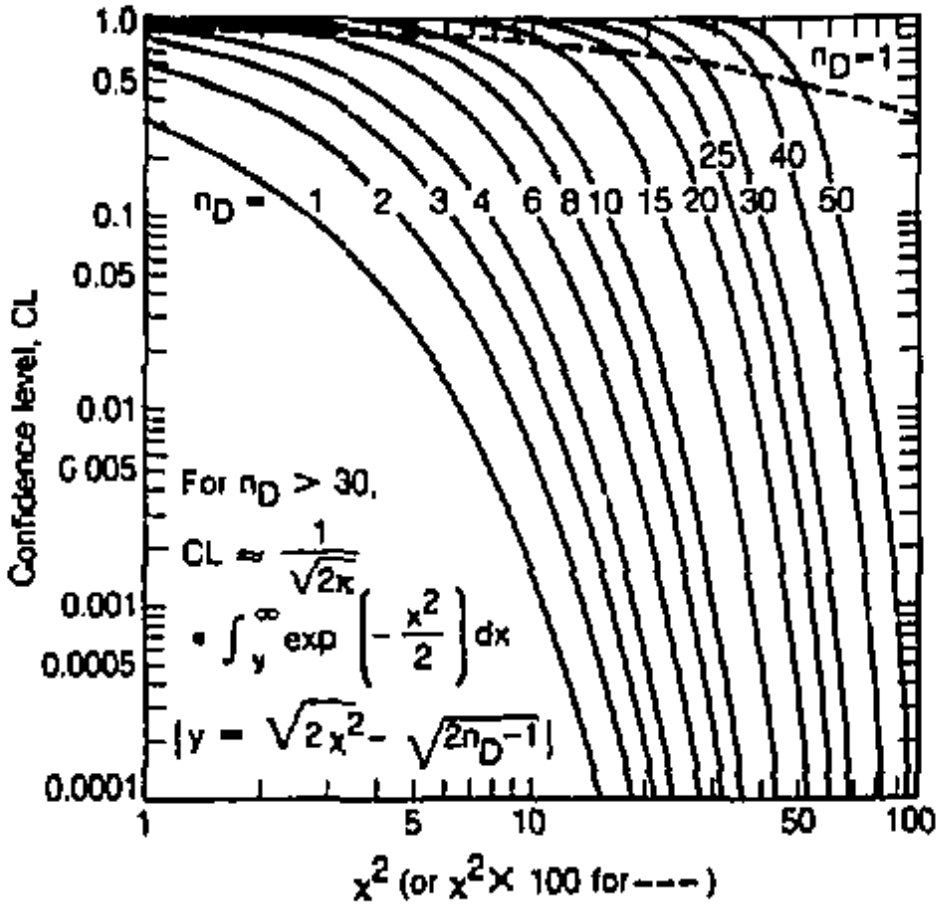

Fig. 8-1. *Confidence level as a function of χ^2 for several values of n_D, the number of degrees of freedom.*

since the distribution is symmetric about $\bar{x}$. The small figure in Eq. (2) is drawn with $\delta = 2\sigma$. CL is given by the ordinate *of the $n_D = 1$ curve in Fig. 8-1 at $\chi^2 = (\delta/\sigma)^2$.* The confidence level for $\delta = 1\sigma$ is 31.7%; 2σ, 4.6%; 3σ, 0.3%. The *odds* against exceeding δ, (1 − CL)/CL, for $\delta = 1\sigma$ are 2.15:1; 2σ, 21:1; 3σ, 370:1; 4σ, 16,000:1; 5σ, 1,700,000:1. Relations between σ and other measures of the *width*: probable error *(CL = 0.5) = 0.67σ; mean absolute deviation* = 0.80σ; RMS deviation = σ; half width at half maximum = 1.18σ.

A.2 χ^2 distribution

The χ^2 distribution for n_D degrees of freedom is

$$P_{n_D}(\chi^2)d\chi^2$$

$$= \frac{1}{2^h \Gamma(h)} (\chi^2)^{h-1} e^{-\chi^2/2} d\chi^2 \quad (\chi^2 \geq 0), \qquad (3)$$

where h (for "half") $= n_D/2$. The mean and variance are n_D and $2n_D$ respectively. In evaluating Eq. (3) one may use *Stirling's approximation*:

$$\Gamma(h) \simeq 2.507\, e^{-h}\, h^{(h-1/2)} (1 + 0.0833/h),$$

which is accurate to ±0.1% for all $h \geq 1/2$. The *confidence level* associated with a given value of n_D and an observed value of χ_0^2 is the probability of the χ^2 exceeding the observed value, i.e.,

$$CL = \int_{\chi_0^2}^{\infty} d\chi^2\, P_{n_D}(\chi^2) \qquad (4)$$

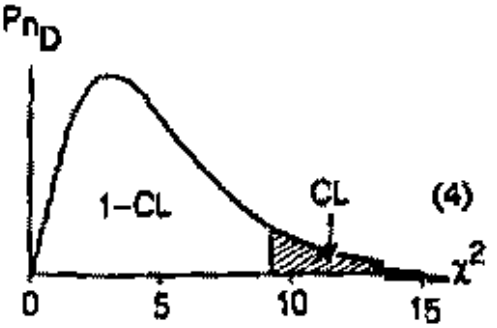

The small figure in Eq. (4) is drawn with $n_D = 5$ and CL = 10%. CL is plotted as a function of χ^2 for several values of n_D in Fig. 8-1. For *large* n_D, χ^2 becomes normally distributed about n_D. Thus,

$$y_1 = (\chi^2 - n_D)/\sqrt{2n_D} \qquad (5)$$

becomes normally distributed with unit standard deviation and mean zero. A *better* approximation is that χ, not χ^2, becomes normally distributed; specifically,

$$y_2 = \sqrt{2\chi^2} - \sqrt{2n_D - 1} \qquad (6)$$

approaches normality with unit standard deviation and mean zero. For small CLs in particular, y_2 is much more accurate than y_1. Thus, for $n_D = 50$ and $\chi^2 = 80$, the true CL = 0.45%, but y_1 is 3.0, corresponding to a CL of 0.13%, while y_2 is 2.7, corresponding to a CL of 0.35%.

A.3 Poisson distribution

The Poisson distribution with mean $\bar{n}$ is

$$P_{\bar{n}}(n) = \frac{e^{-\bar{n}}\bar{n}^n}{n!} \quad (n = 0, 1, 2, \cdots). \tag{7}$$

The variance is equal to the mean. *Confidence levels* for Poisson distributions are usually defined in terms of quantities called "*upper limits*" as follows: The confidence level associated with a given upper limit N and an observed value n_0 of n is the probability that $n > n_0$ if $\bar{n} = N$, i.e.,

$$\mathrm{CL} = \sum_{n=n_0+1}^{\infty} P_N(n) = 1 - \sum_{n=0}^{n_0} P_N(n) \tag{8}$$

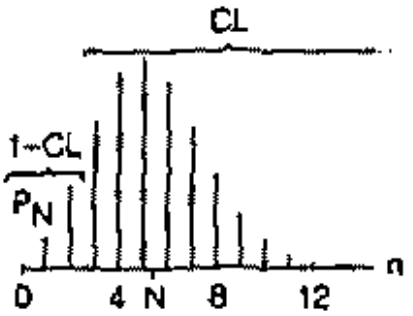

The small figure in Eq. (8) is drawn with $n_0 = 2$ and CL = 90%. A useful relation between Poisson and χ^2 confidence levels allows one to look up this quantity in Fig. 8-1. Specifically, the quantity 1 − CL is given by the ordinate of the $n_D = 2(n_0 + 1)$ curve at $\chi^2 = 2N$. Thus, 90% confidence level upper limits for $n_0 = 0$, 1, and 2 are given by half the χ^2 value corresponding to an ordinate of 0.1 on the $n_D = 2$, 4, and 6 curves, respectively; the values are $N = 2.3$, 3.9, and 5.3.

Tables of confidence levels for all three of these distributions, the relation between Poisson and χ^2 confidence levels, and numerous other useful tables and relations may be found in Ref. 1.

B. STATISTICS

Suppose one is presented with N independent data, $y_n \pm \sigma_n$, and it is desired to make some *inference* about the "true" value of the quantity represented by these data. For this purpose we interpret each datum y_n as a single sample point drawn randomly (and independently of the other data) from a distribution having true mean $\bar{y}_n$ (*which we wish to estimate*) and variance σ_n^2. We do not require that they be normally distributed. (Identification of the true σ_n with the σ_n datum is often an *approximation* which may become seriously inaccurate when σ_n is an appreciable fraction of y_n.) Some commonly used methods of estimation are given below; see Ref. 2

for numerous applications. Section B.1 deals with the case in which all $\bar{y}_n$ are the same, e.g., several different measurements of the same quantity; Sec. B.2 deals with the case in which $\bar{y}_n = \bar{y}(x_n)$, where x_n represents some set of independent variables.

B.1 Single mean and variance estimates

(1) If the y_n represent a set of values all supposedly drawn from a single distribution with mean $\bar{y}$ and variance σ^2 (i.e., the σ_n are all the same, but their common value is unknown), then

$$\hat{y} = \frac{1}{N} \sum_{n=1}^{N} y_n \tag{9}$$

and

$$\hat{\sigma}^2 = \frac{1}{N-1} \sum_{n=1}^{N} (y_n - \hat{y})^2$$

$$= \frac{N}{N-1} \left[\langle (y^2) \rangle - (\hat{y})^2 \right] \tag{10}$$

are unbiased estimates of $\bar{y}$ and σ^2; the angular brackets denote an average over the data. The variance of $\hat{y}$ is σ^2/N. If the parent distribution is normal and N is large, the variance of $\hat{\sigma}^2$ is $2\sigma^4/N$.

(2) If the y_n are independent estimates of the same $\bar{y}$, and the σ_n are known, then the weighted average

$$\hat{y} = \frac{1}{w} \sum_{n} w_n y_n, \tag{11}$$

where $w_n = 1/\sigma_n^2$ and $w = \Sigma\, w_n$, is an appropriate unbiased estimate of $\bar{y}$. This choice of weighting factors in Eq. (11) minimizes the variance of the estimate; the variance is $1/w$.

B.2 Linear least-squares fit

We wish to determine the best fit of independent unbiased data $y_n \pm \sigma_n$, measured at points x_n, to the form $y(x) = \Sigma a_j f_j(x)$, where the f_j are known, linearly independent functions (e.g., Legendre polynomials), one-to-one over the allowed range of x. The estimates for the linear coefficients a_j which minimize the sum of the squared deviations are

$$\hat{a}_i = \sum_{j,n} V_{ij} f_j(x_n) y_n / \sigma_n^2 . \tag{12}$$

Here V is the covariance matrix of the fitted parameters

$$V_{ij} = \overline{(\hat{a}_i - \bar{a}_i)(\hat{a}_j - \bar{a}_j)} , \tag{13}$$

where the overbar denotes the unknown true value; V is estimated by

$$(V^{-1})_{ij} = \sum_n f_i(x_n) f_j(x_n) / \sigma_n^2 . \tag{14}$$

The estimated variance of an interpolated or extrapolated value of y at point x, $\hat{y} = \sum \hat{a}_i f_i(x)$, is

$$(\hat{y} - \bar{y})^2|_{\text{est}} = \sum_{ij} V_{ij} f_i(x) f_j(x) . \tag{15}$$

For the case of a *straight line fit*, $y(x) = a + bx$, one obtains the following estimates of a and b:

$$\begin{aligned} \hat{a} &= (S_y S_{xx} - S_x S_{xy})/D , \\ \hat{b} &= (S_1 S_{xy} - S_x S_y)/D , \end{aligned} \tag{16}$$

where

$$\begin{aligned} S_1, S_x, S_y, S_{xx}, S_{xy} \\ = \sum (1, x_n, y_n, x_n^2, x_n y_n)/\sigma_n^2 , \end{aligned} \tag{17}$$

respectively, and

$$D = S_1 S_{xx} - S_x^2 .$$

The covariance matrix of the fitted parameters is:

$$\begin{pmatrix} V_{aa} & V_{ab} \\ V_{ab} & V_{bb} \end{pmatrix} = \frac{1}{D} \begin{pmatrix} S_{xx} & -S_x \\ -S_x & S_1 \end{pmatrix} . \tag{18}$$

The estimated variance of an interpolated or extrapolated value of y at point x is

$$(\bar{y} - \bar{y})^2|_{\text{est}} = \frac{1}{S_1} + \frac{S_1}{D}\left[x - \frac{S_x}{S_1}\right]^2 . \tag{19}$$

A least-squares fit gives estimates for the a_l [Eq. (12)] with the smallest variance, under the conditions that the expansion of y in terms of $a_l f_l$ is the correct model and that the y_n are independent, unbiased measurements whose variances σ_n^2 are known.

C. ERROR PROPAGATION

Suppose one wishes to calculate the value and error of a function of some other quantities with errors, e.g., in a Monte Carlo program. Let $\{y\}$ be a set of random variables with means $\{\bar{y}\}$ and covariance matrix V. Then the mean and variance of a function of these variables are approximately (to second order in $\{y - \bar{y}\}$)

$$\bar{f} \simeq f(\{\bar{y}\}) + \frac{1}{2}\sum_{mn} V_{mn}\left(\frac{\partial^2 f}{\partial y_m \partial y_n}\right)_{\{y\}=\{\bar{y}\}} \tag{20}$$

and

$$\overline{(f - \bar{f})^2} \simeq \sum_{mn} V_{mn}\left(\frac{\partial f}{\partial y_m}\right)_{\{y\}=\{\bar{y}\}}\left(\frac{\partial f}{\partial y_n}\right)_{\{y\}=\{\bar{y}\}} . \tag{21}$$

E.g., the mean and variance of a function of a *single variable* with mean $\bar{y}$ and variance σ^2 are

$$\bar{f} \simeq f(\bar{y}) + \frac{1}{2}\sigma^2 f''(\bar{y}) \tag{22}$$

and

$$\overline{(f - \bar{f})^2} \simeq \sigma^2 f'(\bar{y})^2 . \tag{23}$$

Note that these equations will usually be applied by substituting measured quantities, $\{\bar{y}\}$ say, for the true means, $\{\bar{y}\}$. If, as is often the case, $\bar{y}_n - \bar{y}_n$ is of order $\sqrt{V_{nn}}$, then the second-order terms in Eqs. (20) and (22) may be small compared with the first-order errors introduced by the substitution.

REFERENCES

1. M. Abramowitz and I. Stegun, Eds., *Handbook of Mathematical Functions* (Dover, New York, 1972).
2. W. T. Eadie, D. Drijard, F. E. James, M. Roos, and B. Sadoulet, *Statistical Methods in Experimental Physics* (North Holland, Amsterdam and London, 1971); S. L. Meyer, *Data Analysis for Scientists and Engineers* (John Wiley and Sons, Inc., New York, 1975); A. G. Frodesen, O. Skjeggestad, and H. Tøfte, *Probability and Statistics in Particle Physics* (Universitetsforlaget, Oslo, Norway, 1979).

This section was adapted, with permission, from the April 1984 edition of the *Particle Properties Data Booklet*.

8.2 ELECTROMAGNETIC RELATIONS

Quantity	Gaussian CGS	MKSA
Units and conversions:		
Charge:	2.99792×10^{9} esu	= 1 coul = 1 amp-sec
Potential:	(1/299.792) statvolt = (1/299.792) erg/esu	= 1 volt = 1 joule/coul
Magnetic field:	10^{4} gauss = 10^{5} dyne/esu	= 1 tesla = 1 nt/amp-m
Electron charge:	$e = 4.803\,242\times10^{-10}$ esu	$= 1.602\,189\,2\times10^{-19}$ coul
Lorentz force:	$\mathbf{F} = q(\mathbf{E} + \frac{\mathbf{v}}{c}\times\mathbf{B})$	$\mathbf{F} = q(\mathbf{E} + \mathbf{v}\times\mathbf{B})$
Maxwell equations:	$\nabla\cdot\mathbf{D} = 4\pi\rho$	$\nabla\cdot\mathbf{D} = \rho$
	$\nabla\times\mathbf{E} = -\frac{1}{c}\frac{\partial\mathbf{B}}{\partial t}$	$\nabla\times\mathbf{E} = -\frac{\partial\mathbf{B}}{\partial t}$
	$\nabla\cdot\mathbf{B} = 0$	$\nabla\cdot\mathbf{B} = 0$
	$\nabla\times\mathbf{H} = \frac{4\pi}{c}\mathbf{j} + \frac{1}{c}\frac{\partial\mathbf{D}}{\partial t}$	$\nabla\times\mathbf{H} = \mathbf{j} + \frac{\partial\mathbf{D}}{\partial t}$
Materials:	$\mathbf{D} = \varepsilon\mathbf{E}$, $\mathbf{B} = \mu\mathbf{H}$	$\mathbf{D} = \varepsilon\mathbf{E}$, $\mathbf{B} = \mu\mathbf{H}$
Dielectric constant:	$\varepsilon_{vac} = 1$	$\varepsilon_{vac} = \varepsilon_0$
Magnetic susceptibility:	$\mu_{vac} = 1$	$\mu_{vac} = \mu_0$
Fields:	$\mathbf{E} = -\nabla\Phi - \frac{1}{c}\frac{\partial\mathbf{A}}{\partial t}$	$\mathbf{E} = -\nabla\Phi - \frac{\partial\mathbf{A}}{\partial t}$
	$\mathbf{B} = \nabla\times\mathbf{A}$	$\mathbf{B} = \nabla\times\mathbf{A}$
Static potentials: (coulomb gauge)	$\Phi = \sum_{\text{charges}}\frac{q}{r}$	$\Phi = \frac{1}{4\pi\varepsilon_0}\sum_{\text{charges}}\frac{q}{r}$
	$\mathbf{A} = \frac{1}{c}\sum_{\text{currents}}\frac{\mathbf{I}}{r}$	$\mathbf{A} = \frac{\mu_0}{4\pi}\sum_{\text{currents}}\frac{\mathbf{I}}{r}$
Relativistic transformations: (v is the velocity of primed system as seen in unprimed system)	$\mathbf{E}'_{\parallel} = \mathbf{E}_{\parallel}$	$\mathbf{E}'_{\parallel} = \mathbf{E}_{\parallel}$
	$\mathbf{E}'_{\perp} = \gamma(\mathbf{E}_{\perp} + \frac{1}{c}\mathbf{v}\times\mathbf{B})$	$\mathbf{E}'_{\perp} = \gamma(\mathbf{E}_{\perp} + \mathbf{v}\times\mathbf{B})$
	$\mathbf{B}'_{\parallel} = \mathbf{B}_{\parallel}$	$\mathbf{B}'_{\parallel} = \mathbf{B}_{\parallel}$
	$\mathbf{B}'_{\perp} = \gamma(\mathbf{B}_{\perp} - \frac{1}{c}\mathbf{v}\times\mathbf{E})$	$\mathbf{B}'_{\perp} = \gamma(\mathbf{B}_{\perp} - \frac{1}{c^2}\mathbf{v}\times\mathbf{E})$
	$4\pi\varepsilon_0 = \frac{1}{c^2}10^{7}\frac{\text{coul}^2}{\text{nt}\,\text{s}^2} = \frac{1}{8.987\,55}\times10^{-9}\frac{\text{coul}^2}{\text{nt}\,\text{m}^2}$	
	$\frac{\mu_0}{4\pi} = 10^{-7}\frac{\text{nt}\,\text{s}^2}{\text{coul}^2}$, $c = 2.997\,924\,58\times10^{8}\ \text{m}\,\text{s}^{-1}$	

Impedances (MKSA)

ρ = resistivity in 10^{-8} Ωm:

~ 1.7 for Cu	~ 5.5 for W
~ 2.4 for Au	~ 73 for SS 304
~ 2.8 for Al	~ 100 for Nichrome
(Al alloys may have double this value.)	

For alternating currents, instantaneous current I, voltage V, angular frequency ω:

$$V = V_0 e^{i\omega t} = ZI .$$

Impedance of self-inductance L: $Z = i\omega L$.

Impedance of capacitance C: $Z = 1/i\omega C$.

Impedance of free space: $Z = \sqrt{\mu_0/\epsilon_0} = 376.7\ \Omega$.

Impedance per unit length of a flat conductor of width w (high frequency, ν):

$$Z = \frac{(1+i)\rho}{w\delta} \text{ , where } \delta = \text{effective skin depth ;}$$

$$\delta = \sqrt{\frac{\rho}{\pi\nu\mu}} \simeq \frac{6.6\text{ cm}}{\sqrt{\nu[\text{sec}^{-1}]}} \text{ for Cu .}$$

Capacitance $\hat{C}$ and inductance $\hat{L}$ per unit length (MKSA)

Flat rectangular plates of width w, separated by $d \ll w$:

$$\hat{C} = \epsilon\frac{w}{d} ; \quad \hat{L} = \mu\frac{d}{w} ;$$

$\frac{\epsilon}{\epsilon_0}$ = 2 to 6 for plastics; 4 to 8 for porcelain, glasses.

Coaxial cable of inner radius r_1, outer radius r_2:

$$\hat{C} = \frac{2\pi\epsilon}{\ln(r_2/r_1)} ; \quad \hat{L} = \frac{\mu}{2\pi}\ln(r_2/r_1) .$$

Transmission lines (no loss):

Impedance: $Z = \sqrt{\hat{L}/\hat{C}}$.

Velocity: $v = 1/\sqrt{LC} = 1/\sqrt{\mu\epsilon}$.

Motion of charged particles in a uniform, static, magnetic field

The path of motion of a charged particle of momentum p is a helix of constant radius R and constant pitch angle λ, with the axis of the helix along $\mathbf{B}$:

$$p\,[\mathrm{GeV}/c]\cos\lambda = 0.29979\,qB\,[\mathrm{tesla}]\,R\,[\mathrm{m}]\,,$$

where the charge q is in units of the electronic charge. The angular velocity about the axis of the helix is

$$\omega\,[\mathrm{rad\ s^{-1}}] = 8.98755\times10^{7}\,qB\,[\mathrm{tesla}]/E\,[\mathrm{GeV}]\,,$$

where E is the energy of the particle.

This section was adapted, with permission, from the April *1984 edition of the Particle Properties Data Booklet. See J. D.* Jackson, *Classical Electrodynamics*, 2d ed. (John Wiley & Sons, New York, 1975) for more formulas and details.

9.3 RADIOACTIVITY AND RADIATION PROTECTION

The International Commission on Radiation Units and Measurements (ICRU) recommends the use of SI units. Therefore, we list SI units first, followed by cgs (or other common) units in parentheses, where they differ.

Unit of activity = becquerel (curie):
1 Bq = 1 disintegration/s [= $1/(3.7\times10^{10})$ Ci].

Unit of exposure, the quantity of x- or γ-radiation at a point in space integrated over time, in terms of charge of either sign produced by showering electrons in a small volume of air about the point:
= 1 coul/kg of air (roentgen; 1 R = 2.58×10^{-4} coul/kg = 1 esu/cm^3 = 87.8 erg released energy per g of air); implicit in the definition is the assumption that the small test volume is embedded in a sufficiently large uniformly irradiated volume that the number of secondary electrons entering the volume equals the number leaving.

Unit of absorbed dose = gray (rad):
1 Gy = 1 joule/kg (= 10^4 erg/g = 10^2 rad)
= 6.24×10^{12} MeV/kg deposited energy.

Unit of dose equivalent (for biological damage) = sievert [= 10^2 *rem* (roentgen equivalent for man)]:
Dose equivalent in Sv = grays × Q, where Q (quality factor) expresses long-term risk (primarily cancer and leukemia) from low-level chronic exposure; it depends upon the type of radiation and other factors. For γ rays and β particles, $Q \cong 1$; for protons, $Q \simeq 1$ at ~10 MeV, rising gradually to $\cong 2$ at ~1 GeV; for thermal neutrons, $Q \simeq 3$; for fast neutrons, Q ranges up to 10; and for α particles and heavy ions (assuming internal deposition — skin and clothing are usually sufficient protection against external sources), $Q \cong 20$.

Natural annual background, all sources: Most world areas, whole-body dose equivalent rate $\cong$ (0.4–4) mSv (40–400 millirems). Can range up to 50 mSv (5 rems) in certain areas. U.S. average $\simeq$ 0.8 mSv. The lungs receive an additional $\simeq$ 0.1 mSv ($\cong$ 10 mrem) from inhaled natural radioactivity, mostly radon and radon daughters (good to $\simeq$

factor of 2 in open areas; can range an order of magnitude higher in buildings and up to 1000× in poorly ventilated mines).

Cosmic ray background in counters (Earth's surface):
$\sim 10^4$/min/m^2/sr.

Fluxes (per m^2) to deposit one Gy in one kg of matter, assuming uniform irradiation:
≈ (charged particles) $6.24\times10^{12}/(dE/dx)$, where dE/dx (MeV m^2/kg), the energy loss per unit length, may be obtained from range-energy data.
≈ 3.5×10^{13} minimum-ionizing singly charged particles in carbon.
≈ (photons) $6.24\times10^{12}/\{E[\text{MeV}](\mu_{en}/\rho)[\text{m}^2/\text{kg}]\}$, for photons of energy E, mass energy absorption coefficient μ_{en}, and density ρ, for samples thick enough to contain the secondary electrons but $\ll 1/\mu_{en}$.
≈ 2×10^{15} photons of 1 MeV energy on carbon.
(Quoted fluxes good to about a factor of 2 for all materials.)

U.S. maximum permissible occupational dose for the whole body:
50 mSv/year (5 rem/year).

Lethal dose: Whole-body dose from penetrating ionizing radiation resulting in 50% mortality in 30 days (assuming no medical treatment), 2.5–3.0 Gy (250–300 rads) as measured internally on body longitudinal center line; surface dose varies due to variable body attenuation and may be a strong function of energy.

For a recent review, see E. Pochin, *Nuclear Radiation: Risks and Benefits* (Clarendon Press, Oxford, 1983).

This section was adapted, with permission, from the April 1984 edition of the *Particle Properties Data Booklet.*

8.4 PROPERTIES OF VACUUM SYSTEMS

A. THROUGHPUT AND CONDUCTANCE

The throughput of any conducting element in a vacuum system is given by

$$q_{pV} = PV/t \,, \tag{1}$$

where P is the pressure and V is the volume of gas passed in time t. For a pump, if P and V are constant,

$$q_{pV} = PS \,, \tag{2}$$

where S is the pumping speed at the intake pressure P. Throughput for a passive element can also be expressed as

$$q_{pV} = C\Delta P \,, \tag{3}$$

where ΔP is the difference between the pressures at the entrance and exit of the element and C is the conductance. In high and ultrahigh vacuums, C is effectively independent of pressure. By analogy to Ohm's law, conductance for parallel constructions is given by

$$C_{tot} = C_1 + C_2 + \ldots \tag{4}$$

and for series constructions by

$$1/C_{tot} = 1/C_1 + 1/C_2 + \ldots \tag{5}$$

The effective pumping speed of a pump depends on both the nominal pumping speed and the conductance of connections between the pump and the volume to be evacuated:

$$1/S_{eff} = 1/S + 1/C_{tot} \,. \tag{6}$$

In the regime of molecular flow (see Table 8-3, below), the conductance, for air (in $l \cdot s^{-1}$), of an aperture of area A (in cm^2) is

$$C_{air} = 11.6\,A \,. \tag{7}$$

For a long straight tube of uniform circular cross section having length L and diameter D,

$$C_{air} = 12.1\,D^3/L \,. \tag{8}$$

For short tubes, Eqs. (7) and (8) must be combined:

$$C_{air} = \frac{1}{\frac{1}{11.6\,A} + \frac{L}{12.1\,D^3}} . \tag{9}$$

The equivalent diameter of a tube that tapers from diameter D_1 to diameter D_2 is

$$D_e = \left(\frac{2D_1^2 D_2^2}{D_1 + D_2} \right)^{1/3} . \tag{10}$$

The equivalent length of an elbow is

$$L_e = L + 1.33 \frac{\theta}{180} D , \tag{11}$$

where θ is the angle of the elbow in degrees.

B. GAS LOADS AND ULTIMATE PRESSURE

Sources of gas in a vacuum system include (a) the residual gas in the system; (b) the vapor in equilibrium with the materials present; and (c) the gases produced or introduced by leakage, outgassing, and permeation. In high-vacuum systems, the ultimate system pressure P_u usually depends only on (c):

$$P_u = Q_G / S_{eff} , \tag{12}$$

where Q_G is the gas load due, in this case, to leakage, outgassing, and permeation. Where Q_G is constant, as in the case of a leak, P_u is also constant; whereas, if $Q_G = f(t)$, as it is when outgassing dominates, P_u is also a function of time. Reference 1 contains nomograms relating gas loads, ultimate pressures, and various physical system parameters. Table 8-1 gives outgassing rates for several vacuum materials. Extensive outgassing data can be found in Ref. 2.

By assuming that the process is dominated by residual gas, pumpdown in the high-vacuum region can be described by

$$P = P_i \exp\left[-(S_{eff}/V_{tot})/t \right] , \tag{13}$$

where P is the pressure after time t, P_i is the pressure at $t = 0$, and V_{tot} is the total system volume.

Table 8-1. Approximate outgassing rate K_1 for several vacuum materials, after one hour in vacuum at room temperature.

Material	K_1 (mbar · l · s^{-1} · cm^{-2})
Aluminum (fresh)	9×10^{-9}
Aluminum (20 h at 100°C)	5×10^{-14}
Stainless steel (304)	2×10^{-8}
Stainless steel (304, *electropolished*)	6×10^{-9}
Stainless steel (304, mechanically polished)	2×10^{-9}
Stainless steel (304, electropolished, 30 h at 250°C)	4×10^{-12}
Perbunan	5×10^{-6}
Pyrex	1×10^{-8}
Teflon	8×10^{-8}
Viton A (fresh)	2×10^{-6}

C. MISCELLANEOUS VACUUM PROPERTIES

The mean free path λ of a gas is inversely proportional to the pressure:

$$\lambda P = c^* , \tag{14}$$

where c^* is a constant characteristic of a given gas. Values for several gases are given in Table 8-2.

For ultrahigh-vacuum systems, it is common to quote the *monolayer time* τ, which is defined as the time required for a monomolecular layer to form on a gas-free surface, assuming that every impinging gas molecule finds and binds to a vacant site. The monolayer time, in seconds, can be conveniently estimated from

$$\tau = 3.2 \times 10^{-6}/P , \tag{15}$$

Table 8-2. Values for the product c of the mean free path λ and the pressure P for several gases at 20°C.*

Gas	c * (cm · mbar)
Hydrogen	12.00×10^{-3}
Helium	18.00×10^{-3}
Nitrogen	6.10×10^{-3}
Oxygen	6.50×10^{-3}
Argon	6.40×10^{-3}
Mercury	3.05×10^{-3}
Water	3.95×10^{-3}
Air	6.67×10^{-3}

where P is expressed in mbar.

Table 8-3 lists for several pressures rough values for λ, τ, the impingement rate Z_f (the number of particles incident on a unit surface per unit time), and the volume collision rate Z_v (the number of collisions in a unit volume per unit time).

REFERENCES

1. A. Roth, *Vacuum Technology*, 2d ed. (North-Holland, Amsterdam, 1982), p.142.
2. R. J. Elsey, "Outgassing of Vacuum Materials," *Vacuum* 25, 299, 347 (1975).

Table 6-3. Values for characteristic vacuum parameters at five representative pressures.

	Pressure				
	10^{3}	10^{0}	10^{-3}	10^{-6}	10^{-9} mbar
	7.5×10^{2}	7.5×10^{-1}	7.5×10^{-4}	7.5×10^{-7}	7.5×10^{-10} Torr
	10^{5}	10^{2}	10^{-1}	10^{-4}	10^{-7} Pa
Particle density, n (cm^{-3})	10^{19}	10^{16}	10^{13}	10^{10}	10^{7}
Mean free path, λ (cm)	10^{-5}	10^{-2}	10	10^{4}	10^{7}
Impingement rate, Z_A ($s^{-1} \cdot cm^{-2}$)	10^{23}	10^{20}	10^{17}	10^{14}	10^{11}
Collision rate, Z_V ($s^{-1} \cdot cm^{-3}$)	10^{29}	10^{23}	10^{17}	10^{11}	10^{5}
Monolayer time, τ	10 ps	10 μs	10 ms	10 s	3 h
Type of gas flow	← viscous		Knudsen		molecular →